1972

VOLUME I

SEMINARS

COURSE LECTURES

ABSTRACTS

Notes on the 1972

Summer Study Program

in

GEOPHYSICAL FLUID DYNAMICS

at

The WOODS HOLE OCEANOGRAPHIC INSTITUTION

Reference No. 72-79

Contents of the Volumes

Participants and Staff Members

Browand, Frederick K.	University of Southern California
Hinch, E. John	University of Cambridge, England
Howard, Louis N.	Massachusetts Institute of Technology
Huppert, Herbert E.	University of Cambridge, England
Ingersoll, Andrew P.	California Institute of Technology
Kopell, Nancy J.	Northeastern University
Lindberg, William A.	Woods Hole Oceanographic Institution
Malkus, Willem V.R.	Massachusetts Institute of Technology
Maxworthy, Tony	University of Southern California
Nemias, Jerome	Scripps Institution of Oceanography
Parlange, Jean-Yves	Yale University
Schwartz, Leanard W.	Stanford University
Simmons, William F.	Woods Hole Oceanographic Institution
Spiegel, Edward A.	Columbia University
Stern, Melvin E.	University of Rhode Island
Thompson, Rory	Woods Hole Oceanographic Institution
Turner, Stewart	University of Cambridge, England
Veronis, George	Yale University
Whitehead, John A.	Woods Hole Oceanographic Institution

Fellows

de Szoeke, Roland A.	Nova University
Flierl, Glenn R.	Harvard University
Hickie, Brian P.	Northwestern University
Huthnance, John M.	Cambridge University, England
McCartney, Michael S.	Case Western Reserve University
Schott, Friedrich A.	University of Kiel, Germany
Schwartz, Leonard W.	Stanford University

Editor's Preface

The effect of gravity on fluids of varying density is of fundamental importance in natural flows. This subject formed the topic of concentration for the fourteenth summer program in Geophysical Fluid Dynamics at the Woods Hole Oceanographic Institution. We had the good fortune to hear Stewart Turner lecture on stratified flows just after he had completed the manuscript for his book on the subject. Turner chose to emphasize nonlinear and turbulent aspects of stratified flows and, therefore, had to give up the deductive approach in favor of treatments based on dimensional analysis and similarity arguments. This summary of the many experimental studies of these flows increased our awareness of the fascinating variety of phenomena in which stratification plays so vital a role.

Turner's lecture series was preceded by introductory lectures by Veronis, Ingersoll, Simmons, Stern, Maxworthy and Huppert. The students' reports of the entire series are recorded in the following pages. As in previous years, the reports reflect the students' understanding and interpretation of the lectures rather than a verbatim report of the talks.

This year the program was supported by the Division of Fluid Dynamics, Oceanography and Applied Mathematics of the Office of Naval Research. The Advanced Training Projects Section of the NSF, which had supported our program for thirteen summers, had been abolished and for a time it appeared that the fire of our GFD dragon was to be extinguished. But Dr. Ralph Cooper of ONR came to our rescue and arranged for support which enabled us to continue our exploration of problems in Geophysical Fluid Dynamics. We are deeply grateful to him for his efforts and to ONR for its support.

Finally, all of us wish to express our gratitude to Mary Thayer, who emerged from a serious hip operation this winter with an increased vigor and determination. Once again she has managed the program with her incredible efficiency and enthusiasm.

George Veronis

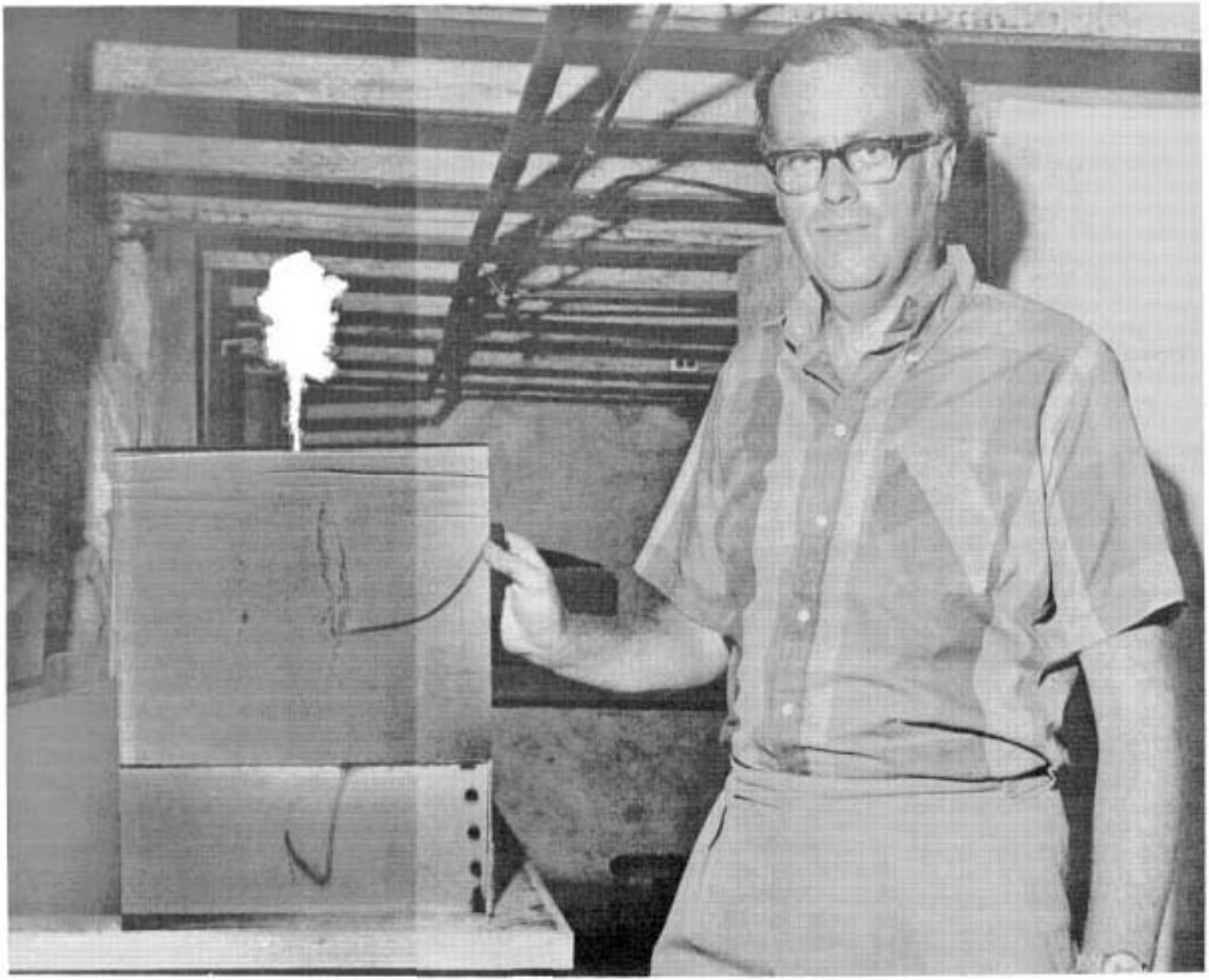

Stewart Turner, Principal Lecturer, in the basement laboratory of Walsh Cottage. Space was limited, but he managed to fit in various experiments on convection in the atmosphere, the ocean and the earth's mantle.

CONTENTS OF VOLUME I

Seminars, Course Lectures and Abstracts

COURSE LECTURES

by

Stewart Turner
University of Cambridge, England

MIXING IN STRATIFIED FLUIDS

CONTENTS OF VOLUME I (continued)

ABSTRACTS

CONTENTS OF VOLUME I (continued)

THE BOUSSINESQ APPROXIMATION

George Veronis

For multi-component fluids the density is given by the equation of state

$$\rho = \rho(s, T, p) \tag{1}$$

where s is the salinity (the mass ratio of dissolved solids to water).

The properties of seawater in tables, formulas, and graphs may be found in

(a) article by Fofonoff, The Sea, v.1

(b) H. Sverdrup *et al.*, The Oceans.

The extreme variation in seawater specific gravity is

$$1.02 \leq \rho \leq 1.07 \tag{2}$$

where the smaller number is characteristic of warm fresh water near the surface and the larger is appropriate to the cold water near the bottom of deep oceans,

If we define ρ_m as the mean value of seawater density then

$$\frac{|\rho - \rho_m|}{\rho} \approx .025 << 1 \tag{3}$$

For an adiabatic hydrostatic fluid the vertical pressure gradient is balanced by the gravitational force

$$\nabla p = -\rho g \quad \text{or} \quad \frac{\partial p}{\partial z} = -g\rho \tag{4}$$

We will not consider molecular diffusion and will take the salinity as a constant in the adiabatic state

$$s_a = \text{const.} = 34.85\ ^{o}/_{oo}$$

From the first law of thermodynamics

$$\delta q = T d\eta = c_p\, dT + T\left(\frac{\partial \eta}{\partial p}\right)_T dp \tag{5}$$

where η denotes entropy,

But, since only adiabatic processes are considered, $\delta q \equiv 0$, the vertical gradient of temperature is

$$\left(\frac{\partial T}{\partial z}\right)_\eta = -\frac{T}{c_p}\left(\frac{\partial \eta}{\partial p}\right)_T \frac{\partial p}{\partial z} = \frac{g\rho T}{c_p}\left(\frac{\partial \eta}{\partial p}\right)_T \tag{6}$$

where we have used (4) and (5). From thermodynamics

$$\left(\frac{\partial \eta}{\partial p}\right)_T = -\left(\frac{\partial V}{\partial T}\right)_p \tag{7}$$

where V is specific volume. Finally

$$\left(\frac{\partial T}{\partial z}\right)_\eta = -\frac{g\alpha T}{c_p} \tag{8}$$

where α, the coefficient of thermal expansion is

$$\alpha = \frac{1}{V}\left(\frac{\partial V}{\partial T}\right)_p \tag{9}$$

The computed bounds of the adiabatic temperature gradient are

$$\frac{.016^\circ C}{km} \leq \left|\left(\frac{\partial T}{\partial z}\right)_\eta\right| \leq \frac{.21^\circ C}{km}$$

where the smaller number corresponds to a surface measurement at $T = -2^\circ C$, and the larger to a depth of 10 km at $4^\circ C$.

Integrating (8) over the top 4 km of the ocean, we get

$$\Delta T\Big|_{-4km}^{0} \sim -0.6^\circ C$$

Note that the adiabatic gradient predicts that the colder water is on top. The observed ΔT is about $+20^\circ C$. In the surface region (upper two kilometers, say)

$$\left|\frac{\partial T}{\partial z}\right|_{adiabatic} \qquad \left|\frac{\partial T}{\partial z}\right|_{observed}$$

and, in addition has the wrong sign. Under the adiabatic hydrostatic assumption we can compute the vertical density gradient. In this case we find

$$\left(\frac{\partial \rho}{\partial z}\right)_{\text{adiabatic}} \approx \left(\frac{\partial \rho}{\partial z}\right)_{\text{observed}}$$

The adiabatic variation of density with depth is

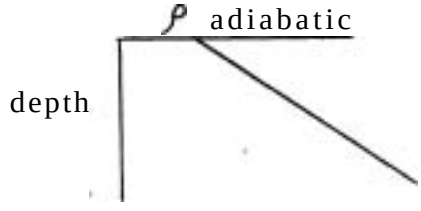

We remove the adiabatic variation, defining a "potential density"

$$\rho \text{ potential} = \rho - \rho \text{ adiabatic}$$

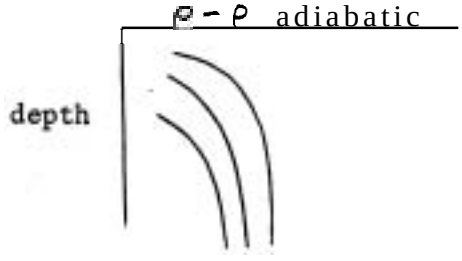

Variations here are due to gradients of salinity and temperature,

The Boussiaesq Equations

Starting with the simple force equation

$$\rho \frac{dv}{dt} = -\nabla p - g\rho \qquad (10)$$

we assume small perturbations from the hydrostatic adiabatic solution, Thus

$$p = p_a + \tilde{p},\ \rho = \rho_a + \tilde{\rho},\ T = T_a + \tilde{T},\ s = s_a + \tilde{s}$$

Since

$$\frac{|\rho - \rho_m|}{\rho_m} \approx .01$$

for typical ocean regions we may replace ρ by ρ_m on the left-hand side of (10) with small error. Subtracting the hydrostatic force balance. we get

$$\frac{d\chi}{dt} = -\frac{\nabla \tilde{p}}{\rho_m} - \frac{g\tilde{\rho}}{\rho_m} \tag{11}$$

Expanding Equation (1) for small deviations from the adiabatic state:

$$\rho = \rho_a + \left(\frac{\partial \rho}{\partial T}\right)_{p,s} \tilde{T} + \left(\frac{\partial \rho}{\partial p}\right)_{s,T} \tilde{p} + \left(\frac{\partial \rho}{\partial s}\right)_{p,T} \tilde{s} + \ldots \tag{12}$$

or

$$\frac{\tilde{\rho}}{\rho_a} \approx \frac{\tilde{\rho}}{\rho_m} = -\alpha \tilde{T} + K\tilde{p} + \gamma \tilde{s} \tag{13}$$

plus second-order small quantities. Here we have defined

$$\alpha = -\frac{1}{\rho_m}\left(\frac{\partial \rho}{\partial T}\right)_{p,s}, \quad K = \frac{1}{\rho_m}\left(\frac{\partial \rho}{\partial p}\right)_{s,T}, \quad \gamma = \frac{1}{\rho_m}\left(\frac{\partial \rho}{\partial s}\right)_{p,T}. \tag{14}$$

The coefficients α , , and γ are determined experimentally. Note the minus sign in the definition of α . The right-hand side sf the equation of motion (10) is equal to

$$-\frac{1}{\rho_m}\frac{\partial \tilde{p}}{\partial z} + g\alpha\tilde{T} - gK\tilde{p} - g\gamma\tilde{s} \tag{15}$$

The order of magnitude of the first term is

$$\frac{1}{\rho_m}\frac{\partial \tilde{p}}{\partial z} \sim \frac{\tilde{p}/\rho_m}{H}$$

where H, the ocean depth $\sim$ 5 km,

But $gK\tilde{p} = \frac{\tilde{p}/\rho_m}{H_s}$

The height $H_s = \frac{1}{\rho_m g K} \approx$ 200 km, hence $\frac{\text{3rd term}}{\text{1st term}}$ in (15) $\ll 1$ and the "sound waves" term may be neglected,

Thus $$\frac{\tilde{\rho}}{\rho_m} = -\alpha\tilde{T} + \gamma\tilde{s} \tag{16}$$

The mass conservation law may be written as

$$w\frac{\partial \rho_a}{\partial z} + \frac{\partial \tilde{\rho}}{\partial t} + \underset{\sim}{v}\cdot\nabla\tilde{\rho} + \rho\nabla\cdot\underset{\sim}{v} = 0. \tag{17}$$

But

$$\left| w \frac{\partial \rho_a}{\partial z} \right| , \quad \left| \underset{\sim}{v} \cdot \nabla \tilde{\rho} \right| \sim \frac{|\rho - \rho_m|}{\rho_m}$$

and may be neglected.

The term $\frac{\partial}{\partial t}$ may be estimated by recognizing that changes occur on a convective time scale; that is

$$\frac{\partial}{\partial t} \simeq \frac{V}{L}$$

and thus

$$\left| \frac{\partial \tilde{\rho}}{\partial t} \right| \sim \frac{|\rho - \rho_m|}{\tau_n}$$

and this term may be neglected also.

Hence our conservation of mass equation is identical to the one for an incompressible fluid:

$$\nabla \cdot \underset{\sim}{v} = 0 \tag{18}$$

We must also specify a conservation equation for salinity. We ignore molecular diffusion and take

$$\frac{d\tilde{s}}{dt} = 0 \tag{19}$$

We state our energy equation assuming no sources or sinks of energy. Then the change in internal energy $\tilde{e}$ is balanced by the work done

$$\rho \frac{d\tilde{e}}{dt} = -p \nabla \cdot \underset{\sim}{v} \tag{20}$$

In general, however, the internal energy may be affected by changes in temperature and salinity.

$$\rho \frac{d\tilde{e}}{dt} = c_p \frac{d\tilde{T}}{dt} - p \nabla \cdot \tilde{v} + c_s \frac{d\tilde{s}}{dt} \tag{21}$$

By subtracting (20) from (21), we get

$$c_p \frac{d\tilde{T}}{dt} + c_s \frac{d\tilde{s}}{dt} = 0$$

But the second term has been assumed to be zero. Thus

$$\frac{d\tilde{T}}{dt} = 0 \tag{22}$$

is our energy equation.

In summary the adiabatic hydrostatic state is described by

$$s = \text{const.}$$

$$\nabla p = -g\rho$$

$$\frac{\partial T}{\partial z} = \frac{-g\alpha T}{C_p}$$

$$\rho = \rho(s, T, p)$$

The Boussinesq equations for the perturbed state are

$$\frac{d\chi}{dt} = -\frac{1}{\rho_m}\nabla p - \frac{g\tilde{\rho}}{\rho_m}$$

$$\nabla \cdot \chi = 0$$

$$\frac{\tilde{\rho}}{\rho_m} = -\alpha\tilde{T} + \gamma\tilde{S} \qquad \alpha, \gamma \text{ taken constant}$$

$$\frac{d\tilde{s}}{dt} = 0$$

$$\frac{d\tilde{T}}{dt} = 0$$

$$\frac{d\tilde{p}}{dt} = 0$$

The concept of potential density, formed by subtracting the adiabatic variation from the actual density, can lead to erroneous conclusions if one is comparing water of different salinity at great depth. For example, looking at a section down the mid-Atlantic from north to south poles, we see:

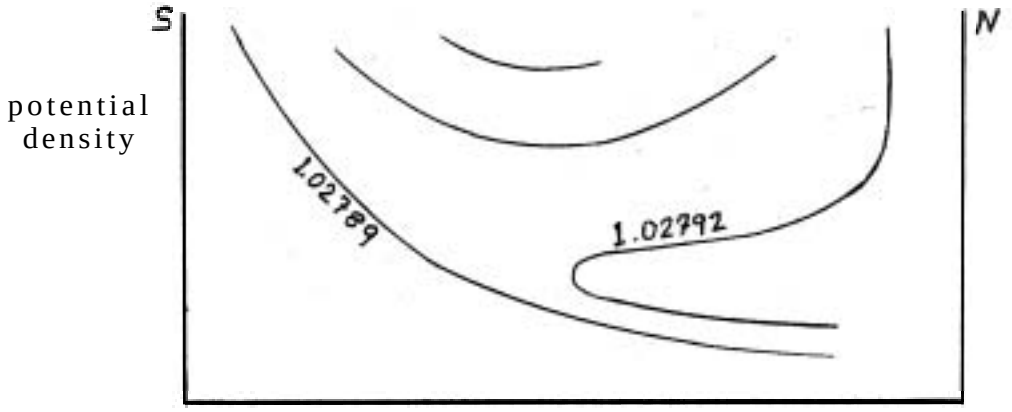

Thus by using the surface as the reference level for the potential density we conclude, erroneously, that the water is statically unstable as in the figure on the left below.

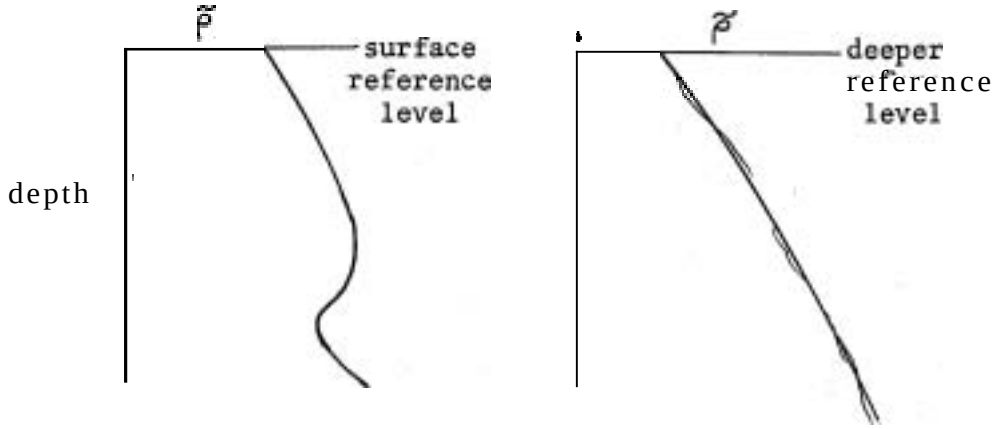

The representation on the right shows stable stratification. The error arises from taking too shallow a reference level.

References

(a) Spiegel, E.A. and G. Veronis 1960 "Boussinesq Approximation for Compressible Fluids", Astrophysical J. 131: 442-447.

(b) Mihaljan, J.M. 1962 Astrophysical J. 136: 1126-1133.

(c) Malkus, W.V.R. 1964 G.F.D. lecture notes 1: 1.

(d) Bretherton, F.P. 1965 G.F.D. lecture notes 1: 10.

Notes submitted by
Leonard W. Schwartz

SMALL AMPLITUDE INTERNAL GRAVITY WAVES

Andrew P. Ingersoll

By the small-amplitude approximation, in this context, we mean that in the derivative following the motion d/dt, the contribution from the time derivative $\partial/\partial t$ outweighs the effect of fluid advection $\vec{v} \cdot \nabla$ in the equations of motion. Expressed another way, since we are considering wave motions we can replace the $\partial/\partial t$ operator by a wave frequency ω and ∇ by a wavenumber k, so that the small amplitude assumption implies that $\omega >> Uk$, where U is a

typical value of the fluid velocity, i.e., that the phase speed of the wave ($= \omega/k$) is far greater than,a typical fluid velocity.

We make use of the Boussinesq approximation which in essence assumes that the only sensible effect of density variation is a buoyancy force in the vertical momentum equation. This vertical buoyancy force per unit mass is given by

$$\sigma' = \alpha g \theta'$$

where θ' is a part of the temperature field T partitioned as follows:

$$T = \bar{\theta}'(z) + \theta'$$

(z is 'the vertical coordinate, taken positive in the upward direction), $\bar{\theta}(z)$ is a basic given stratification, the departures from which, θ' , will interest us. Similarly the pressure field is partitioned into

$$p = \bar{p}(z) + p'$$

where $\bar{p}(z)$ is the pressure required to balance hydrostatically the basic temperature stratification $\bar{\theta}(z)$, i.e.,

$$\bar{p}_z = \rho_0 \alpha g \bar{\theta}$$

Here ρ_0 is the mean density, α the thermal coefficient of expansion, and g the acceleration of gravity, all of which are constants in the context of the Boussinesq approximation.

The fluid velocity components, small in the sense we have described above, we write formally as

$$u = u', \quad v = v', \quad w = w'$$

(primed quantities are taken to be small), Then the equations of motion and continuity are

$$\begin{aligned} u'_t + \frac{1}{\rho_0} p'_x &= 0 \\ v'_t + \frac{1}{\rho_0} p'_y &= 0 \\ w'_t + \frac{1}{\rho_0} p'_z - \alpha g \theta' &= 0 \\ u'_x + v'_y + w'_z &= 0 \end{aligned}$$

Note that these equations are linear in the primed quantities,

We need one more equation: the heat conservation equation (heat conduction is neglected) expressed exactly by

$$\frac{dT}{dt} = 0$$

Substituting directly into this equation and neglecting only terms containing products of primed quantities, we obtain

$$\theta'_t + w' \frac{d\bar{\theta}}{dz} = 0$$

Let us define $\pi' = p'/\rho_0$ and use σ' rather than θ' in the above equations so that they can be rewritten (dropping primes now) as

$$u_t + \pi_x = 0 \tag{1}$$

$$v_t + \pi_y = 0 \tag{2}$$

$$w_t + \pi_z - \sigma = 0 \tag{3}$$

$$u_x + v_y + w_z = 0 \tag{4}$$

$$\sigma_t + N^2 w = 0 \tag{5}$$

where

$$N = \left(\alpha g \frac{d\bar{\theta}}{dz} \right)^{1/2}$$

is called the Brunt-Väisälä frequency and in general is a function of z.

These equations are linear with constant coefficients except for N^2 so that we can anticipate separability of the x, y, t dependence of the equations, but not necessarily the z-dependence.

If we look for wavelike solutions we might expect typical frequencies to depend dimensionally on N: $\omega \sim O(N)$. This may be seen most simply in the special case of constant N (linear basic stratification) with vertical homogeneity $(\partial/\partial z = 0)$ of the perturbations. (In this case all the fluid particles in a vertical column "pulsate" in unison.) With these assumptions the horizontal components of velocity decouple from the system and the vertical motion is governed by

$$w_t - \sigma = 0$$

$$\sigma_t + N^2 w = 0$$

from which σ may be eliminated to give

$$w_{tt} + N^2 w = 0$$

so that our solution must have an e^{iNt} dependence.

A typical magnitude for N from the temperature gradients in the oceans and atmosphere is

$$\frac{2\pi}{N} \sim 10^3 \text{sec} \doteq 15 \text{min.}$$

Let us return to the full equations (1) - (5). We perform the following manipulations:

$$\frac{\partial}{\partial x}\left[\frac{\partial}{\partial x}(3) - \frac{\partial}{\partial z}(1)\right] = w_{xxt} - \sigma_{xx} - u_{xzt} = 0$$

$$\frac{\partial}{\partial y}\left[\frac{\partial}{\partial y}(3) - \frac{\partial}{\partial z}(2)\right] = w_{yyt} - \sigma_{yy} - v_{yzt} = 0$$

Adding these two, and using (4), we obtain

$$\nabla^2 w_t - \nabla_1^2 \sigma = 0$$

where

$$\nabla_1^2 = \partial^2/\partial x^2 + \partial^2/\partial y^2$$

is the horizontal Laplacian operator and

$$\nabla^2 = \nabla_1^2 + \partial^2/\partial z^2$$

is the full Laplacian.

Eliminating σ between this equation and Eq. (5), we obtain finally

$$\nabla^2 w_{tt} + N^2 \nabla_1^2 w = 0 \qquad (6)$$

In what follows, as in the simple example above, we assume N^2 to be constant. This assumption is motivated primarily by considerations of simplicity so that the equations are separable in all coordinates, but physically we may suppose our attention is restricted to a small vertical extent of the ocean in which the assumption is approximately satisfied. Let all dependent variables behave like

$$\exp\left[i(kx + \ell y + mz - \omega t)\right]$$

Without loss of generality, since the coordinate system can be rotated about a vertical axis we can set $\ell = 0$. Substituting this dependence into (6), we obtain the dispersion relationship

$$\omega = \pm \frac{Nk}{(k^2+m^2)^{1/2}} \tag{7}$$

Notice that $\omega \geq 0$ is always a solution. If we therefore define $\omega \geq 0$, the orientation of the wavenumber vector $\vec{k} = k\hat{x} + m\hat{z}$ gives the direction of propagation of the wave (see Figure 1) and

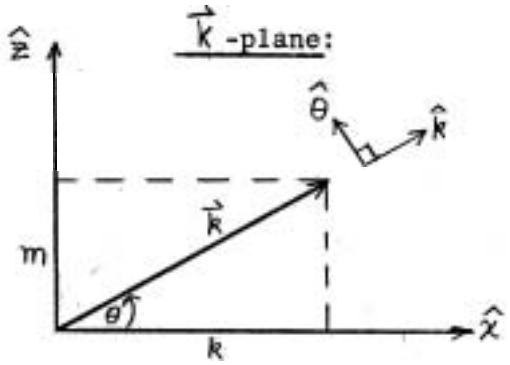

Figure 1

(7) may be written

$$\omega = N|\cos\theta| \tag{8}$$

where θ is the angle shown in Figure 1. Notice that $|\omega| \leq N$.

The fluid velocity for this wave motion is given by

$$\vec{v} = \vec{A}e^{i(kx+my-\omega t)}$$

which, through the continuity equation $\nabla \cdot \vec{v} = 0$, implies that

$$\vec{k} \cdot \vec{A} = 0$$

i.e., that the wave motion is transverse.

Alternative physical derivation of the dispersion relation

We offer an alternative derivation of the dispersion relationship, Consider a column of fluid with axis in the $\hat{\theta}$ direction [Figure 1) which is displaced a distance S along this axis. The

vertical component of this displacement is $S\cos\theta$. The vertical buoyancy force per unit mass tending to expel this column from its surroundings of different density and restore it to its equilibrium position is then $-N^2 S\cos\theta$. Resolving this force into a component parallel to the original displacement $(-N^2 S\cos^2\theta)$ and balancing it by the acceleration in that direction S, we obtain

$$\ddot{S} + N^2\cos^2\theta\, S = 0$$

which represents simple harmonic motion with frequency $\omega = \pm N\cos\theta$.

The group velocity of these waves, defined by

$$\vec{C}_g = \vec{\nabla}_k |\omega| ,$$

is in fact, using (7) or (8) with $\omega > 0$,

$$\vec{C}_g = \frac{\hat{\theta}}{(m^2+k^2)^{1/2}} \frac{\partial(N|\cos\theta|)}{\partial\theta}$$
$$= \mp \frac{N\sin\theta}{(m^2+k^2)^{1/2}}\hat{\theta} ,$$

where the minus sign applies for $-\frac{\pi}{2} < \theta < \frac{\pi}{2}$ and the plus sign for $\frac{\pi}{2} \le \theta \le \frac{3\pi}{2}$. The phase velocity, defined by

$$\vec{C}_p = \left|\frac{\omega}{k}\right|\hat{k} = \frac{N|\cos\theta|}{(k^2+m^2)^{1/2}}\hat{k} ,$$

is thus perpendicular to the group velocity such that the vertical component of $\vec{C}_p$ is equal and opposite to that of $\vec{C}_g$ (see Figure 2).

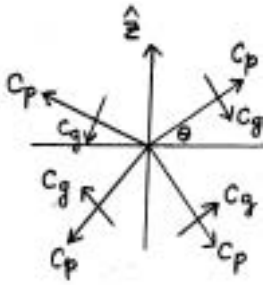

Figure 2

A physical justification for the term "group" velocity, meaning the speed of a group of waves in a wave packet, can be obtained by considering the graphical superposition of two wave trains of the same

wavenumber, slightly differing frequencies, and so progressing in slightly different directions, If the pattern formed by the constructive and destructive interference of the two wave trains is studied this pattern is observed to progress approximately transversely to the directions of progression of the wave trains. Moreover, since the wave train whose wavenumber vector is more nearly horizontal has the greater phase velocity, the velocity of the interference pattern will have an upward vertical component when that of the phase velocity is downward, and conversely. Thus when waves are generated by an object moving with a velocity u through an otherwise motionless fluid, the horizontal component of the phase velocity must be u, to insure that the pattern moves with the object, and the vertical component of the phase velocity must be downward at levels above that of the object, and vice versa,

The effects of rotation

When, one might ask, is rotation going to be an important influence on internal gravity waves in a geophysical situation? We have already remarked that in the oceans and atmosphere

$$\frac{2\pi}{N} \sim 10^3 \text{ sec.}$$

whereas the rotational period of the earth is

$$\frac{2\pi}{\Omega} \sim 10^5 \text{ sec.}$$

Clearly, for internal gravity waves propagating with a significanr horizontal component (i.e., $k/m = O(1)$) we have $\omega = O(N)$ and the rotational modification will be negligible. For waves propagating nearly vertically (i.e., horizontal wavelength much greater than the vertical wavelength), that is for

$$k << m$$

the dispersion relationship will become, to good approximation

$$\omega \simeq N \frac{k}{m}$$

Then in the situation $\frac{k}{m} = O(10^{-2})$, it happens that

$$\omega \simeq \frac{Nk}{m} \sim \Omega$$

and the modifications due to roatation must be incorporated. This can be done by including the terms $-2\Omega v$, $2\Omega u$ on the left-hand sides of Eqs. (1) and (2) respectively and rederiving the dispersion relationship. It can be shown that

$$\omega^2 \simeq N^2 \frac{k^2}{k^2+m^2} + (2\Omega)^2 \frac{m^2}{k^2+m^2}$$

which, in the limit $k/m \longrightarrow 0$, behaves like

$$\omega^2 \simeq N^2 \frac{k^2}{m^2} + (2\Omega)^2$$

The functional dimensionless parameter which determines the importance of the role played by rotation is

$$B = \frac{N^2 k^2}{\Omega^2 m^2}$$

or, using instead of the wavenumbers k and m the horizontal scale L and the vertical scale H of the motion:

$$B = \frac{N^2 H^2}{\Omega^2 L^2} = \frac{\alpha g \frac{d\bar{\theta}}{dz}}{\Omega^2} \frac{H^2}{L^2}$$

When this parameter is large, rotational effects are negligible, but when it is of order unity, rotation ought to be taken into consideration.

Notes submitted by
Roland A. de Szoeke

WAVE-WAVE INTERACTION

William F. Simmons

Consider internal waves whose motion is governed by the following system of equations:

incompressibility $\nabla \cdot u = 0$ (1)

continuity $\frac{D\rho}{Dt} = 0$ (2)

momentum $\rho \frac{Du_i}{Dt} + \frac{\partial p}{\partial x_i} + \rho g_i = 0$ (3)

Using the cartesian axis system shown below

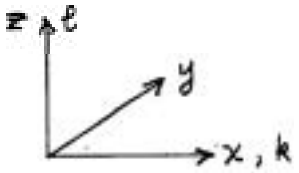

the acceleration $g_i = (0, 0, -g)$. k and ℓ are the horizontal and vertical wave numbers respectively. Let $\hat{}$ denote dimensionless quantities formed as follows:

$$\hat{x} = kx, \quad \hat{z} = \ell z, \quad \hat{t} = Nt$$
$$\hat{\omega} = \frac{\omega}{aN} \qquad \hat{u} = \frac{u}{(aN)(\ell/k)} \tag{4}$$

where a is the semi-wave amplitude defined in the figure

N is the Brunt frequency where

$$N^2 = -\frac{\partial \bar{\rho}}{\rho_0}\frac{g}{\rho_0}. \tag{5}$$

We also define $\delta = \ell/k$, and also the aspect ratio $\epsilon = a\ell \ll 1$, i.e. the vertical distance over which sensible changes in the wave form occur is much greater than the wave amplitude. We will see that ϵ measures the strength of nonlinear effects. The density

$$\rho = \bar{\rho}(z) + \rho'$$
$$\bar{\rho}(z) = \rho_0\left(1 - \frac{1}{\rho_0}\frac{\partial \bar{\rho}}{\partial z} z\right) = \rho_0\left(1 + \frac{N^2}{g\ell}\hat{z}\right) \tag{6}$$

The quantity, $\sigma = \frac{N^2}{g\ell} \sim 10^{-4}$ typically for the ocean, measures the strength of effects due to varying inertial mass. We consider that variations in density at points in space arise from up and down wave motion, Thus

$$\rho' = \left(-\frac{\partial \bar{\rho}}{\partial z}\alpha\right)\hat{\rho}' = \rho_0 \sigma \epsilon \hat{\rho}' \tag{7}$$

defines the fluctuating component of density in dimensionless variables.

By taking the curl of the momentum equation and retaining only the component normal to the plane of the motion, we obtain a vorticity equation

$$\frac{\partial}{\partial x}\left(\rho \frac{Dw}{Dt}\right) - \frac{\partial}{\partial z}\left(\rho \frac{Du}{Dt}\right) + g\frac{\partial \rho}{\partial x} = 0 \tag{8}$$

The system of Equations (1), (2), and (8) may be rewritten in terms of dimensionless variables. For convenience we will omit the symbol $\hat{}$. We get

$$\frac{\partial u}{\partial x} + \frac{\partial w}{\partial z} = 0 \tag{1}$$

$$\frac{\partial p'}{\partial t} - w + \epsilon \frac{\partial p'}{\partial x_j} u_i = 0 \tag{9}$$

$$\left\{\frac{\partial \rho'}{\partial x} + \left(\frac{\partial w}{\partial x} - \delta^2 \frac{\partial u}{\partial z}\right)_t\right\} + \epsilon\left\{\left(\frac{\partial w}{\partial x_j} u_j\right)_x - \delta^2\left(\frac{\partial u}{\partial x_j} u_j\right)_z\right\} =$$
$$= \sigma\left\{-\delta^2 \frac{\partial u}{\partial t} + z\left(\frac{\partial w}{\partial x} - \delta^2 \frac{\partial u}{\partial z}\right)_t\right\} + O(\sigma\epsilon) + O(\sigma\epsilon^2) + \ldots \tag{10}$$

where repeated subscripts i or j imply summation over the three cartesian components. Since $\sigma \sim 10^{-4}$ and $\epsilon \sim 10^{-1}$ say, the right-hand side of (10) is quite small. For our present purposes we will neglect it completely, setting the left-hand side of (10) equal to zero, σ terms can be treated in the same way that nonlinear terms will be treated, They give rise to vertical variations of semi-wave amplitude on the length scale g/N^2,*

Consider now a wave pair whose wave vectors lie at angles θ and $-\theta$ with the horizontal.

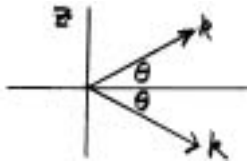

*They will henceforth be ignored.

Further, let us introduce a stream function Ψ so that

$$u = \frac{\partial \psi}{\partial z}, \quad w = -\frac{\partial \psi}{\partial x}$$

Select as boundary conditions those appropriate to rigid horizontal planes on the top and bottom

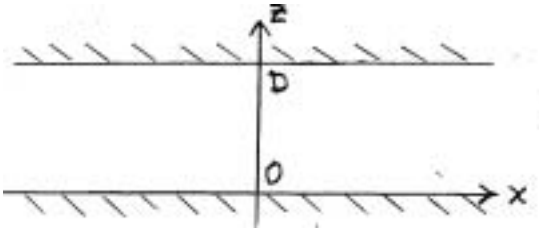

$$w(x,y,0) = w(x,y,D) = 0 \tag{11}$$

The linear (infinitesimal amplitude) approximation to the stream function Ψ is, in dimensional form for this wave pair (taking $\epsilon = 0$)

$$\psi = \frac{a\omega}{k} \cos(kx - \omega t) \sin \ell z \tag{12}$$

where we will take

$$\begin{aligned} kx - \omega t &= \chi \\ \ell z &= \theta \end{aligned} \tag{13}$$

The condition (11) is satisfied by taking $\ell D = n\pi$. From the continuity equation we get, as a first approximation, in dimensionless variables

$$0 = \frac{\partial \rho'}{\partial t} + \frac{\partial \psi}{\partial x} = -\omega \frac{\partial \rho'}{\partial \chi} + k \frac{\partial \psi}{\partial \chi} \tag{14}$$

Thus

$$\rho' = \rho_0 \frac{N^2 a}{g} \cos \chi \sin \theta. \tag{15}$$

By eliminating density and combining the first approximations to the continuity and vorticity equations, we get

$$\begin{aligned} \mathcal{L}(\psi) &= \nabla^2 \psi_{tt} + N^2 \psi_{xx} \\ &= N^2 (k^2 + \ell^2) \left[\frac{\omega^2}{N^2} - \frac{k^2}{k^2 + \ell^2} \right] \psi = 0 \end{aligned} \tag{16}$$

The solution is represented graphically for the first three modes permitted by the boundary condition.

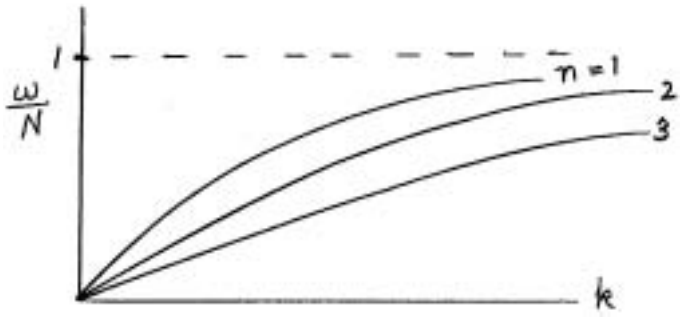

The continuity and vorticity equations, retaining terms of $O(\epsilon)$, may be represented schematically as

$$\mathcal{L}_1(\psi) + \epsilon \mathcal{N}_1(\psi, p') =$$
$$\mathcal{L}_2(\psi) + \epsilon \mathcal{N}_2(\psi, p') = 0$$

These may be combined to form one equation for ψ, correct to $O(\epsilon)$.

$$\mathcal{L}(\psi) + \epsilon \mathcal{N}(\psi, \psi) = 0 \tag{17}$$

One might consider solving an equation of this form by a Stokes expansion

$$\psi = \sum_{n=0} \epsilon^n \psi^{(n)} = \psi^{(0)} + \epsilon \psi^{(1)} + \epsilon^2 \psi^{(2)} + \cdots \tag{18}$$

However the homogeneous solutions will be periodic and ultimately secular terms will appear in the particular integrals. Thus the perturbation expansfon (18) will cease to be valid for large t or x.

We will search for a uniformly valid solution by the method of multiple scales:

We replace the x and t derivatives in the equations as follows:

$$\begin{aligned} \frac{\partial}{\partial x} &\longrightarrow \frac{\partial}{\partial x} + \epsilon \frac{\partial}{\partial X_1} + \epsilon^2 \frac{\partial}{\partial X_2} + \cdots \\ \frac{\partial}{\partial t} &\longrightarrow \frac{\partial}{\partial t} + \epsilon \frac{\partial}{\partial T_1} + \epsilon^2 \frac{\partial}{\partial T_2} + \cdots \end{aligned} \tag{19}$$

Now a typical second derivative is computed as

$$\frac{\partial^2}{\partial x^2} \longrightarrow \left(\frac{\partial}{\partial x} + \epsilon \frac{\partial}{\partial X_1} + \cdots \right)^2 = \frac{\partial^2}{\partial x^2} + 2\epsilon \frac{\partial^2}{\partial x \partial X_1} + O(\epsilon^2)$$

Symbolically we replace the operator $\mathcal{L}$ by

$$\mathcal{L} \longrightarrow \mathcal{L} + \epsilon \mathcal{S}_1 + \epsilon^2 \mathcal{S}_2 + \cdots$$

where the $\mathcal{L}$'s contain derivatives with respect to slowly varying quantities. Note that $\mathcal{L}_1$ is a 1st order slowly varying differential operator, $\mathcal{L}_2$ a 2nd order, and so on. Equation (17) with ψ expanded in a series of the form (18) and the independent variables treated as in (19) becomes

$$\left\{ \rho_0 \left(\frac{\partial^2}{\partial t^2} \nabla^2 + N^2 \frac{\partial^2}{\partial x^2} \right) \psi^0 + \right.$$
$$+ \epsilon \left\{ 2\rho_0 \left[\frac{\partial^2}{\partial t \partial T} \nabla^2 + \frac{\partial^2}{\partial t^2} \left(\frac{\partial^2}{\partial x \partial X} + \frac{\partial^2}{\partial z \partial Z} \right) + N^2 \frac{\partial^2}{\partial x \partial X} \right] \psi^0 + \right.$$
$$\left. \left. + \rho_0 \left(\frac{\partial}{\partial t^2} \nabla^2 + N^2 \frac{\partial^2}{\partial x^2} \right) \psi' - \eta(\psi^0, \psi^0) \right\} + O(\epsilon^2) = 0 \qquad (20)$$

where we consider only first-order slow variation, letting $T_1 \rightarrow T$, etc. Consider a family of experiments in whish two waves are generated simultaneously by a paddle, One wave has parameters

$$a_1, \omega_1, \ell_1, k_1,$$

considered as fixed for all experiments, The other wave has parameters

$$a_3, \omega_3, \ell_3, k_3$$

which are fixed for a given experiment, but ω_3 and a_3 may vary from one experiment to the next, The approximate stream function for the two-wave system, in terms of "slow" and "fast" variables, is of the form

$$\psi^0 = \sum_{i=1,3} \frac{a_i(X, Z, T)}{k_i} \omega_i \cos \left[k_i x - \omega_i t + \eta_i(X, Z, T) \right] \cdot \sin \left[\ell_i z + \mu_i(X, Z, T) \right] \qquad (21)$$

where η_i , and μ_i are slowly varying phase angles. Substituting this form in Equation (20) we get

$$\sum_{i=1,3} \frac{a_i \omega_i}{k_i} \left(k_i^2 + \ell_i^2 \right) N^2 \left\{ \frac{\omega_i^2}{N^2} - \frac{k_i^2}{k_i^2 + \ell_i^2} \right\} \cos \chi_i \sin \theta_i +$$
$$+ \epsilon \left\{ \sum_{i=1,3} 2N^2 k_i \left[\left\{ \frac{\partial}{\partial T} + c_{gix} \frac{\partial}{\partial X} \right\} a_i \sin \chi_i \cos \theta_i - \left\{ c_{giz} \frac{\partial}{\partial Z} \right\} a_i \cos \chi_i \cos \theta_i \right] + \right.$$
$$\left. + \mathcal{L}(\psi') \right\} + \text{terms in } \cos(\chi_i \pm \chi_j) \sin(\theta_i \pm \theta_j) = 0 \qquad (22)$$

In (22) the term represented symbolically as $\mathcal{L}(\psi')$ will be of the form

$$\frac{a\omega}{k} \left(k^2 + \ell^2 \right) N^2 \left\{ \frac{\omega^2}{N^2} - \frac{k^2}{k^2 \ell^2} \right\} \cos \chi \sin \theta$$

where $k = k_1 \pm k_3$

$\ell = \ell_1 \pm \ell_3$

$\omega = \omega_1 \pm \omega_3$

Ordinarily the new wave k, ℓ will not lie on any dispersion curve. That is

$$\left\{\frac{\omega^2}{N^2} - \frac{k^2}{k^2+\ell^2}\right\} = O(1) \qquad \text{(case A)}$$

We define this situation as "ordinary mutual interaction". Schematically, in the (,) plane

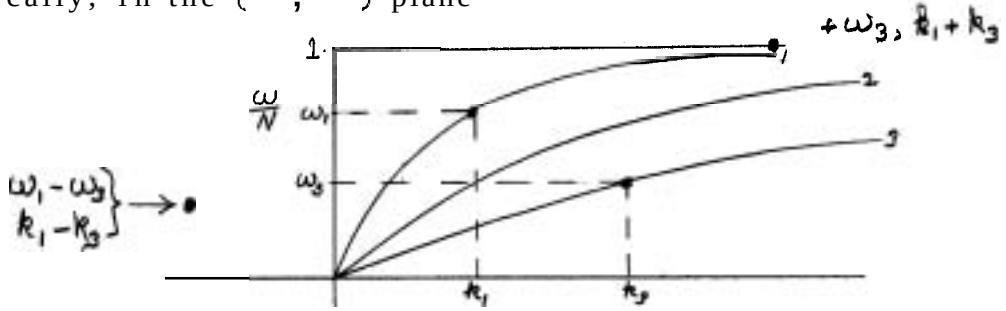

We can, however, by a careful choice of (, , ,) and (, ,), construct a case where the wave ω , k , ℓ does lie on a dispersion curve. That is

$$\left\{\frac{\omega^2}{N^2} - \frac{k^2}{k^2+\ell^2}\right\} = 0. \qquad \text{(case C)}$$

We call this situation "resonant mutual interaction". Graphically: a resonance between a 1- and 3-wave producing a 2-wave as shown by the , .

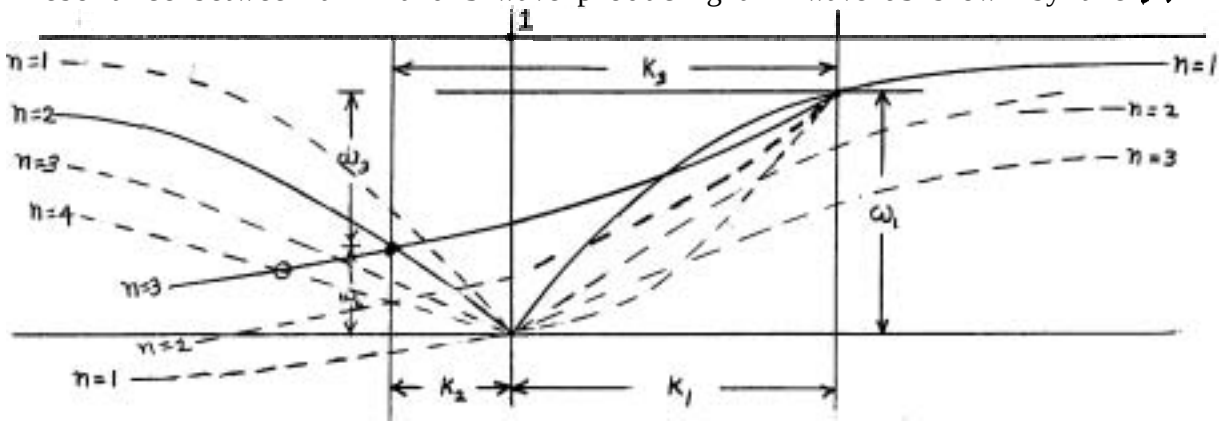

A second resonance with 1 and 3 producing a 4-wave is indicated at "0".

Note, the dispersion curve for the 3-wave has been shifted to the point (ω_1, k_1) to perform the superposition.

A third situation arises when the sum or difference wave lies very close to, but not exactly on, the proper dispersion curve. That is

$$\left\{\frac{\omega^2}{N^2} - \frac{k^2}{k^2+\ell^2}\right\} = O(\epsilon) \qquad \text{(case B)}$$

This is called "nearly resonant interaction".

The magnitude of the terms in (22) is shown for the three cases in tabular form. For case A:

	$O(1)$	$O(\epsilon)$			$O(\epsilon^2)$
	$\mathcal{L}(\psi^0)$	$\mathcal{L}(\psi')$	$\mathcal{J}(\psi^0)$	$\eta(\psi^0,\psi^0)$	
$\psi = \frac{a_1\omega_1}{k_1}\cos\chi_1\sin\theta_1$	0	N.T.	$O(1)$	N.T.	
$+\frac{a_3\omega_3}{k_3}\cos\chi_3\sin\theta_3$	0	N.T.	$O(1)$	N.T.	
$+\epsilon\frac{\beta\omega}{k}\cos\chi\sin\theta$	N.T.	$O(1)$	N.T.	$O(1)$	

where N.T. means no term is present. Here, no terms can balance slow variations at $O(\epsilon)$, so the 1 and 3 waves have fixed parameters, and order ϵ "harmonics" are present at $k, \pm k_3, \ell_1 \pm \ell_3, \omega_1 \pm \omega_3$, with amplitudes given by balancing $\mathcal{L}(\psi')$ against $\eta(\psi^0,\psi^0)$.

For case B the table looks like

0	N.T.	$O(1)$	$O(1)$
0	N.T.	$O(1)$	$O(1)$
N.T.	$O(\epsilon)$	N.T.	$O(1)$.

In order to achieve a balance of $\mathcal{L}(\psi')$ against $\eta(\psi^0,\psi^0)$ for this case we must have

$$\beta \sim (O(\epsilon))^{-1}.$$

But this violates the scaling by requiring that the "harmonic" waves be order 1, If we rescale case B according to this plan we obtain case B. Here, slow variations in the 1- and 3-waves are required to balance terms arising from η, and the $O(\epsilon)$ term arising from the almost tuned $\mathcal{L}(\psi_2^0)$ wave contributes, together with the slowly varying term, to balance

case B (re-scaled)	0	N.T.	O(1)	O(1)
	0	N.T.	O(1)	O(1)
	O(∈)	N.T.	O(1)	O(1)

$\eta(\Psi_1^*, \Psi_2^*)$, and for case C we obtain the table

	0	N.T.	0.1	0.1
	0	N.T.	0.1	0.1
	0	N.T.	0.1	0.1

which indicates the familiar balance of slowly varying terms against nonlinear terms for a perfectly tuned resonant triad.

References

Martin, S., W.Simmons and C.Wunsch 1972 The excitation of resonant triads by single internal waves, J.Fluid Mech. 53: 17.

Martin, S., W.Simmons and C.Wunsch 1969 Resonant internal wave interactions. Nature 224: 1014.

McEwan, P.B. 1971 Resonant degeneration of standing internal gravity waves. J.Fluid Mech, 50: 431,

McGoldreich, L.F. 1970 J.Fluid Mech.

Phillips, O.M. 1966 The dynamics of the upper ocean, Cambridge University Press.

Notes submitted by
Leonard W. Schwartz

THE EFFECTS OF STRATIFICATION ON ROTATING CRITICAL FLOW

Melvin E. Stern

Let us first review some notions about vorticity in homogeneous fluids. Consider a closed curve C encompassing an area A which moves with the fluid, Then the strength of the bundle of vortex lines enclosed by C is constant, This is the theorem of conservation of absolute vorticity $\xi = \nabla \times \underset{\sim}{v}$ expressed mathematically by

$$\frac{d}{dt}\iint_A \underset{\sim}{\xi} \cdot d\underset{\sim}{A} = 0$$

in an inertial frame of reference, Transforming to a system of coordinates rotating with angular velocity $\underset{\sim}{\Omega}$ the absolute vorticity in

the above theorem must be written as $\xi + 2\Omega$, where ξ is now the vorticity relative to the rotating frame, and 2Ω is the so-called planetary vorticity imparted to each fluid particle by the rotation. Consider now a system of coordinates in which $\Omega = \Omega \hat{k}$ and denote the vertical components of planetary vorticity by $f = 2\Omega$ and of relative vorticity by $\xi = \nabla \times \vec{v} \cdot \hat{k}$.

Consider two-dimensional horizontal flows in a horizontal constricted channel (Fig.1) so that relative vorticity has no non-zero component but in the vertical. Then a vertical column of fluid (vortex tube) of cross-sectional area δA remains vertical as it passes through the channel, and the conservation of vorticity implies that

$$(f + \xi)\, \delta A = \text{constant on a streamline along the channel}$$

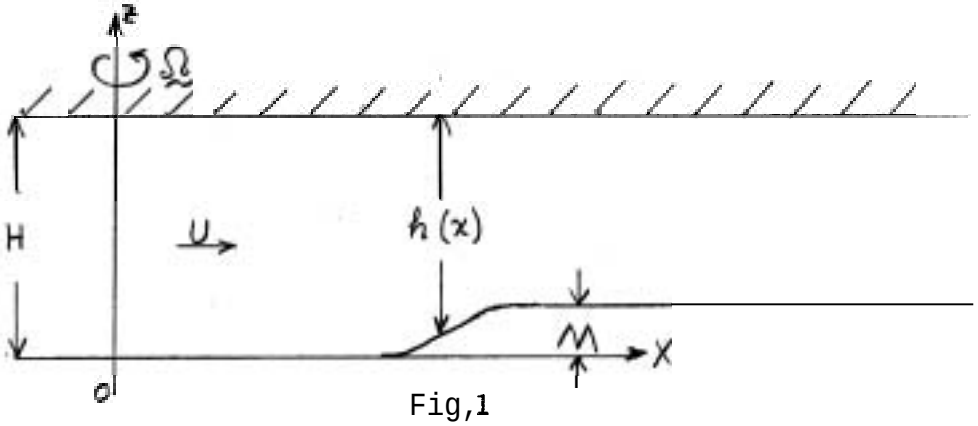

Fig,1

Continuity demands also that

$$h\, \delta A = \text{constant on a streamline}$$

where h = h(x) is the height of the channel. These two laws inply that

$$\frac{f + \xi}{h} = \text{constant on a streamline}$$

This quantity is the potential vorticity, and this property, the conservation of potential vorticity, is a quite general property of bounded homogeneous rotating flows,

In the flow under consideration, the relative vorticity is zero upstream of the depth variation, and du/dy downstream; where u(y) is the distribution, downstream of the obstacle, of velocity across

the channel, Then from the conservation of potential vorticity we have that

$$\frac{f + \frac{du}{dy}}{H - M} = \frac{f}{H}$$

i.e.,

$$\frac{du}{dy} = \frac{fM}{H}$$

Integrating across the channel, we obtain

$$u(y) = \frac{UH}{H-M} + \frac{fM}{H} y$$

The constant of integration is deduced from the continuity of mass, i.e., that the flow integrated over a channel cross section downstream must be the same as that over an upstream section,

The pressure distribution can be obtained from integrating the inviscid Euler equation:

$$\frac{d\underset{\sim}{u}}{dt} + f\hat{K} \times \underset{\sim}{u} = -\frac{1}{\rho}\nabla p$$

The velocity field as shown above is given by

$$\underset{\sim}{u} = (U, 0, 0) \quad \text{upstream,}$$
$$= (u(y), 0, 0) \quad \text{downstream,}$$

so that the substantial derivative of the velocity field vanishes in both cases, Integration yields

$$P - P_{uw} = -\rho f U (y + \tfrac{1}{2}L) \quad \text{upstream,}$$

$$P - P_{dw} = -\frac{\rho f U H}{H-M}(y - \tfrac{1}{2}L) - \tfrac{1}{2}\frac{\rho f^2 M}{H}(y + \tfrac{1}{2}L)^2 \quad \text{downstream,}$$

where P_{uw}, P_{dw} are the pressures on the wall $y = -\frac{1}{2}L$ up- and downstream, respectively.

The step in bottom topography causes a horizontal shearing of current downstream of the step. The sense of the shearing is determined by the direction sf rotation (the sign of f): the flow increases from right to left (looking downstream], The slowest flow is along the right wall $(y = -\frac{1}{2}L)$

$$u(-\tfrac{1}{2}L) = \frac{UH}{H-M} - \frac{fML}{2H}$$

and it is possible that this flow can stagnate or reverse on the right

wall, in which case the simple analysis presented here would break down. (See reference to Phillips (1963) at end of these notes,) The necessary condition for such a critical flow is then

$$\frac{UH}{H-M} - \frac{fML}{2H} \leq 0$$

We introduce the Rossby number

$$R_o = \frac{U}{fL} = \frac{\text{inertial (nonlinear] terms}}{\text{rotational terms}}$$

considered small in the present flow, Then an approximate condition for criticality is the following inequality for the aspect ratio of the step

$$2R_o \leq \frac{M}{H} \leq 1 - 2R_o$$

This aspect ratio is considered to be small and nearer to the lower edge of the range,

Define the ratio of the differences between the central ($y = 0$) and wall ($y = -\frac{1}{2} L$) pressures downstream and upstream:

$$\gamma = \frac{P_d(y=0) - P_{dw}}{P_u(y=0) - P_{uw}}$$

In the case of marginal criticality

$$\frac{UH}{H-M} = \frac{fML}{2H}$$

or, approximately,

$$\frac{M}{H} = 2R_o$$

this ratio becomes in the limit $R_o \longrightarrow 0$ (or equivalently, $M/H \rightarrow 0$

$$\gamma = \frac{1}{2}$$

for homogeneous flows.

Consider now the corresponding situation in a stratified flow whose density field is given by

$$\rho = \bar{\rho}(z) + \rho_0 \rho'(x, y, z)$$

where $\bar{\rho}(z)$ is a basic linear stratification, ρ_0 a reference density, say $\rho_0 = \bar{\rho}(0)$, and ρ' are the deviations (non-dimensional) from the basic stratification, The <u>static stability</u> is defined by

$$S = -\frac{1}{\rho_0}\frac{d\bar{\rho}}{dz}$$

Consider the same channel as before with a topographic step, except that we now take the channel height to be infinite in order to forestall complications due to such things as reflection of internal waves at the upper boundary. A uniform flow U is supposed to exist upstream of the step as before. The Boussinesq approximation is used throughout the following analysis.

Now suppose the slope of the bottom variation is so small that sufficiently far downstream no lee waves will be observed nor will waves be reflected upstream, so that the motion can be considered steady. Suppose also that the deviations (u,v,w) from the upstream flow U, induced by the bottom variation, are everywhere small. Then the equations of motion can be linearized about the basic flow U:

$$U\frac{\partial u}{\partial x} - fv = -\frac{1}{\rho_0}\frac{\partial p}{\partial x}$$
$$U\frac{\partial v}{\partial x} + fu = -\frac{1}{\rho_0}\frac{\partial p}{\partial y}$$

The omitted terms are of higher order. From these equations we can obtain the alternative set

$$\left(f^2 + U^2\frac{\partial^2}{\partial x^2}\right)u = -\rho_0^{-1}\left(U\frac{\partial^2 p}{\partial x^2} + f\frac{\partial p}{\partial y}\right)$$
$$\left(f^2 + U^2\frac{\partial^2}{\partial x^2}\right)v = -\rho_0^{-1}\left(f\frac{\partial p}{\partial x} - U\frac{\partial^2 p}{\partial x \partial y}\right)$$

From the boundary condition

$$v = 0 \quad \text{on} \quad y = \pm\tfrac{1}{2}L$$

the second of these equations, integrated along the wall implies that

$$fp - U\frac{\partial p}{\partial y} = C_\pm \quad \text{on} \quad y = \pm\tfrac{1}{2}L.$$

These conditions are satisfied by a pressure of the form

$$P_0 = C_+/f + \left(U/fL - \tfrac{1}{2}\right)(C_+ - C_-) - \left(\frac{C_+ - C_-}{fL}\right)y$$

but such a pressure has no effect other than to induce a constant downstream flow additional to U.

Without loss of generality, then, we can set

$$C_+ = C_- = 0$$

so that the boundary conditions become

$$fp - U\frac{\partial p}{\partial y} = 0 \quad \text{on} \quad y = \pm \tfrac{1}{2}L .$$

The vertical pressure balance is hydrostatic:

$$\frac{1}{\rho_0}\frac{\partial p}{\partial z} = -g\rho'$$

Neglecting diffusive effects, the advection of perturbation density by the basic flow must be balanced by the vertical flux of buoyancy:

$$U\frac{\partial}{\partial x}(\rho' g) = w S g$$

Combining the last two equations, we obtain

$$w = -\frac{\partial}{\partial x}\left(\frac{U}{\rho_0 g S}\frac{\partial p}{\partial z}\right)$$

Applying the operator $(f^2 + U\partial^2/\partial x^2)$ to the continuity equation

$$\frac{\partial u}{\partial x} + \frac{\partial v}{\partial y} + \frac{\partial w}{\partial z} = 0,$$

and substituting from the equations above, we get

$$U\frac{\partial}{\partial x}\left\{\left(f^2 + U^2\frac{\partial^2}{\partial x^2}\right)\frac{\partial}{\partial z}\left(\frac{1}{gS}\frac{\partial p}{\partial z}\right) + \frac{\partial^2 p}{\partial x^2} + \frac{\partial^2 p}{\partial y^2}\right\} = 0$$

Since this equation is linear in p we can formally Fourier analyze with respect to x, so that the operator $U\partial/\partial x$ is replaced everywhere by ikU, k being a downstream wavenumber. Physically, this corresponds to analyzing the topography $M(x)$ into a (continuous) Fourier spectrum and calculating the pressure adjustment $p(y, z; k)$ for each component $M(k)e^{ikx}$. Clearly, for a general topography $M(x)$ there will be small scale effects (i.e., large wavenumber k) caused by the large k components of the topography, however, since the smoother $M(x)$ the more quickly its spectrum $M(k)$ falls off as $k \to \infty$, let us consider only topographies sufficiently smooth that large wavenumber effects can be neglected. That is, we consider wavenumbers for which $kL \ll 1$. Thus, the $\partial^2/\partial x^2$ operator may be neglected in comparison with the $\partial^2/\partial y^2$ operator, and the factor

$$\left(f^2 - U^2k^2\right) = f^2\left(1 - R_0^2(kL)^2\right), \quad R_0 = \frac{U}{fL}$$

may be approximated by f^2 for any Rossby number, $R_0 \leq 1$. Finally, the equation we shall consider is written

$$\frac{\partial}{\partial z}\frac{f^2}{gS}\frac{\partial p}{\partial z}+\frac{\partial^2 p}{\partial y^2}=0$$

We require a bottom boundary condition and a radiation condition as $z \longrightarrow \infty$. Since we consider small amplitude bottom variations, the bottom condition can be imposed at the mean level z = 0:

$$w(x,y,0)=U\frac{\partial M(x)}{\partial x}$$

Thinking in terms of Fourier components, we may write this as

$$w(y,0;k)=ikUM(k)$$

This condition must be expressed in terms of the pressure field. By combining the hydrostatic and density conservation equations

$$wSg=U\frac{\partial}{\partial x}(\rho' g)=-U\frac{\partial}{\partial x}\left(\frac{1}{\rho_0}\frac{\partial p}{\partial z}\right)$$
$$=-\frac{ikU}{\rho_0}\frac{\partial p}{\partial z}$$

Hence,

$$\frac{\partial p}{\partial z}=-\rho_0 g S M \quad \text{at } z=0.$$

Non-dimensionalize the equations and boundary conditions by:

$$y=L\left(y_1+\tfrac{1}{2}\right), \qquad z=\frac{fL}{\sqrt{gS}}z_1,$$
$$p(y,z)=\rho_0\sqrt{gS}\,MfL\,\phi(y_1,z_1),$$

so that the equations can be written as (dropping the subscripts 1 now):

$$\frac{\partial^2\phi}{\partial y^2}+\frac{\partial^2\phi}{\partial z^2}=0$$
$$\frac{\partial\phi}{\partial z}=-1 \quad (z=0)$$
$$\phi-R_0\frac{\partial\phi}{\partial y}=0 \quad (y=0,1)$$

A rough argument for the onset of critical flow is now given. The ratio γ of pressure differences introduced in the homogeneous case is given by

$$\gamma=\left[\phi\left(\tfrac{1}{2},0\right)-\phi(0,0)\right]\left(\frac{\rho_0\sqrt{gS}\,MfL}{\tfrac{1}{2}\rho_0 fUL}\right)$$
$$=2\left[\phi\left(\tfrac{1}{2},0\right)-\phi(0,0)\right]\left(\frac{\sqrt{gS}\,M}{U}\right)$$

In the quasi-geostrophic limit of small Rossby number, $R_o \to 0$, the sidewall boundary conditions become

$$\phi = 0 \quad (y = 0, 1).$$

The form of solution to be expected from the boundary conditions may be sketched schematically (Fig. 2). The situations correspond

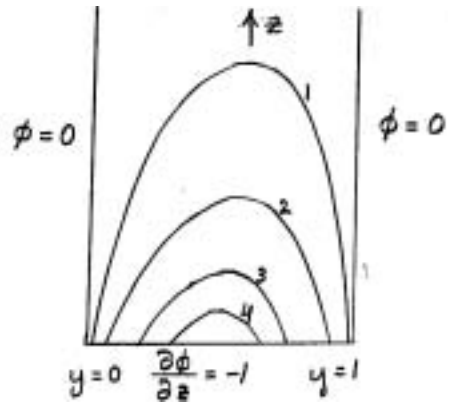

Fig, 2

Schematic of the solution for Ro = 0. Arbitrary units for ϕ.

to heating from below a body whose sides are held at a constant temperature,

The sidewall boundary conditions and the Laplaee equation suggest eigenfunctions of the form $e^{-n\pi z}\sin(n\pi y_1)$ (n is an integer), The necessary superpositions of these functions to satisfy the bottom boundary condition turns out to be

$$\phi = \sum_{n\ \mathrm{odd}} \frac{4}{(n\pi)^2} e^{-n\pi z} \sin(n\pi y).$$

From this we obtain:

$$2\left[\phi\left(\tfrac{1}{2}, 0\right) - \phi(0,0)\right] = \sum_{n\ \mathrm{odd}} \frac{8}{(n\pi)^2} \sin\left(\tfrac{1}{2}n\pi\right)$$

$$\doteq 0.5$$

Mence

$$\gamma \doteq 0.5\left(\frac{\sqrt{g}SM}{\nu}\right) \text{ for } R_o = 0$$

If the validity of this model may be stretched to $\sqrt{g}SM\nu^{-1} \doteq 1$, a value of γ corresponding to critical conditions in the homogeneous

case is obtained. In the corner $y = z = 0$ the perturbed velocity field

$$u \propto -\frac{\partial \phi}{\partial y}$$

has a singularity which we may consider associated with the critical flow.

A treatment for non-zero Rossby number (derived by Dr. Herbert Huppert after the lecture) may be given which resolves the ambiguities in the $R_0 = 0$ situation,

The sidewall boundary conditions

$$\phi - R_0 \frac{\partial \phi}{\partial y} = 0 \qquad (y = 0, 1)$$

suggest an expansion of the solution in the non-orthogonal set of functions

$$e^{-n\pi z}\left[\sin(n\pi y) + R_0 n\pi \cos(n\pi y)\right].$$

However, another type of solution with shorter length scales $[O(R_0)]$ is suggested:

$$\exp\left[\frac{1}{R_0}(y \pm iz)\right]$$

This solution corresponds to Kelvin waves* trapped along the right-hand wall, (Notice that the exponential decline can be in the negative y-direction only.) Because of the remarkable property of these waves that their group velocity is in the opposite z-sense from their phase velocity, the plus sign represents a wave radiating energy to infinity and the minus sign a wave radiating energy from infinity, The appropriate radiation condition eliminates the latter.

Consider then a solution of the form

$$\phi = \sum_{n\,\mathrm{odd}} \frac{A_n}{(n\pi)^2} e^{-n\pi z}\left[\sin(n\pi y) + R_0 n\pi \cos(n\pi y)\right] - iB R_0^2 e^{(y+iz)/R_0}$$

*Although the present model is steady ($\partial/\partial t = 0$) it is equivalent to the situation of an obstacle being towed with velocity $-U$ through a rotating channel filled with motionless fluid, in which ease the factor e^{ikx} implicit above is replaced by $e^{ik(x+Ut)}$. This is the sense in which, we mean "waves".

B, A_n are constants to be determined. For the time being, replace the bottom condition by the weaker condition:

$$\frac{\partial^2 \phi}{\partial y \partial z} = 0 \quad (z = 0)$$

The problem is now homogeneous and can be solved to within a constant factor. This condition demands that

$$\sum_{n\ odd} A_n \left[\cos(n\pi y) - R_o n\pi \sin(n\pi y)\right] - B e^{y/R_o} = 0$$

for $0 < y < 1$. This condition can be extended into the range $-1 < y < 0$ by substituting -y for y:

$$\sum_{n\ odd} A_n \left[\cos(n\pi y) + R_o n\pi \sin(n\pi y)\right] - B e^{-y/R_o} = 0$$

for $0 < y < 1$. Adding these, we obtain:

$$\sum_{n\ odd} A_n \cos(n\pi y) = B \cosh(y/R_o)$$

Hence,

$$A_n = B \int_{-1}^{1} \cos(n\pi y) \cosh(y/R_o)\, dy$$

Note that by differentiating the previous relation in the range $0 < y < 1$:

$$-\sum_{n\ odd} A_n R_o\, n\pi \sin(n\pi y) = B \sinh y/R_o ,$$

and adding, we recover the original condition:

$$\sum_{n\ odd} A_n \left[\cos(n\pi y) - R_o n\pi \sin(n\pi y)\right] = B e^{y/R_o}$$

We now use

$$\frac{\partial \phi}{\partial z} = -1 \ (y = z = 0)$$

to obtain the constant B:

$$-R_o\left(\sum_{n\ odd} A_n - B\right) = -B R_o\left(\sum_{n\ odd} \int_{-1}^{1} \cos(n\pi y) \cosh(y/R_o)\, dy - 1\right)$$

$$= -1$$

i.e.,

$$B = R_o^{-1}\left(2\sum_{n\ odd} \int_{0}^{1} \cos(n\pi y) \cosh(y/R_o)\, dy - 1\right)^{-1}$$

This determines B in terms of the Rossby number.

The minimum velocity U (possibly negative) occurs in the corner y = z = 0, and is proportional, in the geostrophic limit $R_o \to 0$, to $\partial\phi/\partial y$. So we must evaluate

$$\phi_y(0,0) = \sum_{n\ odd} \frac{A_n}{n\pi} - i B R_o$$

Straightforward integration shows that

$$\int_0^1 \cos(n\pi y)\cosh(y/R_0)\,dy = -\frac{R_0 \sinh(1/R_0)}{2(1+n^2+\pi^2 R_0^2)}$$

so that

$$(BR_0)^{-1} = -\left[1 + \sum_{n\,\text{odd}} \frac{R_0 \sinh(1/R_0)}{1+n^2+\pi^2 R_0^2}\right]$$

and

$$\sum_{n\,\text{odd}} \frac{A_n}{n\pi} = -2(BR_0) R_0 \sinh(1/R_0) \sum_{n\,\text{odd}} \frac{1}{n\pi R_0 (1+n^2+R_0^2)}$$

$$= \frac{2\sum_{n\,\text{odd}} \frac{1}{n\pi R_0 (1+n^2+\pi^2 R_0^2)}}{\sum_{n\,\text{odd}} \left(\frac{1}{1+n^2\pi^2 R_0^2}\right) + R_0 \sinh(1/R_0)}$$

The infinite sums can be replaced by integrals in the limit $R_0 \longrightarrow 0$ Consider as integration variable, $\theta = n\pi R_0$; then the differential $d\theta$ replaces the summation interval πR_0. Hence, in the limit $R_0 \longrightarrow 0$:

$$\phi_y(0,0) \cong \frac{2\int_{\pi R_0}^{\infty} \frac{d\theta}{\theta(1+\theta^2)} + \frac{1}{R_0 \sinh(1/R_0)}}{\int_{\pi R_0}^{\infty} \frac{d\theta}{1+\theta^2} + \frac{1}{R_0 \sinh(1/R_0)}}$$

Now

$$\int_{\pi R_0}^{\infty} \frac{d\theta}{1+\theta^2} = \frac{\pi}{2} - \tan^{-1}(\pi R_0) \cong \frac{\pi}{2},$$

$$\int_{\pi R_0}^{\infty} \frac{d\theta}{\theta(1+\theta^2)} = -\ln \frac{\pi R_0}{\sqrt{1+\pi^2 R_0^2}} \cong -\ln(\pi R_0).$$

Hence

$$\phi_y(0,0) \cong -\frac{4}{\pi} \ln(\pi R_0)$$

asymptotically as $R_0 \longrightarrow 0$, and there is a logarithmic sfngularity in the corner $y = z = 0$.

For small Rossby number, the geostrophic approximation holds, so that, in <u>dimensional</u> units:

$$-\frac{u}{v} = \frac{1}{\cdots} P_y = \frac{\sqrt{gSM}}{v} \phi_{y_1}(y_1, z_1)$$

Clearly, in the critical case of stagnation in the corner where this ratio must approach and exceed unity, the geostrophic assumption under which this formula was obtained is invalid. That is, however small the Rossby number, geostrophy is violated in the corner at onset of stagna-

tion because the perturbation velocity u is the same magnitude as the basic flow U. Nevertheless, we may regard the criterion for stagnation obtained by substituting for ϕ_y in the corner,

$$-\left(\frac{\sqrt{g S M}}{U}\right)\frac{4}{\pi}\ln(\pi R_0) = 1$$

as at least a necessary condition for critical flow in an homogeneous fluid.

Reference

Phillips, N. A. 1963 Rev.Geophys. 1: 123-172.

Notes submitted by
Roland A. deSzoeke

EXPERIMENTS IN STRATIFIED FLUIDS

Tony Maxworthy

We will concentrate on two main areas of research after discussing the parameters involved and types of experimental methods which have been used:

1) "flatness" effects: the tendency of stratified fluid flows to be one-dimensional,

2) wave phenomenon: in particular lee waves, solitary waves and shear layer instability.

See Lecture, p.14, for a discussion of internal waves.

I Non-dimensional parameters

A) Reynolds number

$$Re = Ud/\nu \sim \frac{\text{inertial forces}}{\text{viscous forces}}$$

B) Prandtl and Schmidt numbers

$$Pr, Sc = \nu/D \sim \frac{\text{heat or species diffusion time}}{\text{viscous diffusion time}}$$

These define within the fluid a variety of length scales. In wave and stability problems if $Sc >> 1$, then the length scale for viscous diffusion is much greater than that for species diffusion. This strongly affects the stability characteristics of shear flow.

C) Richardson's number: several different definitions are used depending on circumstances under discussion.

1) Layer Richardson number

$$Ri = \frac{-g}{\rho_0}\frac{\partial \rho}{\partial z}\frac{d^2}{\nu^2} \quad \text{(when } \frac{\partial}{\partial z} \text{ is well-defined and continuous)}$$

$$\sim \frac{\text{buoyancy forces}}{\text{inertial forces}} \quad \text{or} \quad \frac{(\text{buoyancy frequency})^2}{(\text{shear frequency})^2}$$

If Ri $>>$ 1 then the wave speed is much greater than the flow speed. Information is then transmitted upstream at essentially infinite speed, leading to flatness effects.

2) Layer Richardson number, when $\Delta\rho$ is well defined and ρ is constant on either side of layer.

$$Ri = \frac{-g}{\rho_0}\frac{\Delta\delta}{(\Delta v)^2}\Delta z$$

In the field this is the easiest to measure.

3) Gradient Richardson number: locally defined

$$J = \frac{-g}{\rho_0}\frac{\partial \rho}{\partial z}\frac{1}{(\partial U/\partial z)^2}$$

J occurs in stability analysis. A generally used criterion is that if J $\lesssim$ 1/4 then the flow will tend to be unstable to infinitesimal disturbances.

4) Flux Richardson number: useful for energy considerations:

$$R_f = Ri/P_r = \frac{-g}{\delta_0}\frac{\partial \delta}{\partial z}\left(\frac{\partial U}{\partial z}\right)^{-2}\left(\frac{K}{\nu}\right)$$

II How to do experiments

A) Equipment

1) Tanks

Generally with a free surface, Several methods used to produce the stratified density field:

a) Old method: put in several thin layers of progressively lighter fluid, using salt as the density variation-producing agent, Molecular diffusion will then smooth out the profile. The time scale involved is on the order of $d^2/D \sim 10^5$ seconds for one centimeter layers, and is too long for practical use to be made of this method.

b) External mixing,

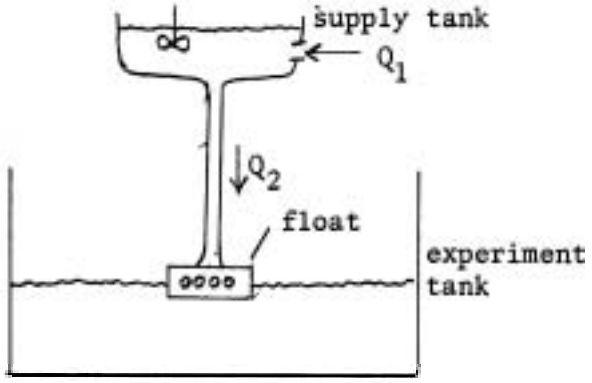

The fluid in the supply tank is initially at the maximum density desired, As fluid is fed to the experiment tank at rate Q via the feed float, the supply tank is continuously replenished at rate Q_2 by less dense fluid. The paddle ensures uniformity of the supply, If $Q_2 = Q_1$, then the resultant stratification will be exponential; if $Q_2 = 2Q_1$, then the resultant stratification will be linear.

c) Modern variation on a) (Internal mixing)

Put two thick layers into the tank, and tow an object through the interface, creating internal waves and turbulence. The associated turbulent eddy diffusivity is much greater than the molecular diffusivity, so the smoothing-out time scale is correspondingly decreased to a fairly reasonable value. With some practice, a nearly linear profile can be generated.

d) Heating is sometimes used, both for water and for air. There are serious problems with side wall convective effects,

2) Tunnels

a) Berkeley tunnel (air)

Open return, Used to study shear layers in stratified fluids. Problems with wall convection and also with flow stagnation and wave formation if operating parameters are not in correct range,

b) MIT tunnel (air)

Used to study smokestack plumes in stratified cross-flows. The twelve radiators are used to tailor the density field, while the twelve jet pumps can be used to tailor the velocity field.

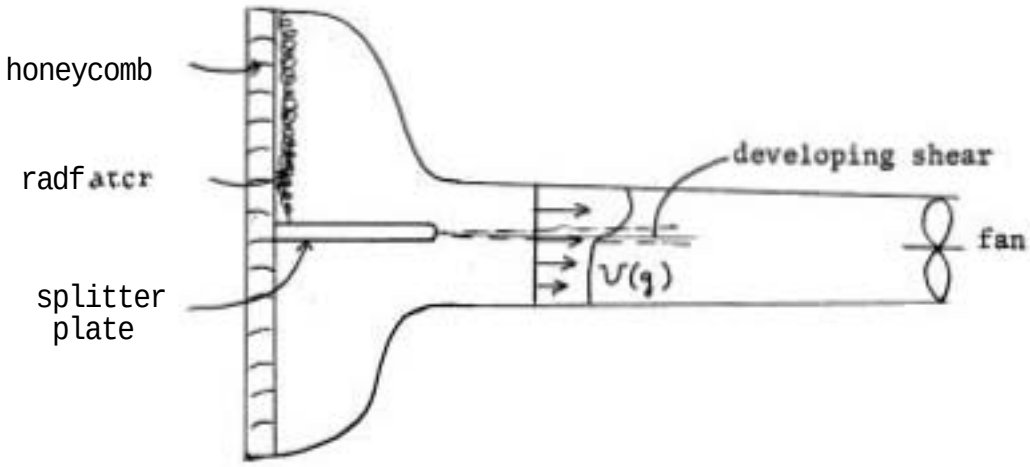

Berkeley tunnel

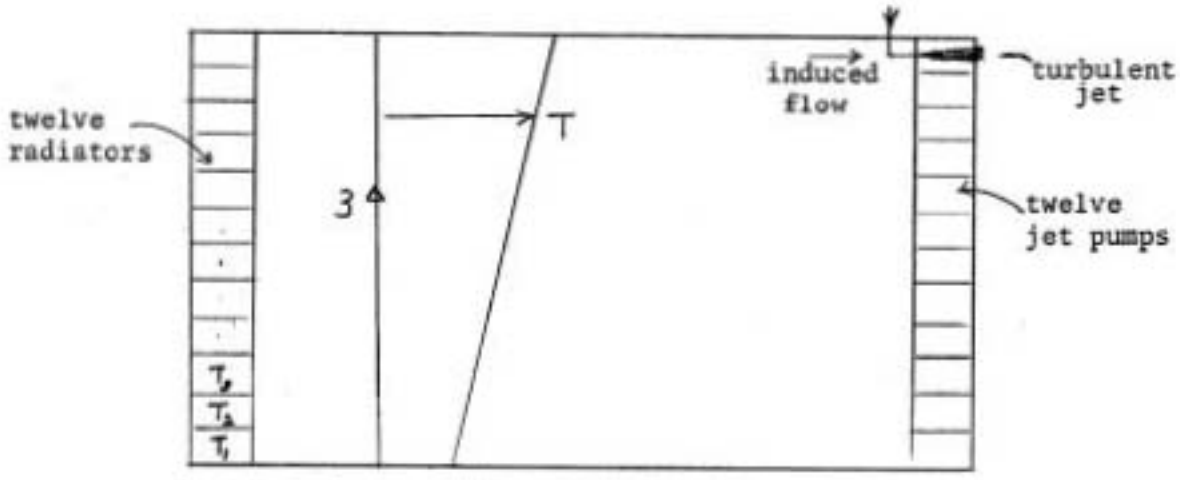

M.I.T. tunnel

c) USC tunnel (water)

Four brine layers are fed into the tunnel from four supply reservoirs, pass through the tunnel, mixing slightly, and are removed by four scoops at the tunnel end, and returned to the reservoirs. Due to the slight mixing, there is a slight drift in the supply densities, but runs of less than one hour this presents no difficulties,

A series of paddles just downstream of the inlets can be used to smooth out the density discontinuities.

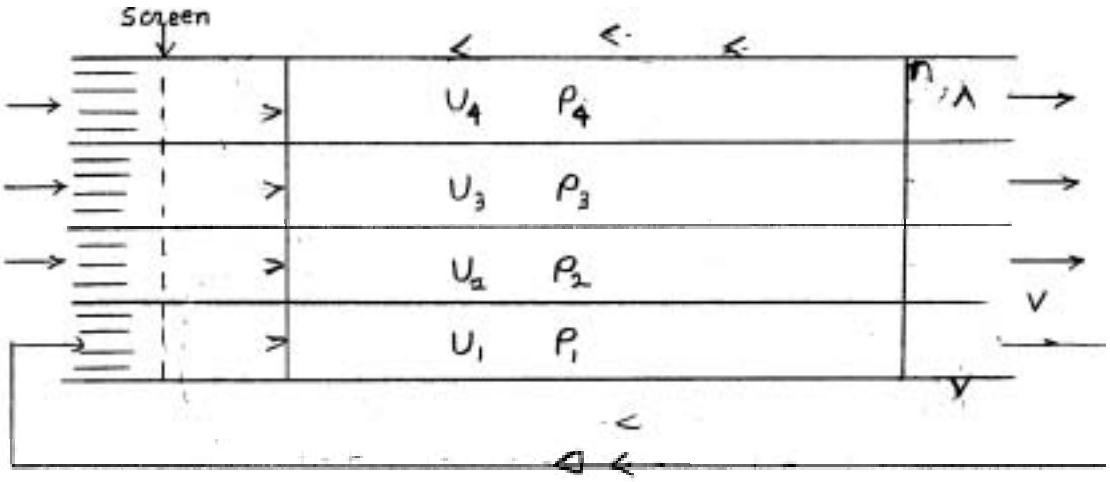

d) Johns Hopkins tunnel (water)

Closed loop tunnel using a novel pumping technique to pump a series of layers more or less independently

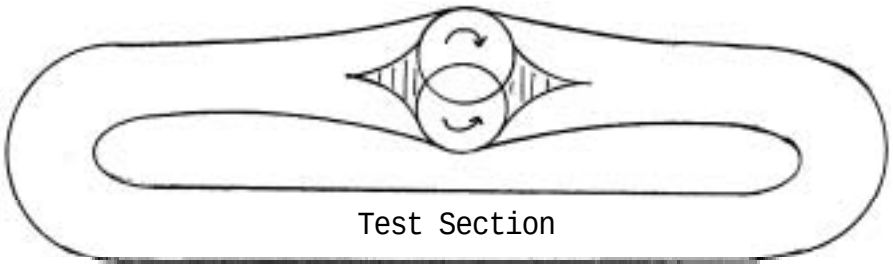

The overlapping circles represent two stacks of disks meshed together. The fluid is pumped by the viscous drag on the disks. The meshed area prevents backflow. At the present too much mixing occurs downstream of the disk stack.

B) Instrumentation

1) Dye: useful for marking layers, and showing streamline distortion. Can also be used for indicating velocity profiles - if a potassium permanganate crystal is dropped into the tank, it leaves a straight colored wake, which will distort in direct proportion to the velocity field.

2) Neutrally buoyant particles: density can be tailored to anywhere in the range 1.0 to 1.4 (gm/cm^3).

3) Hot-film probes: usually run at constant temperature. The current is proportional to ρu, so an independent measure of density is needed, Usually the Boussinesq approximation is made.

4) Conductivity probes: these make use of the fact that there is a direct one-to-one relationship between electrical conductivity and salt content (and therefore density). The probe has two electrodes: one a flat conductive plate, the other a small platinum bead on a wire:

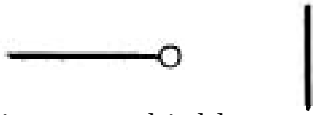

The electric field lines are highly concentrated at the bead, ensuring that most of the contribution to the measurement comes from the bead, and not the supporting structure,

5) PH method: (see Baker) this method is useful for low velocities [from 0 to 5 cm/sec). Two electrodes are placed in a solution of thymol blue near its end point. A D.C. voltage is applied to the electrodes. This induces a proton exchange reaction near the positive electrode that causes the solution to change its color from yellow to blue. In practice, the positive electrode is a fine wire (or a set of fine wires), while the other electrode is just a plate located in an unimportant region of the flow field. The voltage is pulsed, so that cylindrical marked regions of fluid are created at the wires and carried along by the fluid as Lagrangian markers,

III Specific problems

A) Flatness effects

1) Body flows: first examined by Long, who towed shallow bodies along the bottom of a tank, At high Richardson number he found a blocked region ahead of the body where the fluid moved at essentially the same velocity as the body. Above the blocked region, the velocity profiles exhibited a number of alternate jet-like flow regions.

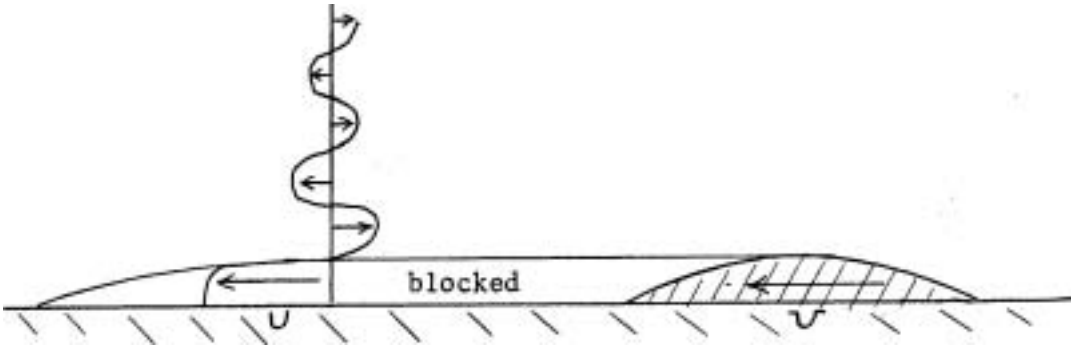

This kind of behavior is a general characteristic of flows in which the body force is transverse to the object velocity.

More recently, Browand and Winant have looked at the flow about a towed cylinder. The experimental conditions were:

$$Re \sim 50 \qquad 400 \leq Ri \leq 6000$$
$$(Re/Ri)^{1/4} \ll 1 \qquad Ri/Sc \ll 1$$

The experiments were run in a forty-foot channel eighteen inches deep. The cylinder was one inch diameter. The condition $Ri/Sc \ll 1$ means that the salt field does not have enough time to diffuse during the experiment. The condition $(Re/Ri)^{1/4} \ll 1$ means that the flow field can be considered to be inertialess. The flow field they observed looked like this:

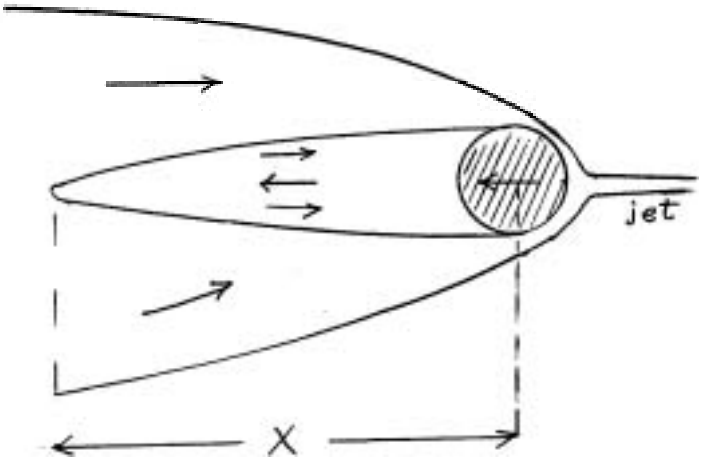

The velocity field was strongly perturbed far ahead of the blocked region, and there was recirculation inside it, Its length correlated well with existing theories, and was

$$x/d = (0.155)^4 \text{ ReRi}$$

Even in this long tank, the effects of the end wall were easily seen:

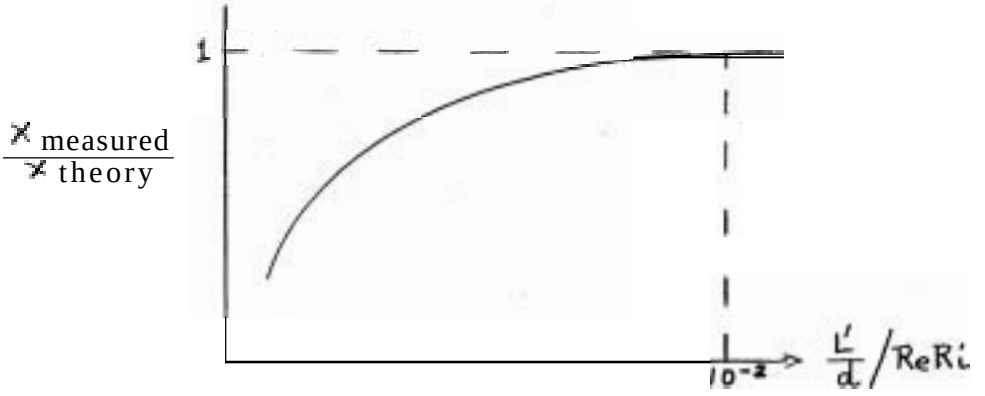

In the experiments ReRi ranged from 2×10^4 to 3×10^5 (L' is the distance from the cylinder to the end wall).

If the same experiment is run with a flat plate, a forward growing boundary layer is found:

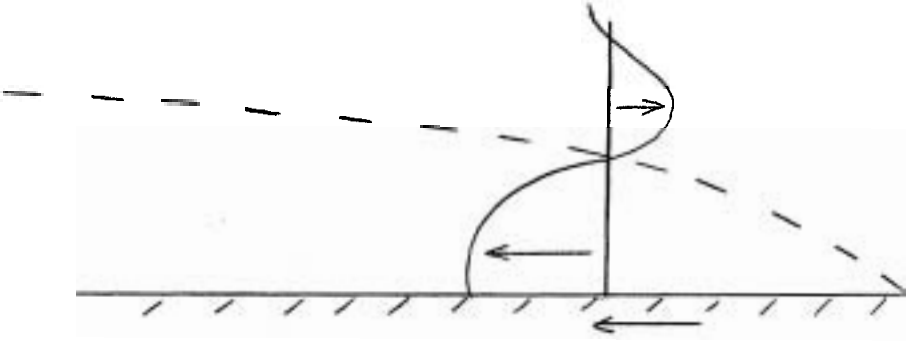

The blocking phenomenon can be predicted simply by taking inertialess limit ($Ri \to \infty$) and the inviscid limit ($ReRi \to \infty$) in the equations of notion, This leads to, for flow in the x-direction:

$$u, v, w \neq f(x)$$

23 Fluid source/sink problems

Injecting fluid of density (z_1) along a line z_1. For a constant volume flux, similarity theory predicts that the slug width is propor-

tional to $t^{1/6}$, and that the slug length is proportional to $t^{5/6}$. Maxworthy experimentally verified this. Again, strong velocity perturbations were found a considerable distance upstream of the slug.

The corresponding problem of withdrawal of fluid has also been examined,

3) Layering phenomenon

a) If a hemispherical blob of fluid at $z = z_1$ and $\rho = \rho(z_1)$ is released, it undergoes gravitational collapse. In the process it radiates gravitational waves - mostly corresponding to $(\omega/N \sim .8)$. The final configuration resembles the above slug configuration. Close examination of the slug shows small scale density striations.

b) If an object is oscillated vertically, it generates waves, which propagate at an angle which depends on ratio of the oscillation frequency to Brunt frequency. Mixing phenomena occur. The final state again shows density striations due to the mixing and subsequent spreading of blobs of constant density.

c) Closer examination of the thermocline region of the ocean over the recent years has revealed striations of many scales superimposed on the mean density profile. Layering of the mixed regions created by internal wave breaking, for example, is one explanation of this phenomenon.

B. Wave Phenomenon

1) Shear instability

a) case where $Sc >> 1$

For this case the viscous diffusion length is greater than the density diffusion length, leading to a distribution of the gradient Richardson number shown below (see Brownand and Wang for details), $J < \frac{1}{4}$ somewhere, so instability is to be expected. Initially linear waves of two types develop: classical Kelvin-Helmholtz type, and so-called Holmboe waves: separate waves in the top and bottom which interact through the interface. Next, in the nonlinear regime of K-H waves a regular series of vortices is observed, which grow, interact and

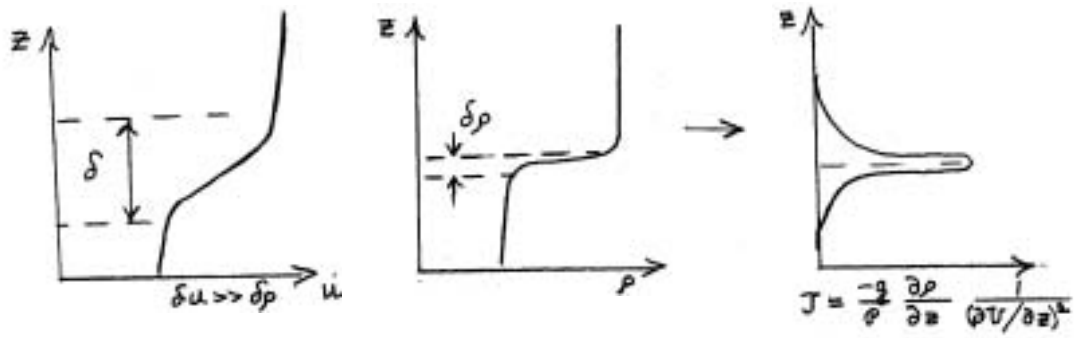

generate subharmonics. Eventually, this system collapses, generating internal waves and turbulence.

Finally, the system stabilizes, with new characteristic thicknesses:

$$\delta_\rho' \approx \delta_u' \gg \delta_u$$

If the system is allowed to continue to develop, eventually the entire process could repeat.

b) Case with Pr = O(1)

See Scotti and Corcos for details. They investigated statically stable stratified shear layers using the Berkeley wind tunnel described in earlier section. The minimum gradient Richardson number J could be adjusted over the range 0.07 to 0.76. They obtained, among other things, three values of growth rates of disturbances, for three values of minimum J. The extrapolation of this data showed that the growth rate disappeared for J_{min} = 0.22, which is in good agreement with the often quoted stability criterion of J = 0.25.

2) Lee waves

Long, in the references mentioned before, found that for a two-layer system with an obstacle height very much less than the undisturbed lower layer thickness, oscillations occurred downstream of the obstacle (provided that the flow was subcritical: layer Richardson number $(Ri > \pi^2)$. In the continuously stratified case, the same kind of patterns were observed, with the patterns becoming more complicated as the Richardson number was increased.

3) Solitary waves

Davis and Acrivos investigated the formation of solitary waves in a stratified, incompressible fluid. Their analysis is based on the inviscid equations of motion, assuming that the characteristic wavelength of the motion is very much greater than the characteristic thickness of the density variation. They made a numerical computation of some streamline patterns which compared well with those observed in their experiments, A simpler analytical calculation by Benjamin gave essentially the same results. For larger amplitude waves they observed a region of closed streamlines accompanying the wave and ultimately wave breaking, The former was also indicated by their numerical solutions, but the assumptions used in the formulation of the problem break down when the closed streamlines occur. Note that the disturbances in this problem decay exponentially away from the interface region,

References

Baker, J. 1966 J.F.M. 26: 573,

Benjamin, B, 1966 J.F.M. 25: 241.

Browand, F. and Y. Wang 1972 Int.Sym. on Stratified Flow, Novosibirsk.

Browand, F. and C. Winant (to be published) Geophysical Fluid Dynamics.

Davis, R. and A. Acrivos 1968 J.F.M. 29: 593

Long, R. 1954 Tellus 6: 297.

Long, R. 1955 Tellus 7: 341.

Scotti, R. and G. Corcos 1972 J.F.M. 52: 499.

Notes submitted by
Michael S. McCartney

DOUBLE -DIFFUSIVE CONVECTION

Herbert E. Huppert

I. The occurrence of double-diffusive convection

The occurrence of double-diffusive convection has the following minimum requirements:

1) the fluid must consist of two (or more) components: e.g., heat and salt in the ocean;

2) the components must have different diffusivities;

3) the opponents must make opposing contributions to the vertical density gradient.

II. Mechanisms

We will utilize the Boussinesq approximation:

$$\rho = \rho_0 (1 - \alpha T + \beta S)$$

which gives for the vertical gradient of density (note: z is vertically ypward):

$$\frac{1}{\rho_0} \frac{\partial \rho}{\partial z} = -\alpha \frac{\partial T}{\partial z} + \beta \frac{\partial S}{\partial z}$$

i.e., we can distinguish two cases fitting the requirements of I, and having statically stable ($\frac{\partial \rho}{\partial z} < 0$) density profiles:

case i $\left(-\alpha \frac{\partial T}{\partial z} < 0 \qquad \beta \frac{\partial S}{\partial z} > 0\right)$

such that $\frac{\partial \rho}{\partial z} < 0$

case ii $\left(-\alpha \frac{\partial T}{\partial z} > 0 \qquad \beta \frac{\partial S}{\partial z} > 0\right)$

Case (i) leads to a monotonic mode, while case (ii) leads to an oscillatory mode; for infinitesimal disturbances.

A. Monotonic mode

Case (i) corresponds to the case of hotter, saltier water over colder, fresher water (H, S/C, F). This might occur in the tropical oceans due to the effect of surface heating and evaporation, and the presence of antarctic bottom water.

Stommel et al. (1956) proposed the following thought experiment: Suppose that a long thin tube is lowered into the ocean, in such a way that the elevation of fluid elements is not altered. If the column of fluid is lifted slightly by applying a pressure difference to the upper end of the tube, then a given fluid element finds itself cooler than its neighbors outside the tube, as well as less salty. Heat is con-

ducted through the tube wall, and thermal equilibrium is reached. The tube wall is, however, impermeable to salt, so the element ends up lighter than its neighbors outside the tube, experiences an upwards buoyancy force, and accelerates upwards. The motion will now continue without the externally applied pressure difference, which is just necessary to "prime" the so-called salt pump.

The same mechanism works for elements lowered below their static equilibrium point: the element finds itself in a cooler environment, transfers heat to the surroundings, and ends up at the same temperature as, but with more salt than its surroundings. It feels a negative buoyancy force, and accelerates downward. The motion in this salt pump derives the kinetic energy from the potential energy stored in the unstable salt field. An attempt was made by Stommel, Magaard and Howard in 1970 to experimentally verify this in the ocean. A dynamic head of about 60 cm was attained. The result was, however, inconclusive, because of complications involving the flexibility of the tube and the sea swell.

In 1960, Stern noted that the physical tube was actually unnecessary: since $K_T >> K_S$, nature provides its own barrier to salt diffusion, differences, that is temperature differences are smoothed out much more rapidly than salt concentration differences.

Continuity leads us to expect alternate up and down moving columns. This configuration is called the salt-finger configuration:

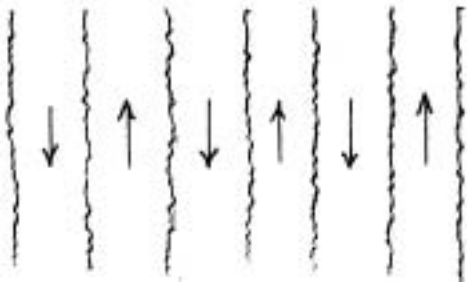

The salt-finger mechanism is most effective for rather thin columns: too thick, and the heat transfer is inhibited; too thin, and the motion is damped out by viscosity.

B. Oscillatory mode

Case (ii) corresponds to colder, fresher water over hotter, saltier water (C, F/H, S).

If, in the same mechanical configuration as the salt pump, a fluid element is lifted up in this density field, it finds itself hotter and saltier than its neighbors. After it gives up its heat, it therefore ends up heavier than its surroundings, and experiences a negative buoyancy force. If the suction is removed from the tube, the column will fall. Even if we ignore inertia, we can see that a given element will tend to overshoot its original level, since it is now colder and therefore denser than its original level. With inertia included, the element will overshoot even its new equilibrium level. It then finds itself in hotter saltier surroundings, is heated, and experiences an upwards buoyancy force, and rises. The same arguments about overshooting can be applied here. This leads to vertical oscillations of the column at a growing amplitude: the so-called "over-stable" mode. In the actual oscillatory process, the element is continuously transferring heat to and from the environment, so the cyclic average of buoyancy forces should be used. On the average over a cycle, the element experiences a net positive temperature induced buoyancy force, and a net negative salinity induced buoyancy force. Viscosity acts to damp any motion. When the temperature effect is greater than the salinity and viscosity effects, the over-stable mode can occur.

As before, the tube is unnecessary, due to the difference in diffusivities for heat and salt, The continuity equation leads us to expect the motion to be oppositely directed in adjacent columns, leading to an oscillating cell-like structure. The physical configuration is the same as the salt finger one above, but now the velocities in the "fingers" are periodic in time (and change direction).

III. The Rayleigh-Bénard problem

We consider two horizontal surfaces, infinite in extent, and separated by H. The upper is maintained at zero temperature and salinity, the lower at ΔT and ΔS.

A. Nondimentionalization, equilibrium state, and governing equations.

Scale lengths by H, times by $\frac{H^2}{K_T}$, velocities by $\frac{K_T}{H}$, and temperature and salinity by ΔT and ΔS.

The equilibrium state is

temperature = $\Delta T(1-z)$ salinity = $\Delta S(1-z)$

Substitution of the nondimensional variables into the two-dimensional linearized equations of motion gives:

$$\frac{1}{\sigma}\nabla^2\psi_t = -R_T T_x + R_S S_x + \nabla^4\psi$$
$$T_t + \psi_x = \nabla^2 T$$
$$S_t + \psi_x = \tau\nabla^2 S$$

The first equation represents the time rate of production of vorticity by horizontal gradients of temperature and salinity, and by viscous diffusion. The other two equations are the diffusion equations for salt and heat. In the equations, T and S represent the nondimensional deviations of the temperature and salinity fields from the equilibrium state. The following parameters appear

σ = Prandtl number = ν/K_T

$\tau = K_S/K_T$

R_T = thermal Rayleigh number = $\alpha g \Delta T H^3/K_T\nu$

$\sim \frac{\text{thermal buoyancy force}}{\text{viscous force}}$

R_S = solutal Rayleigh number = $\beta g \Delta S H^3/K_T\nu$

$\sim \frac{\text{saline buoyancy force}}{\text{viscous force}}$

This choice for R_S over the more obvious one: $\beta g \Delta S H^3/K_S\nu$ proves to be convenient,

The choice of boundary conditions is motivated primarily by mathematical simplicity, and not by a desire to model laboratory experiments, We consider the case of free-free boundaries,

no normal flux: $\psi = 0$ @ $z = 0, 1$

zero stress: $\psi = 0$ @ $z = 0, 1$

zerotemperature and salinity perturbation: $T = S = 0$ @ $z = 0, 1$

B. Normal mode solutions

We look for solutions of the form:

$$\psi = \exp(pt) \sin \pi a x \sin \pi z$$

the z dependence is πz not $m\pi z$ because we anticipate that the lowest order mode will be least damped by viscosity. The appropriate form for salinity and temperature is then: $T, S \propto \exp(pt) \cos \pi a x$ Note that the physical variables will be taken as the real parts of these expressions, since p can be complex: $p = p_r + ip_i$ · $p_r > 0$ corresponds to growth with time,

Substitution of the assumed solution form (see Veronis, 1965 and 1968) gives a third order algebraic equation for p:

$$p^3 + (\sigma + T + 1)K^2 p^2 + \left[(T + \sigma T + \sigma)K^4 - (R_T - R_S)\sigma \frac{\pi^2 a^2}{K^2}\right] p + \sigma T K^6 + (R_S - T R_T)\sigma \pi^2 a^2 = 0$$

where $K^2 = \pi^2(a^2 + 1)$

The equation has real coefficients, so therefore has either three real roots or one real root and two complex conjugate roots. The complex roots are associated with an overstable oscillatory instability for $p_r > 0$, with the stability margin given by $p_r = 0$, $p_i \neq 0$. The real roots are associated with a monotonic instability for $p_r > 0$, with the stability margin given either by $p_r = 0$, and $p_i = 0$ (the "exchange of stabilities" point), or by $p_i \longrightarrow 0$, and $p_r > 0$,

The most dangerous mode is $a^2 = \frac{1}{2}$ that is, the one which gives the minimum value of critical Rayleigh number, If we vary R_S and R_T while keeping all the other parameters fixed, then the stability properties of the problem can be represented by regions of a single diagram: (see p.49).

The diagonal line $R_T = R_S$ represents the static stability margin as defined by the usual ideas of lighter fluid over heavier fluid the region below this line would be statically stable, The line $p = 0$ has the equation

$$R_T = \frac{R_S}{T} + \frac{27\pi^4}{4}$$

The line $p_r = 0$ has a more complex equation, which can be written in

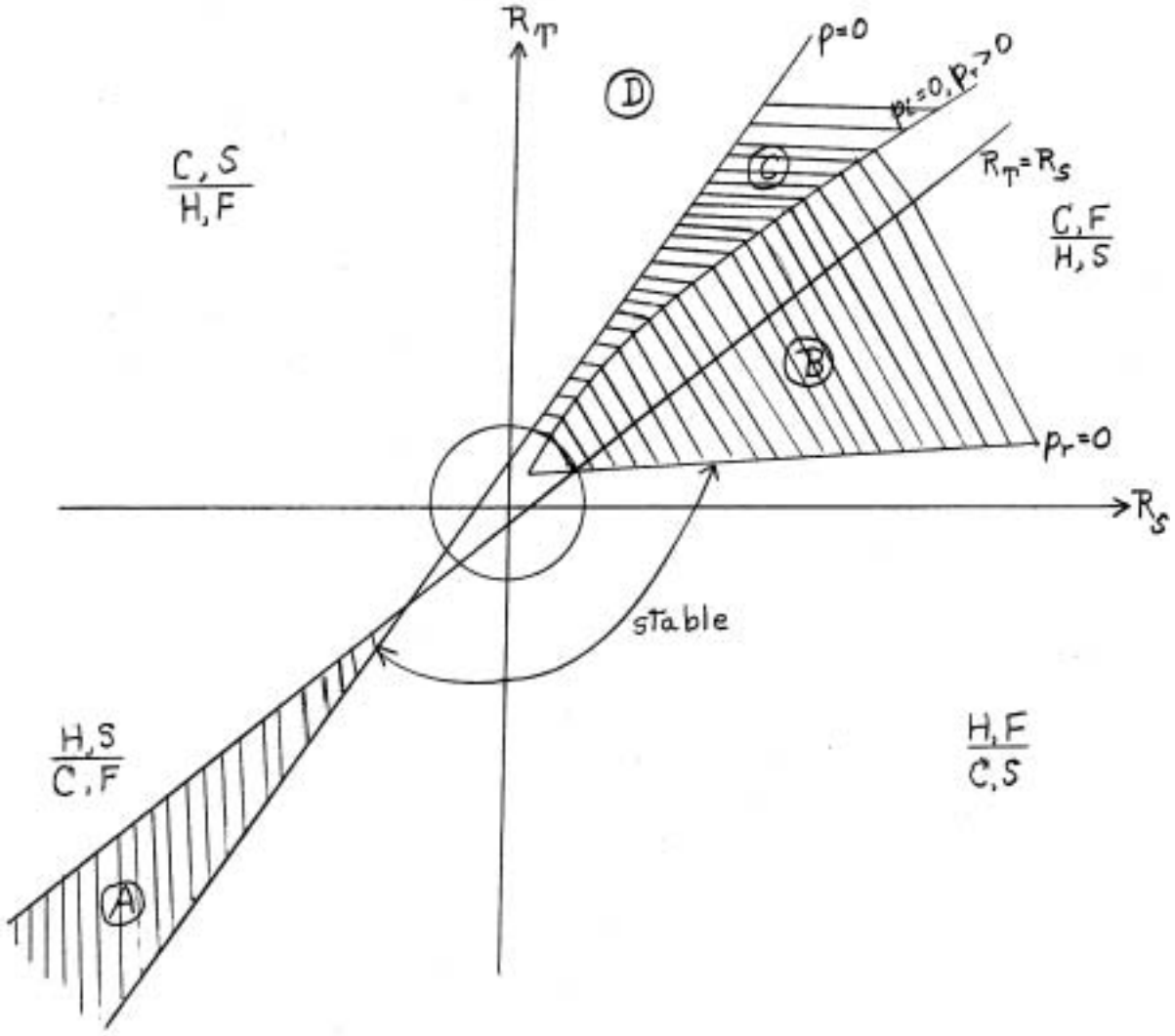

The region inside the circle where all the curves converge represents rather complicated behavior. However, the values of R_T are so low, that the region is of no practical interest.

the form:

$$R_T = \frac{\sigma+\tau}{\sigma+1} R_S + K$$

where K tends to $27\pi^4/4$ in the limit $\tau \to 0$ or $\sigma \to \infty$. The line $p_i = 0$ becomes parallel to the $R_T = R_S$ curve as R_S becomes large.

The region labeled A corresponds to the salt-finger type of instability (case i): monotonic, with $p_r > 0$ and $p_i = 0$:

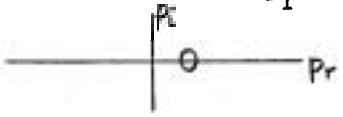

The region labeled B corresponds to the heat driven stability mechanism (case ii of section 1): oscillatory, with $p_r > 0$ and $p_i \neq 0$:

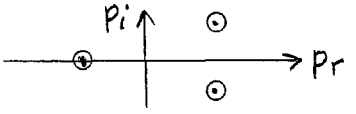

If we imagine running an experiment at fixed R_S and increasing R_T, we move upwards through the region B. The two complex roots move towards the p_r axis until they coalesce at the p_r axis: $p_i = 0$, The modes then change in character from the oscillatory pair of modes of region B to a pair of monotonic modes in region C:

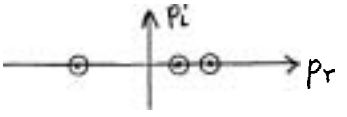

At still larger R_T, the third (previously damped) mode passes through the exchange of stabilities point ($p = 0$, and all three (monotonic) are then amplified, This corresponds to region D of the diagram.

C. Experimental verifications

The salt-finger phenomenon is easily set up in the laboratory, either with heat and salt as the components, or with two solutes, say salt and sugar. The occurrence of salt fingers in the ocean is suspected, but as of yet. has not been conclusively shown.

The oscillatory instabilities of region A have been detected by Shirtcliffe, who heated a tank from below, with a stabilizing salinity gradient, and recorded growing temperature oscillations with a thermocouple.

A more subtle way in which the oscillatory modes may appear follows: The heat flux J_T and the concentration flux J_C can be written in the general linear form:

$$J_T = -K_T \nabla T + \gamma \nabla C$$

$$J_C = -K_C \left[\nabla C + S_T C(1-C) \nabla T \right]$$

where the second terms represent temperature and salinity mutual interaction effects. S_T is called the Soret coefficient, while γ is propor-

tional to the Dufort coefficient, When there is a solid surface in a solution, then the requirement of $J_C = 0$ at the surface requires:

$$-S_T C(1-C) \left.\frac{dT}{dz}\right|_{\substack{\text{surface}\\ \text{applied}}} = K_C \left.\frac{\partial C}{\partial z}\right|_{\substack{\text{surface}\\ \text{involved}}}$$

Therefore, if we apply a temperature gradient to a tank containing initially homogeneous sale solution by heating from below, then a salt concentration gradient will be induced at the wall. Thus, where we might expect to find a simple monotomic mode (since we are heating a homogeneous fluid from below), we may get instead an oscillatory mode due to the induced salt gradient, if the sign of S_T is correct. At the present, little data is available concerning the magnitude and sign of S_T.

IV The nonlinear regime

A, Are sub-critical instabilities due to finite amplitude disturbances possible?

Veronis (1965, 1968) has done two calculations in regard to this. The first employed a two-term series solution, The results indicated that sub-critical instability was possible. In his later calculation, the number of terms sufficient for 1% accuracy were used. The results here indicated that sub-critical instability was not possible, However, values of τ fairly close to 1 were used, while very much smaller values of τ might lead to subcritical instability. More work in this area is needed to resolve this important question.

B. What happens when the motion is in the strongly nonlinear regime?

We first look at the classical case $R_S = 0$. For this problem the stability margin is given by $B_{t,cr} = 658$, The heat transfer can be represented by the Nusselt number: the ratio of the actual heat transfer (H) to the heat transfer that would occur by conduction alone:

$$Nu = H \Big/ \left[K_T \frac{\Delta H}{h}\right]$$

Numerical experiments have shown that for $(R_T/658) > 5$ and for free-free boundaries, the Nusselt number is proportional to the cube root of the thermal Rayleigh number, for Prandtl numbers greater than 1. This parti-

cular power dependence has been given many different interpretations. The simplest is the following: at large R_T, a blob of fluid moves along in a boundary layer and is heated, The blob breaks away from the surface and rises essentially as a thermal. After reaching the upper plate, it moves along the surface boundary layer and gives up its heat, then breaks away and falls as a thermal. In the continuous process nearly all the heat transfer is via the buoyant plume. Since the rise of a plume is only weakly affected by the downstream conditions (i.e. the upper boundary) we postulate that the heat transfer also is only weakly affected: that it becomes independent of the plate spacing h. Since $Nu \propto h$, and $R_T \propto h^3$, this then gives the cube root relation $Nu \propto R_T^{1/3}$.

This argument can be easily extended to the case $R_S \neq 0$, giving

$$Nu_T = f\left(\sigma, \tau, \frac{\beta \Delta S}{\alpha \Delta T}\right) R_T^{1/3}$$

A calculation using the mean field equations (discussed in a later seminar) gives for the case of infinite Prandtl number:

$$Nu_T = 0.224\left(1 - \left(\frac{\beta \Delta S}{\alpha \Delta T}\right)\tau^{1/2}\right)^{1/3} R_T^{1/3}$$

The same calculation gives for the solutal Rayleigh number:

$$Nu_S = \tau^{-1/2} Nu_T$$

Note that the limit $\sigma \to \infty$ is appropriate: for water $\sigma = 6.7$, and experiments (numerical and laboratory) indicate that there is no essential qualitative difference between the moderate σ and the $\sigma \to \infty$ cases.

Comparison of these relations with the highly accurate solutions of Veronis shows good agreement, indicating that in this case the mean field equations are a good approximation.

Note that these calculations correspond to points far above the diagonal in the first quadrant of the R_S - R_T plane.

V. Internal interfaces

With a homogeneous fluid, simple laboratory experiments are constrained to the rigid-rigid or rigid-free configurations. With the double diffusive case we can do more: we can stack up several layers and have internal interfaces. We now will examine the case of hotter

saltier water over colder fresher water. We will imagine that we start with discontinuous profiles of temperature and salinity:

and investigate the stages of formation of salt fingers,

A. Smoothing out of the discontinuities by molecular diffusion.

The conditions at t = 0 are:

$$\{T,S\} = \begin{cases} 0,0 & z<0 \\ \Delta T, \Delta S & z>0 \end{cases}$$

The solution to the diffusion equation is then:

$$\{T,S\} = \{\Delta T, \Delta S\} \, erfC\left[\frac{-z}{\sqrt{K_{T,S}\, t}}\right]$$

These solutions look something like this:

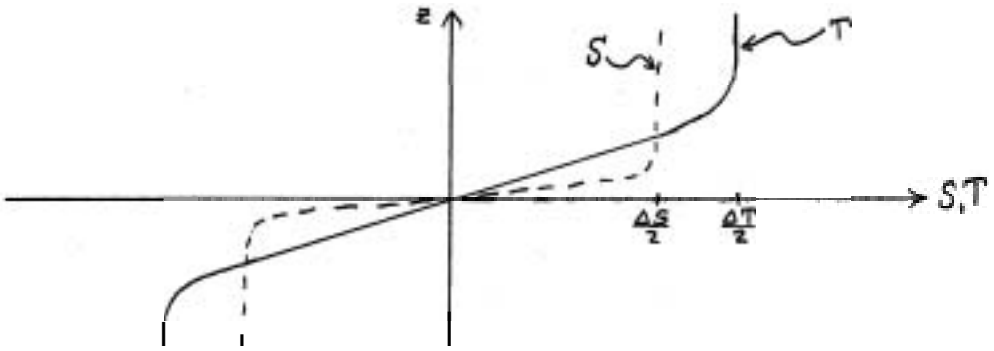

B. Development of infinitesimal instability

We use the previously developed model for horizontal zero stress surfaces, with linear T, S gradients. The stability margin was:

$$-R_T = \frac{1}{\tau} R_S - \frac{27\pi^4}{4}$$

Therefore, the criterion for occurrence of small wavey disturbances is:

$$\left|R_T\right| + \frac{27\pi^4}{4} < \frac{1}{\tau}\left|R_S\right|$$

where the two terms on the left-hand side represent the stabilizing effects of the temperature field and of viscosity, respectively, and the right-hand side represents the destabilizing effect of the salinity field. In most problems of interest to us:

$$R_T, R_S >> 27\pi^4/4$$

Therefore, we neglect the viscosity term, giving:

$$|R_T| < \frac{1}{\tau} |R_S|$$

In this problem the appropriate Rayleigh numbers would be based on the gradients of temperature and salinity, not their net differences. Thus this requirement becomes:

$$\beta \frac{dS}{dz} > \tau \alpha \frac{dT}{dz}$$

The minimum requirement comes from evaluating this at the origin:

$$\frac{\alpha \Delta T}{\beta \Delta S} < \frac{1}{\tau\sqrt{\tau}}$$

C. Development of the quasisteady salt finger configuration

Experimental observations show that the fingers from many long thin rectangular tubes in a quasi-steady condiguration. We therefore adopt the following steady fully-developed flow model:

$$u = 0 \qquad v = 0 \qquad \frac{\partial}{\partial t} = 0$$

The horizontal momentum and the continuity equation then give:

$$p = p(z) \qquad w = w(x, y)$$

The z-momentum equation then gives

$$\frac{1}{\rho_0} \frac{dp}{dz} = (-\alpha T + \beta S) g + \nu \nabla^2 w(x, y)$$

Differentiating once with respect to z gives:

$$\frac{1}{\rho_0} \frac{d^2 p}{dz^2} = \left(-\alpha \frac{\partial T}{\partial z} + \beta \frac{\partial S}{\partial z}\right) g$$

But the left-hand side is at most a function of z:f(z), therefore, a single integration gives:

$$-\alpha T + \beta S = f(z) + h(x, y)$$

We now assume that this relation can be extended:

$$-\alpha T = f_T(z) + h_T(x, y)$$
$$+\beta S = f_S(z) + h_S(x, y)$$

The conservation equations can be written:

$$w \frac{d}{dz}(f_{T,S}) = K_{T,S}\left[\frac{d^2}{dz^2} f_{T,S} + \nabla_1^2 h_{T,S}\right]$$

Horizontally averaging these, using $\overline{w} = 0$ $\overline{\nabla_1^2} = 0$ then gives:

$$K_{T,S} \frac{d^2}{dz^2} f_{T,S} = 0$$

Therefore:

$$\frac{df_T}{dz} = \gamma_T \qquad \frac{df_S}{dz} = \gamma_S \qquad \gamma_T, \gamma_S \text{ constants}$$

The z-momentum equation splits into two equations: one involving functions of z, the other functions of x and y. The second of these is:

$$0 = (h_T + h_S)g + \nu \nabla_1^2 w$$

The conservation equations are:

$$w\gamma_T = K_T \nabla_1^2 h_T$$
$$w\gamma_S = K_S \nabla_1^2 h_S$$

We now look for solutions of the form:

$$\{w, h_T, h_S\} = \{W, H_T, H_S\} \cos mx \cos hy$$

This leads to

$$(m^2 + h^2)^2 = \frac{g}{\nu}\left(\frac{\gamma_T}{K_T} + \frac{\gamma_S}{K_S}\right)$$

Since the left side is greater than zero, we obtain:

$$\gamma_T > -\gamma_S/\tau$$

Therefore

$$\beta \frac{dS}{dz} > \tau\alpha \frac{dT}{dz}$$

This criterion for fully developed salt fingers is identical to that derived from the infinitesimal disturbance theory, This suggests that the initial infinitesimal disturbance field can lead to the final fully developed configuration, and then any finite amplitude, sub-critical disturbance field must lead to some other final configuration.

Huppert and Mannis carried out a series of experiments at Cambridge to attempt to verify this relation criterion, Experiments using NaCl and sugar and $MgSO_4$ and sugar gave excellent agreement with the theory; while that with NaCl and $MgSO_4$ gave only fair agreement, although in the second case the problem may have been complicated by the electrolytic properties of the solution.

References

Huppert, H. and P. Mannis 1973 (to be published in Deep-Sea Research).

Shirtcliffe, T.S.C. 1967 Nature, 215: 409-490.

Stern, M.E. 1960 Tellus 12: 172-175.

Stommel, H., A.B.Arons and D. Blanchard 1956 Deep-sea Research 3: 152-153.

Veronis, G. 1965 J.Mar.Res. 25: 1-15.

Veronis, G. 1968 J.Fl.Mech. 34: 315-336.

Notes submitted by
Michael S. McCartney

COURSE LECTURES
by
Stewart Turner
University of Cambridge, England

MIXING IN STRATIFIED FLUIDS

Lecture #1. CLASSIFICATION OF MIXING MECHANISMS IN A STRATIFIED FLUID.

Introduction: These lectures discuss the physical mechanisms responsible for mixing in large bodies of stratified fluid: first by identifying the various processes, secondly by studying the smaller scale phenomena in isolation through both theory and results of laboratory experiments, thirdly be combining these isolated processes together into overall descriptions of the behavior of the fluid.

Stratified fluid: The equilibrium state of a heterogeneous fluid is defined by $p(x,y,z) = p_0(x,y) - g\int_0^z \rho(x,y,z)\,dz$

For a homogeneous fluid ρ = constant and this state is one of neutral equilibrium; no restoring force acts on an idealized displaced particle.

A fluid will be described as "stratified" if, in the equilibrium state, constant pressure surfaces correspond to constant density surfaces, i.e. the isopycnal surfaces are horizontal. A "stable" strati-

fication has light fluid overlying heavier fluid, Tilting of the interface (or isopycnal lines) is opposed by buoyancy forces and tends to generate oscillating vorticity. An "unstable" stratification has heavy fluid over light, and a tilting of the interface will be magnified and generate increasing vorticity.

The models of oceanic processes to be considered will be stably stratified in the mean throughout, Rotation effects will be considered only in the thermal wind relationship for a shear of the mean field

$$f \frac{\partial u}{\partial z} = \frac{g}{\rho} \frac{\partial \rho}{\partial y},$$

but will be neglected in considering the small length and short time scale mixing processes.

The vertical structure in general consists of a thin region where transient effects of local winds and heating occur, then a mixed region with weak stable gradients and small velocities such that it can be treated one-dimensionally, At 50 - 100 m is the seasonal thermocline; at 500 - 1000 m is the main thermocline whose structure can only be described by incorporating advection effects.

Parameters describing the state of the fluid: The first characterization of a stratified fluid must of course be the density gradient, which is coupled with gravity in the buoyancy force term, The parameter used is

$$N^2 = -\frac{g}{\rho} \frac{\partial \rho}{\partial z}$$

N is the buoyancy frequency (more cryptically known as the Brunt-Väisälä frequency) and is the natural oscillation frequency of a particle displaced in the density gradient. Typical values of N ($\frac{2\pi}{N}$ = period) are: seasonal thermocline 10^{-2} sec^{-1} (5 cycles/hr) or for the main thermocline 2×10^{-2} sec^{-1} (2 cycles/hr). For discrete density differences, the reduced gravity

$$g' = \frac{\Delta \rho}{\rho} g$$

is a parameter which frequently arises.

The shear $\frac{\partial u}{\partial z}$ also has the dimensions T^{-1}; thus a dimensionless local parameter, the gradient Richardson number

$$Ri = N^2 \left(\frac{\partial u}{\partial z}\right)^{-2} = -\left(\frac{g}{\rho}\frac{\partial \rho}{\partial z}\right)\left(\frac{\partial u}{\partial z}\right)^{-2}$$

can be formed. The overall Richardson number for a layer of thickness L, velocity difference U and density difference $\Delta\rho$ is $Ri_o = \frac{g'L}{U^2}$. The Richardson number relates the buoyancy [mixing inhibiting) to inertial forces (favoring mixing). It can also be viewed as the inverse square of an internal Froude number

overall $Fi = U/\sqrt{g'L}$ or

gradient $F_g = (\partial u/\partial z) N^{-1}$

For oceanic thermal wind flows with the isotherms sloping at an angle $\theta = \frac{\partial \rho}{\partial y}\left(\frac{\partial \rho}{\partial y}\right)^{-1}$

$N \sim 10^{-2} - 10^{-4}$ see^{-1} $\qquad f \sim 10^{-4}$ sec^{-1}

θ — 10^{-3} giving $u \sim 10$ cm/sec

$Ri = -f^2\left(\theta^2 \frac{g}{\rho}\frac{\partial \rho}{\partial z}\right)^{-1} = f^2/N^2\theta^2$

$Ri > 100$ for the mean motion above,

However detailed temperature gradient probe studies show large fluctuations even on mm scales (Gregg and Cox (1972) Deep-Sea Research) - the Ri is not at all uniform, and thus the large value of the mean Ri is not too important,

Classification of mixing processes: The observed microstructure suggests several questions

1) How are these irregular features formed?
2) What mechanisms cause mixing across the associated interfaces?
3) What is the source of energy for the mixing?

Although advection's role in the mixing process has not been considered extensively, it will spread layered structures horizontally and may be responsible for formation of layers by the spread sf intrusions of fluid or mixed fluid caused by internal waves breaking at boundaries.

However small scale ($< 1 - 10$ cm) structure diffuses much too rapidly to be advected over large horizontal distances.

External mixing phenomena occur when the energy source is an identifiable process which lies outside the region which is actually mixed. An oceanic example of external mechanical mixing is from wind stresses causing surface waves and turbulent mixing. Mixed, heated water will form a relatively isothermal layer whose thickness increases in time. Surface cooling, on the other hand, will cause external convective mixing; this is also important in the atmosphere since the lower boundary is heated.

Internal mixing, which occurs when the flow is both produced and used in the same region, can also be in mechanical or convective form. Double diffusive convection uses the potential energy of the unstably stratified component to form convectively unstable layers within an overall stable density gradient. These layers resemble strongly oceanic microstructure characterized by regular sharp steps in both temperature and salinity (c.f. Neal, Neskyba and Denner (1969) Science 166: 377; Stommel and Federov (1967) Tellus 19: 2; Pingree (1969) Deep Sea Research 16: 275.)

Internal mechanical mixing derives its energy from the local shear (for example Kelvin Helmholtz instabilities); frequently this shear can be increased by internal waves passing through the region, Woods (1968) J.F.M. 32: 791 and Met.Mag. 97: 65 has some excellent photographs of this process occurring in the ocean. Regularly spaced cloud billows may also show the presence of this kind of mixing aided by internal waves.

Convective problems can be studied by models of individual convection elements - plumes, threads, etc., while mechanical mixing is studied by considering shear flow processes.

The internal-external classification may not always be apparent: the flow of a heavy liquid down a slope under a lighter fluid may be either depending on the slope. A large slope produces mixing driven by the shear at the interface itself; at low slopes the mixing at the interface may be caused by turbulence induced by bottom stresses (external).

Notes submitted by
Glenn R. Flierl

Lecture #2. CONVECTION FROM ISOLATED SOURCES

Mechanisms sf convection will be discussed in terms of the behavior of isolated convection elements produced by small identifiable sources, Three types will be considered

plume thermal starting plume

1) the plume - produced by a continuous source of heat
2) the thermal - a rising blob of fluid
3) starting plume - the initial stages of a plume

Because of the turbulent nature of these elements even short distances above the source, similarity and dimensional arguments will be used extensively (cf. Batchelor (1954) Quart.J.Roy.Met.Soc. 80: 339; Turner (1969) Ann.Rev.Fluid Mech. 1: 29).

Plumes: The important quantities which characterize the plume are:

assumed known - the rate of heat supply

$F_o = 2\pi \int_0^\infty \omega g' r \, dr$ at source-dimensions $L^4 T^{-3}$

For a constant ρ environment $\rho 2\pi \int_0^m \omega g' r dr$ is independent of z by the conservation of heat equation,

z = height above the source

unknown: $b(z)$ radius of the plume

$\omega(z, r/b)$ vertical velocity

$g'(z, r/b) = \frac{\Delta\rho}{\rho} g$ densitydifference

A similar profile in r/b is assumed where r is the distance from the axis, Dimensional considerations give

$$b = \beta z$$

$$w = F_o^{1/3} z^{-1/3} f(r/b)$$

$$g' = F_o^{1/3} z^{-1/3} f_2(r/b)$$

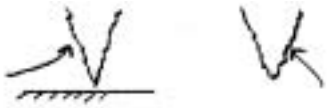

The flow outside the plume for an element on or far from a boundary has been estimated by G.I.Taylor by replacing the plume by a set of sinks of strength $z^{2/3}$ along the axis.

The inflow velocity of entrained fluid cap be calculated from the above forms of b and w and the continuity of mass to be

$$u_e \propto z^{-1/3} \text{ or } u_e \propto w.$$

This can be regarded as a fundamental characteristic of plumes for the purpose of studying their behavior in stratified environments. The resulting equations (the entrainment equations) are

Cons. of mass $\frac{d}{dz}\left(\pi b^2 \bar{w}\right) = 2\pi \alpha b \bar{w}$

Cons, of momentum $\frac{d}{dz}\left(\pi b^2 \bar{w}^2\right) = a b^2 g'$

Cons. of buoyancy $\frac{d}{dz}\left(\pi b^2 \bar{w} g'\right) = -\pi b^2 \bar{w} N^2(z)$

where α is the entrainment constant expressing the proportionality of inflow velocity to vertical velocities in the plume.

The pressure has been neglected (which is a valid assumption for small angles of spread),

$b^2 \bar{w} N^2(z)$ represents the change in the buoyancy flux due to the environment fluid being drawn in. The velocity and width are defined as integrals across the plume,

$$\pi b^2 \bar{w} = 2\pi \int_0^\infty w(r/b, z)\, r\, dr$$

$$\pi b^2 g' = \frac{2\pi \int_0^w \rho(r/b, z) r\, dr - \rho(\infty, z)}{\rho_1}$$

ρ_1 density at source

The boundary conditions are set by the mass, momentum and buoyancy fluxes at the source (z = 0). These equations are valid for a "top hat" profile ($w = \overline{w}$ constant across the plume and zero outside). The solution with $N^2 = 0$ is

$$b = \frac{6\alpha}{5} z$$

$$\overline{w} = \frac{5}{6\alpha}\left(\frac{9\alpha F_0}{10\pi}\right)^{1/3} z^{-1/3}$$

$$g' = \frac{5F_0}{6\alpha\pi}\left(\frac{9\alpha F_0}{10\pi}\right)^{-1/3} z^{-5/3}$$

The conservation equations above can be used for jets where both momentum and buoyancy are injected into the flow, The increased turbulence causes more rapid entrainment and widening of the jet,

Two-dimensional plumes can be treated similarly giving

$$w \propto A^{1/3}$$

$$g' \propto A^{2/3} z^{-1}$$

A: buoyancy flux/unit length

This line source model has been applied by G.I.Taylor to the "bubble breakwater" and can be used to model waste outflow problems,

Batchelor (1954) treats the case of a plume into an unstably stratified environment [or alternatively a plume which from chemical or other means changes buoyancy as it rises) by similarity methods for the case

$$\frac{g}{\rho_1}\left(\frac{\partial \rho}{\partial z}\right) = C z^p \qquad C > 0$$

giving

$$\overline{w} \propto C^{1/2} z^{(1+\frac{1}{2}p)}$$

$$b = 2\alpha\left(3 + \tfrac{1}{2}p\right)^{-1} z$$

$$g' \propto C z^{(1+p)}$$

The buoyancy flux $\overline{w} g' b^2$ is proportional to $z^{4+\frac{3}{2}p}$; thus for $p > -8/3$ the plume requires no heat flux at the source to initiate it.

The ease of a plume rising into a stably stratified environment can be treated by the entrainment equations. The parameters are assumed constant, and Fo at the source.

Non-dimensionalizing

$$z = .49\,\alpha^{-1/2} F_0^{1/4} N^{-3/4} z_1$$
$$\bar{\omega} = .69\,\alpha^{-1/2} F_0^{1/4} N^{1/4} \omega_1$$
$$b = .98\,\alpha^{1/2} F_0^{1/4} N^{-3/4} b_1$$
$$g' = .49\,\alpha^{-1/2} F_0^{1/4} N^{5/4} \Delta_1$$

with the definitions

mass flux $m_1 = b_1^2 \omega_1$

momentum $v_1 = b_1 \omega_1$

buoyancy $f_1 = m_1 \Delta_1$

The resulting equations are

$$\frac{dm_1}{dz_1} = v_1 \qquad \frac{df_1}{dz_1} = -m_1$$
$$\frac{dv_1^2}{dz_1} = f_1 m_1$$

and at $z = 0$

$$f_1 = 1, \quad v_1 = m_1 = 0$$

Solutions are given in Morton, Taylor, and Turner (1956) Proc.Roy.Soc. ~~A 234~~: 1; the height of the top of the plume is 2.8 x $.49\alpha^{-6/5} F_0^{1/4} N^{-3/4}$; experimentally this has been verified by Briggs (1969) for a range of heights from 1 to 10^4 ft.

Thermals: Thermals are individual blobs of rising fluid which grow in size as they entrain fluid from their surroundings, The appropriate similarity parameters are

$F_* = g \frac{\rho_a - \rho}{\rho} V$ the total buoyancy flux ($L^4\ T^{-2}$) and height z

$r_* = \alpha z$ a characteristic radius

$$\omega = F_*^{1/3} z^{-1} f(r/r_*)$$
$$g' = F_* z^{-3} f_2(r/r_*)$$

From the above it follows that

$$\frac{dz}{dt} = K z^{-1} \Rightarrow z^2 \propto t$$

or

$$\omega \propto t^{-1/2}$$

$$r_* \propto t^{1/2}$$

and

$$\omega = C (g' r_*)^{1/2}$$

experimental $C \sim 1.2$

From streak photographs, the internal velocity seems to behave like Hill's spherical vortex (Lamb section 165); a natural extension is to regard this as a special case of a buoyant vortex ring with both the eireulation and the buoyancy supplied by the source specified independently. For Hill's vortex the circulation around the core of the ring $\propto \omega r_*$; this result also holds for the buoyant expanding ring. Since ωr_* is independent of z, K_o is constant.

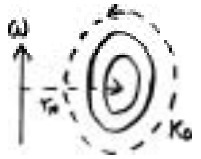

The momentum of the ring is $P = \rho \pi K_o r_*^2$ and $\frac{dP}{dt} = \pi \rho K_o \frac{dr_*^2}{dt} = \rho F_*$ which must arise from buoyant effects $\Rightarrow \pi \rho K_o$

$r_*^2 - r_{*o}^2 = \frac{F_* t}{\pi K_o}$ independent of the detailed motion of the core.

If a similarity assumption for the core is made so that the volume increases when the radius increases

$$\omega = C K_o / r_*$$

$$r_* = \alpha z$$ and since

$$2 r_* \frac{dr_*}{dt} = \frac{F_*}{\pi K_o} = 2 r_* \omega \frac{dr_*}{dz} = 2 r_* \omega \alpha = 2 C K_o \alpha$$

$$\alpha = \frac{F_*}{K_o^2 2 \pi C}$$

Thus unlike the plume, an initial impulse (causing large circulation Ko) will greatly decrease the angle of spread of the buoyant vortex ring.

For thermals and vortex rings in a stratified environment the height of rise is

and since

$$z_{max} = K \alpha^{-3/4} F_*^{1/4} N^{-1/2}$$

$$\alpha = K' F_* K_o^{-2}$$

$$z_{max} = K'' F_*^{-1/2} K_o^{3/2} N^{-1/2}$$

In contrast to the plume which rises higher for large initial buoyancy and low initial momentum (and thus low mixing) the thermal spreads more rapidly when given large buoyancy and low momentum or circulation and rises less high, (At very high initial momentum the plume height begins to increase as the momentum is increased], The rapid increase in maximum rise of a buoyant ring given initial circulation has been suggested as a method of forcing pollution high into the atmosphere, by using a "puffing" smokestack,

Starting plumes: As suggested by the appearance, the starting plume can be treated by stacking a thermal on top of a plume; however, since normal plumes and thermals rise as $\Omega \propto z^{-1/3}$, z^{-1} respectively, a thermal with increasing buoyancy and momentum (pumped through the bottom from the plume) must be used,

Notes submitted by
Glenn R. Flierl

Lecture #3. CONVECTION IN LAYERS

The object of this lecture is to look at the way in which buoyant element models have been used to understand thermal convection and to give a brief introduction to double-diffusive (thermohaline, thermosolutal) convection.

The classic problem of thermal convection is to determine the motion of a layer of fluid contained between horizontal planes, uniformly heated below and cooled above, The importance of the problem from a geophysical point of view is obvious, e.g., heat transfer from the earth's surface, convection patterns in thin layers of clouds, etc. Interest in the problem dates back to Bénard (1901) who showed that a thin layer of fluid becomes unstable when the temperature difference

exceeds a minimum value which depends strongly on the depth and less strongly on the properties of the fluid. The motion that first takes place is a regular steady pattern, but with larger depths and temperature differences it can become unsteady and even turbulent,

The Rayleigh number $R_a = \frac{g\alpha\Delta T d^3}{K\nu} = \frac{g' d^3}{K\nu}$

is the most important dimensionless parameter in describing the state of the fluid over the whole range of unstable conditions. The Rayleigh number can be regarded as a balance between the driving buoyancy forces and the two dfffusfve processes which retard the motion and have a stabilizing effect.

The linear stability theory for the Bénard problem was first formulated and solved for the ease of two free boundaries by Lord Rayleigh (1916). The remaining cases of two rigid boundaries and one rigid and one free boundary were first dealt with by Jeffreys (1926, 1928). Today, the state of knowledge of the linear theory is virtually complete and recent interest has concentrated on the nonlinear problems associated with convection at higher Rayleigh numbers, For comprehensive review of the linear theory see Chandrasekhar (1961).

To obtain information about the steady amplitude and preferred planform of the finite convective motions which are established above R_{a_c} (the critical Rayleigh number, below which the fluid is stable to small disturbances], one must take into account the advection of buoyancy and momentum by the flow field generated by the buoyancy, and therefore must use the nonlinear equations of motion. Malkus and Veronis (1958) showed that the nonlinear equations can be expanded as a sequence of linear equations whose solutions follow from those of the linear problem, Schlüter, Lortz and Busse (1965) extended the Malkus-Veronis expansion technique to investigate the stability of each of the possible steady finite amplitude solutions. They showed for both rigid and free boundaries that all three-dimensional cellular patterns in a fluid with fixed properties can be unstable to infinitesimal disturbances. There

is a range of parameters for which only two-dimensional rolls are stable and the boundary of this region was determined by Busse (1967), with the assumption of infinite P_r ,

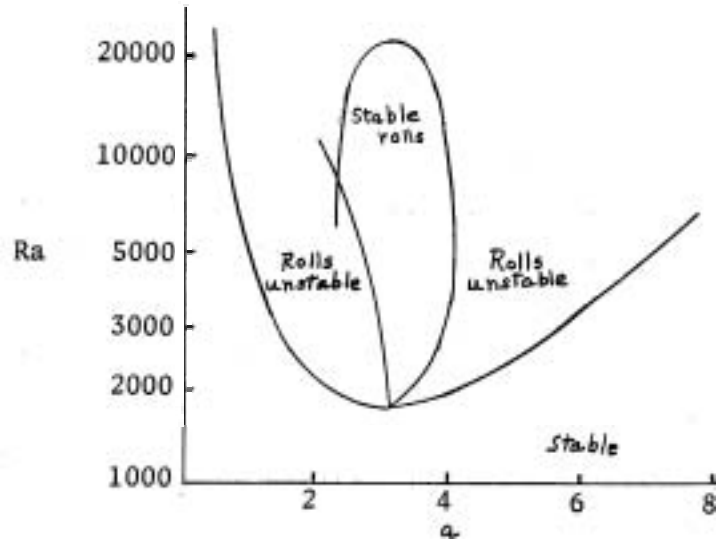

The application of these theories is limited to a small range of Rayleigh numbers near Ra_c. For higher Ra, numerical methods have been developed.

The first quantitative laboratory results were those of Schmidt and Milvertsn (1935) who verified the predicted value of the critical Rayleigh number。 For a history of this work and a general outline of the earlier (prior to 1959) numerical and experimental results see Chandrasekhar (1961), Koschmieder (1967) repeated Bénard's experiments using silicone oil, using various shapes for the convection chamber with free and solid top boundaries, and showed that the initial cellular pattern to form when the bottom is gradually heated uniformly is the two-dimensional roll。 The orientation of the roll depends on the side wall boundaries, For example, in a circular chamber they appear as a series of concentric annular rings, With a free top boundary, the rings break down into hexagonal cells, It seems likely now that variations of surface tension with temperature are an essential element in these and Bénard's original experiments with free surfaces, In experiments with two rigid boundaries, Krishnamurti (1968) has shown that roll cells aligned by the lateral boundaries occur at Ra just above

Ra_c when the mean temperature of the layer is fixed. Hexagons can be realized when the mean temperature of the layer is increasing steadily and the temperature profile is thus nonlinear.

Recently, heat flux experiments by Krishnamurti (1970) have shown that just above Ra_c the nondimensional heat flux expressed as $H = Nu \cdot Ra$ is a linear function of Ra, with slope $\sim$ 2.7 for water and slightly higher for fluids with larger Pr, At a second critical value Ra_{II}, there is a discrete change to higher slope, which was identified with a change in planform from two- to three-dimensional flow caused by finite amplitude instability. Further changes in slope in the heat flux curves at still higher Ra are associated with transitions to time-dependent flows of various kinds,

A feature of convection at high Rayleigh number, which has only recently become clear as experiments have been made in silicone oils of high viscosity and liquid metals, is the strong dependence on Prandtl

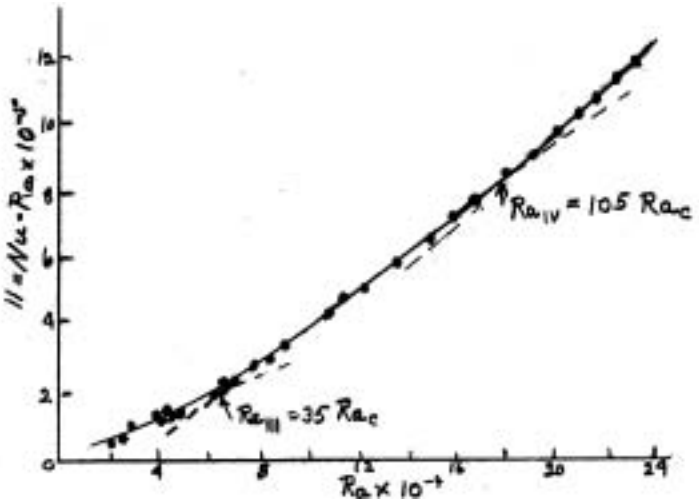

Heat flux H = Nu·Ra as a function of Rayleigh number, showing the 3rd and 4th transitions in a fluid with Pr = 100. (After Krishnamurti 1970).

number. When Pr is large, steady convection can persist to quite high Ra. The flux is then carried by large convection cells across which the velocity is gradually varying, but with temperature anomalies eon-centsated in narrow vertical regions at the cell boundaries which are fed by the boundary layers at the walls. As Re is increased (for a given finite Pr) the motion becomes time dependent; remarkably regular oscillations are first observed and these increase in number and frequency until finally the flow becomes disordered and turbulent. The various regimes observed are shown in the following figure as a function of Re and Pr.

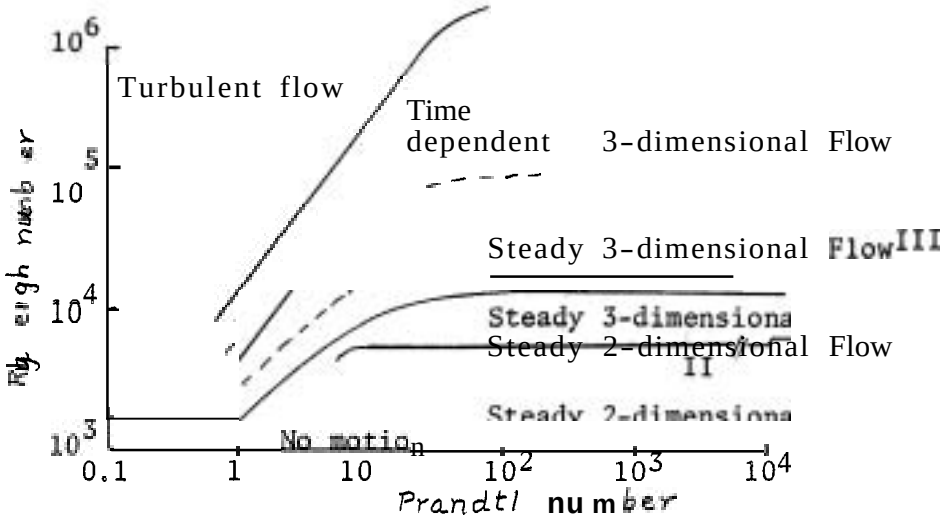

T rbul Convection

In a previous lecture, we discussed the assumption that the heat flux does not depend on plate separation but only on the character of the thermal boundary layers, For this to be true, it is necessary that Nu be independent of d, the plate separation. From this it follows that Nu varies as $Ra^{1/3}$ while H varies as $(\Delta T)^{4/3}$.

The mechanism of the heat transfer was the object of Townsend's (1959) investigation. What he observed was that the flux from the heated boundary was intermittent rather than steady. Buoyant fluid slowly accumulates and then breaks away, either as a thermal, or as an unsteady plume. The following simple model due to Howard (1964) deals with this directly.

Suppose a fluid of depth d is initially at rest and has constant temperature T = 0. At time t = 0 the upper and lower boundaries have temperatures $-\frac{1}{2}\Delta T$ and $+\frac{1}{2}\Delta T$ applied to them. The fluid then heats up by thermal conduction, producing error function profiles of the form

$$T = \tfrac{1}{2}\Delta T \operatorname{erfc}\left(\frac{z}{2\sqrt{\kappa t}}\right)$$

The thickness $\sqrt{\pi \kappa t}$ of the boundary layer increases, until at time t_* the Rayleigh number Ra_δ based on ΔT and $\delta = \sqrt{\pi \kappa t_*}$ reaches a critical value of order 10^3. At this time the buoyant fluid in the boundary layer suddenly breaks away as a discrete entity. With Pr of order unity or greater Howard has shown that this can happen in a time small compared with t_* (the model does not apply to low Pr, since conduction across the whole depth d will than be dominant). Time averages of the conduction profile over the interval $(0, t_*)$ give estimates of the mean temperature profile and heat flux which are equivalent to horizontal averages in the real flow. Howard's results, after averaging in this way, are

$$\bar{T} = \tfrac{1}{2}\Delta T\left(1+2\xi^2\right)\operatorname{erfc}\xi - 2\pi^{-1/2}\xi e^{-\xi^2}$$

$$Nu = d(\pi\kappa t_*)^{-1/2} = d/\delta = \left(Ra/Ra_\delta\right)^{1/3}$$

$$\xi = \tfrac{1}{2}z(\kappa t_*)^{-1/2} = \frac{\sqrt{\pi}}{2}\frac{z}{\delta}$$

If t_* is determined by putting $Re \approx 10^3$ then $Nu = 0.1\ Ra^{1/3}$, is reasonable agreement with experiment.

It is now of interest to examine the heat transfer through the environment by specifying the mechanism sf the transfer. Consider the following experiment. A turbulent plume of salt solution is supplied at the top of a tank of fresh water for a long time. Dye put into the flow at an early stage spreads out along the floor, and this marked fluid becomes part sf the environment, in which turbulence is quickly suppressed. A later marked patch of plume flufd passes through this slightly heavies Payer and as a result of mixing with it, becomes heavier still. The net result of this process is to produce a stably stratified environment.

Baines and Turner (1969) have based a detailed theoretical model on this picture, using the entrainment equations for plumes and two extra equations. The first of these is simply the continuity equation, while the second expresses the fact that the density of a particle in the non-turbulent environment remains constant, and that the only density changes at a fixed height occur because of the vertical motion.

Double-Diffusive Convection

Unlike convection in a single component system, a stratified salt solution heated from below does not overturn top to bottom, but rather overturns in layers starting at the bottom and this layered structure progresses upwards through the fluid. Across the interfaces there is a stable density jump due to the salinity distribution, while the more rapid diffusion of heat provides an unstable buoyancy flux which drives the convection. When heating is begun, the bottom layer passes the point of instability and a well-mixed layer develops. The top of this layer rises as fluid from above the layer is incorporated into it,

Experimentally it is observed that $\alpha \Delta T = -\beta \Delta S$, i.e. the steps in T and S are compensating to within experimental error and the net density structure is shown in the following figure. It has been assumed that the top of the mixed layer is marginally stable,

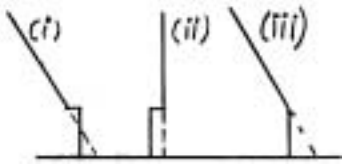

The distributions of (i) density due to salinity, (ii) density due to temperature, and (iii) the net density produced by heating a linear salt gradient from below.

In the opposite case to that described above, when a little hot salty water is poured on top of a stable temperature gradient, 'salt fingers' quickly form: ideally, the planform of the fingers is square, with the upward and downward motions alternating in a closely packed array. Practically, this means that each 'finger' tends to have four nearest neighbors.

If a layer sf lighter sugar solution (the more slowly diffusing component) is placed above a stable gradient of salt, the configuration again gives rise to 'fingers', since the substance of lower diffusivity is again unstably stratified, This setup is convenient for laboratory use since large gradients are easily obtained without any special precautions to prevent losses at the boundaries,

Laboratory experiments on the formation of layers by heating a salt gradient from below can be complicated by heating or cooling of the side walks, The formation and growth of layers in a two-component system is an unsteady process, which is related to the instability of the sidewall thermal boundary layer as it grows by conduction. When instability sets in, salt is lifted by the heated wall layer, but only to a level where the net density is close to that in the interior. Fluid then flows out away from the wall, producing a series of layers which form simultaneously at all levels and grow inwards from the boundaries.

Analogous effects can be obtained using two solutes instead of salt and heat, If opposing gradients are set up, the surfaces of constant concentration are horizontal and the no-flux boundary conditions are satisfied for both properties on vertical walls, At an inclined boundary, density anomalies are produced by diffusion which tend to drive the flow along the wall, The second component prevents this continuing indefinitely and fluid spreads into the interior as a series of layers.

Once layers and interfaces have formed in one of the ways described, the most important property is the flux of S and T across them, The overall behavior of a two-layer convecting system, with a hot salty layer on top sf a cold fresh layer is an example which can be treated by dimensional arguments, The flux sf the driving component F_T across a convecting layer sf depth d, and therefore through the bounding interfaces in a steady state, must be of the form

$$Nu = f\left(Ra, Rs, Pr, \tau\right)$$

where $Nu = \frac{F_T}{k\Delta T/d}$ $\quad Ra = \frac{g\alpha\Delta T d^3}{\nu K}$ $\quad Rs = \frac{g\beta\Delta S d^3}{\nu K}$

$Pr = \nu/K$, $\tau = K_s/K$. ΔT and ΔS are the differences between the center of one layer and the center of the next. In any experiment

$$\beta\Delta S/\alpha\Delta T = R_s/Ra$$

is given and Pr and τ are constants, and a plausible form for f which removes the dependence on d is

$$Nu = f_1\left(\frac{\beta\Delta S}{\alpha\Delta T}\right) Ra^{1/3}$$

This is equivalent to

$$\alpha F_T = A_1 (\alpha\Delta T)^{4/3}$$

where A_1 has dimensions of velocity. f_1 and A_1 can depend on molecular properties, but once the two components are specified, they should be functions only of the density ratio $R_\rho = \frac{\beta\Delta S}{\alpha\Delta T}$.

The deviations of A_1 from the value A obtained for solid boundaries with only a difference ΔT between them are a measure of the effect of an increasing ΔS on F_T. Measurements by Turner (1965) in the heat-salt system, which were compared with the 'solid plane' values in this way confirm that the ratio A_1/A can be expressed as a function of R_ρ alone, For $R_\rho < 2$, the heat flux is greater than it would be above a solid plane. This increase is due to two effects: the interface behaves more like a free surface, so that there is a weaker constraint on the horizontal motion, and it also supports waves which can break, so increasing the effective surface area, When $R_\rho > 2$ the heat flux falls progressively below the solid plane value as R_ρ is increased, reaching about one-tenth of that value when $R_\rho = 7$, Huppert (1971) has suggested that over the whole of the measured range, the empirical form

$$A_1/A = 3.8\,(\beta\Delta S/\alpha\Delta T)^{-2}$$

fits the observations to the experimental accuracy,

Similar arguments can be used to express the salt flux as a functisn of Ra and R_ρ , independent of d. It follows that the ratios of the fluxes, expressed in terms of their respective contributions to the density flux will be

$$\beta F_s / \alpha F_T = f_* \left(\frac{\beta \Delta S}{\alpha \Delta T} \right)$$

This flux ratio should be another systematic function of R_ρ, and this is again borne out experimentally by Turner (1965), as $R_\rho \rightarrow 1$, $\beta F_s / \alpha F_T \rightarrow 1$ also, suggesting that heat and salt are being transported by the samk turbulent motions at a breaking interface. As R_ρ increases to 2, the flux ratio falls rapidly, since molecular processes become important. For $R > 2$, the flux ratio remains constant to within experimental error, the mean value being $\beta F_s / \alpha F_T = 0.15$.

References

Baines, W.D. and J.S.Turner 1969 Turbulent buoyant convection from a a source in a confined region. J.Fluid Mech. 37: 51-80.

Bénard, H. 1901 Les tourbillons dars une nappe liquide transportant de la chaleur par convection en regime permanent. Ann.Chim.Phys. (7) 23: 62-144.

Busse, F.H. 1967 On the stability of two-dimensional convection in a layer heated from below. J.Math.& Phys. 46: 140-150.

Chandrasekhar, S. 1961 Hydrodynamic and Hydromagnetic Stability, Oxford, The Clarendon Press.

Howard, L.N. 1964 Convection at high Rayleigh number, Proc.Eleventh Int. Cong. of Applied Mech., Munich, Ed. H.Görtler,Berlin Springer-Verlag.

Huppert, H.E. 1971 On the stability of a series of double-diffusive layers. Deep-Sea Res. 18: 1005-1021.

Jeffreys, H. 1926 The stability of a layer of fluid heated from below. Phil.Mag. 2: 833-844.

Jeffreys, H. 1928 Some cases of instability in fluid motion. Proc.Roy.Soc. A-118: 195-208.

Kosehmieder, E.L. 1967 On convection under an air surface. J.Fluid Mech. 30: 9-15.

Krishnamurti, R. 1968 Finite amplitude convection with changing mean temperature. J.Fluid Mech. 33: 445-463,

Krishnamurti, R. 1970 On the transition to turbulent convection, J.Fluid Mech. 42:295-320.

Malkus, W.V.R. and G.Veronis 1958 Finite amplitude cellular convection. J.Fluid Mech. 4: 225-260.

Rayleigh,Lord 1916 On convection currents in a horizontal layer of fluid when the higher temperature is on the under side. Phil.Mag.(6) 32: 529-546.

Schlüter, A,, D. Lortz and F. Busse 1965 On the stability of steady finite amplitude convection. J.Fluid Mech, 23: 129-144.

Schmidt, R.J. and S.W.Milverton 1935 On the instability of a fluid when heated from below, Proc.Roy.Soc. A-152: 586-594,

Townsend, A.A. 1959 Temperature fluctuations over a heated horizontal surface. J.Fluid Mech. 4: 361-375.

Turner, J.S. 1965 The coupled turbulent transports of salt and heat across a sharp density interface, Int.J.Heat and Mass.Trans. 8: 759-767,

Turner, J.S. 1973 Buoyancy Effects in Fluids, Cambridge, The University Press,

Notes submitted by
Brian P. Hickie

Lecture #4 SHEAR INSTABILITIES AND TURBULENT GRAVITY CURRENTS

1. Inviscid models

a) Instabilities with different profiles

The two-dimensional, linear theory in case of a sharp interface between two deep uniform layers with different densities ρ_1 , ρ_2 and velocities u_1 , u_2 leads to the Kelvin-Helmholtz instability criterion for wavelike disturbances of wavenumber k:

$$(u_1 - u_2)^2 > \frac{g}{k}\,\frac{\rho_2 - \rho_1}{\rho_1 \rho_2}$$

For small density gradients this can be written as

$$\frac{(\Delta u)^2}{g'} > \frac{1}{\pi}$$

i.e. in the form of a critical internal Froude number based on the wavelength of the disturbance,

If nonlinear terms are taken into account, the development of an originally sinusoidal interface (curve (i) in Fig.1) into a spiral form (ii) due to the interaction of the various parts of the vortex sheet and the distortion of the wave form by the mean flow can be shoen (Fig.1).

More realistic are interfaces of finite thickness, Two of them are presented here (Drazin and Howard, 1966):

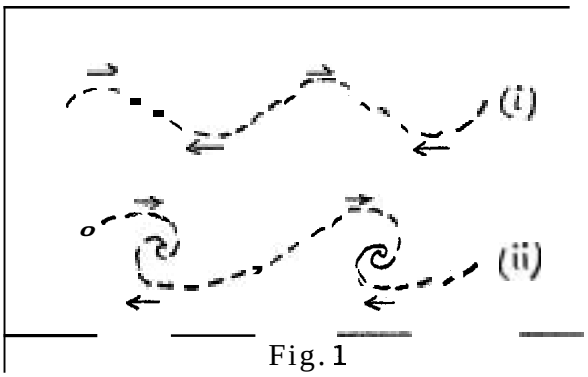

Fig. 1

(i) Layer of intermediate density and thickness h between twb deep uniform layers and with a linear velocity profile in this depth interval. An overall Richardson number can be defined as

$$Ri_o = g(\Delta\rho/\rho)h/(\Delta u)^2$$

Instability, in this case, develops only in a small zone. In contrast

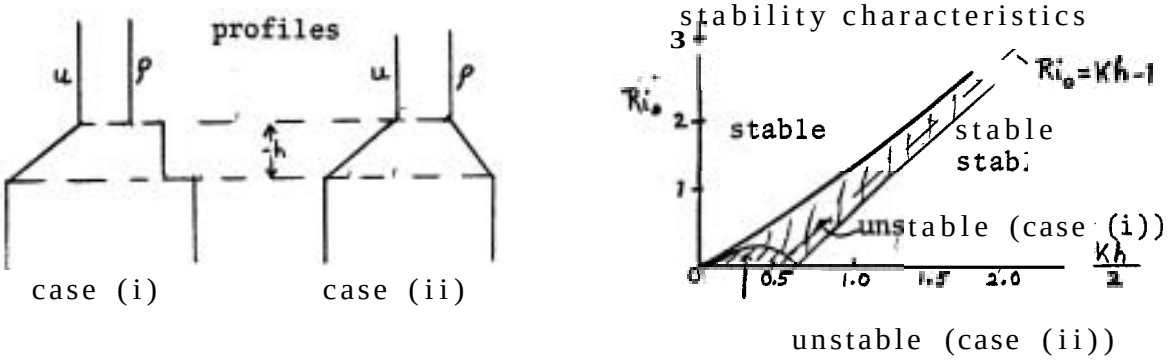

Fig. 2

to the K.H.-case the higher wavenumbers are again stabilized by the finite thickness of the interface (Fig.2).

(ii) Velocity shear as with (i) but linear density gradient.

At low Ri there is again a range of intermediate wavenumbers which are unstable. However, for Ri $\geq$ 1/4 small disturbances of all wavenumbers are stable to infinitesimal disturbances. The first wave to go unstable if Ri is reduced below 1/4 has a wavelength of

$$\lambda = 7.5\,h$$

Different other continuous profiles of u and ρ have been investigated with similar results as case (ii), i.e. with only slightly varying ranges of instability. It turned out that the sufficient condition for an inviscid continuously stratified flow to be stable to small disturbances is $Ri \geq 1/4$. This does, however, not necessarily mean that the flow has to become unstable for $Ri < 1/4$, counterexamples have been found,

b) Experimental results

Scotti and Corcos (1969) have undertaken measurements in a wind tunnel with a two-layer flow stratified by temperature where the lighter layer was flowing Easter than the heavier one. Small waves were generated at the centre of the interface by use of an oscillating wire. Growth and decay of these waves were in good agreement with the inviscid theory.

Thorpe (1969) used a rectangular tank with fresh water above salt water, If this tank was tilted rapidly through a small angle and left there, after a few seconds a regular array of waves suddenly appeared on the interface. The wavelengths and the velocity differences at which the waves occurred were in good agreement with the inviscid theory extended to an accelerated flow, One interesting result of Thorpe's later experiments was that the interfacial instabilitaes with an appearance like those in Fig.1 broke up after a short time to produee a thickened interface. The final mean density gradient seems to be almost linear through this interface with small scale steps superimposed.

Instabilities of the K.-H. type have been observed visually in the atmosphere on cloud patterns and in clear air by means of radar techniques, In the ocean they were observed by Woods (1968) rising dye tracing techniques,

(c) Effects of internal waves on shear instability

As shown by Phillips (1966) the current shear of an internal wave, the wavelength of which is large compared with the interface thickness, is within the interface

$$\frac{du}{dz} = -\left(\frac{N^2}{\omega^2} - 1\right)\omega k a$$

with ω = frequency, k = horizontal wavenumber, a = amplitude at the interface. For long waves $(N^2 >> \omega^2)$.

This means

$$\frac{du}{dz} = \frac{ka}{\omega} N^2$$

The gradient Richardson number then is

$$Ri = \frac{\omega^2}{N^2 k^2 a^2}$$

i.e. the minimum Ri is achieved for the maximum density gradient because of its linear relation to the current shear. [The most unstable interface is the sharpest one!)

The maximum rate of shear occurs at the crests and troughs of progressive waves and if inside the interface

$$Ri < 1/4 \quad \text{or} \quad Ka > 2\frac{\omega}{N}$$

the waves are potentially unstable, The length scales of the instabilities are those discussed in the previous section (Fig.2). The subsequent mixing reduces N so that the stability condition may be restored, even if the wave slope is maintained.

2, Viscosity and stratification

a) Plane flow

The stability of density interfaces like those treated in the previous chapters is well described by the inviscid theory except for very low Reynolds numbers when viscous damping will reduce the growth rate of disturbances.

Viscous theory has been applied to different velocity and density profiles where viscosity was expected to be of importance. The most important example is a parabolic velocity profile with a linear temperature (density) profile, investigated by Gage and Reid (1968). For positive Ri they found numerically the form of stability curves. According to their results the flow will be stable to small disturbances for $Ri > 0.0544$ for all Re, For smaller Ri the flow is stable provided Re is sufficiently small, and at large Re the instability is confined to a particular small wavenumber range,

b) Flow along sloping boundaries

At first the properties of a uniform layer of heavy viscous fluid flowing under lighter fluid are summarized: The integration of the viscous equations of motion through the depth of the lower layer leads to

$$u = \frac{g' \sin\theta}{2\nu}\left(zh - z^2\right) + u_i$$

with u_i = velocity at the interface (Fig.3).

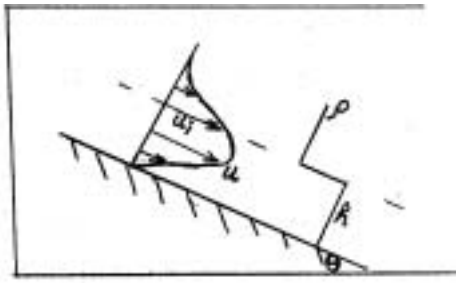

Fig.3

Introduction of the mean velocity5 of the layer leads to

$$\frac{u_i}{\bar{u}} = 2 - \frac{1}{6}\,\frac{g' \sin\theta \cdot h^2}{\bar{u}\,\nu} = 2 - \frac{H}{6}$$

where the dimensionless parameter H may be written as

$$H = Re \sin\theta / F^2 = Re \cdot Ri_o \tan\theta,$$

with

$$Re = \frac{\bar{u}h}{\nu}, \quad F = \frac{\bar{u}}{(g'h)^{1/2}}, \quad Ri_o = \frac{g'h\cos\theta}{\bar{u}^2}$$

Ippen and Harleman (1952) found experimentally H = 7.3 i.e., u_i = 0.79 u for the case of interest here,

The range of H in other cases may vary from 3 for a free surface flow to 12 for a fixed boundary at z = H. The important point is that H has a fixed value, i.e. only one of either Re or Ri is free in the experiment with the slope given,

Convenient parameters have to be chosen to describe the relative importance of buoyancy and viscosity in laminar flows along boundaries:

(1) if the length h scale is the basic property and velocity is produced by gravity then the Grashof number

$$Gr = \frac{g'h^3}{\nu^2} = \frac{Re^2}{F^2}$$

is appropriate, because $\bar{u}$ does not appear,

(ii) if the velocity is given then the Keulegan number

$$K = \frac{\bar{u}^3}{\nu g'} = Re \cdot F^2$$

should be chosen.

Few results on the stability of these flows are available up to now, The experiments of Ippen and Harleman suggest that the two-layer flow becomes unstable for $F = 1$, then the first wave-like disturbance with wavelengths $\lambda \approx 3h$ appear. This result was rather insensitive to slope. Another instructive experiment is the related case of a laminar boundary under a heated sloping plane in air, Tritton (1963) showed that the first instability appeared almost independent of the slope in a wide range of slope between 40° and 90° from the horizontal. The critical Grashof number corresponded to a local value of Re of about 250. However, the attainment of the fully turbulent flow is definitely retarded by the stabilizing effect of the density gradient across the flow as the plane is tilted towards the horizontal.

3. Turbulent flows along sloping boundaries

A turbulent flow along a sloping boundary is assumed to mix with a non-turbulent environment. There do exist various geophysical applications for this type of flow, Examples are turbidity currents in the ocean or the downflow of cold arctic water along the bottom under warmer water. (Attention in the latter case will have to be paid to the effect of rotation,)

The concept sf plumes which has already been discussed in previous Lectures, is also applicable here. In an inclined plume there is a component of gravity normal to the entraining edge so that the densfty gradient has a stabilizing effect,

An overall Ri number can again be defined:

$$Ri_\theta = \frac{g'h\cos\theta}{u^2} = \frac{A\cos\theta}{u^3}$$

where u = mean velocity downslope, h = depth, $A = g'hu$ is the buoyancy flux per unit width.

The entrainment parameter is no longer - as in case of vertical plumes - a constant but it can be a function $E(Ri_\theta)$, as Ellison and

Turner (1959) have pointed out, The mass continuity equation is

$$\frac{d(uh)}{dx} = E(Ri_0)u$$

If bottom friction is disregarded the momentum equation becomes

$$\frac{d(u^2h)}{dx} = g'h \sin\theta$$

From these two equations

$$E = Ri_0 \tan\theta$$

results, a strong dependence of the entrainment upon the slope,

The neglect of bottom friction in the above formulae seems justified, because the experiments of Ellison and Turner have shown that for moderately steep slopes the stress depends mostly on the entrainment at the outer edge. The mixing process can be regarded as an internal one which is effectively isolated from the boundary, The local velocity and buoyancy gradients across the edge of the plume are then given in terms of the imposed differences by

$$\frac{du}{dz} = K_1 \frac{g'}{\Delta u}; \quad N^2 = \frac{g}{\rho}\frac{d\rho}{dz} = K_2^2\left(\frac{g'}{\Delta u}\right)^2$$

In this outer region, the profiles are linear essentially because no external length scale is relevant. A detailed interpretatfon of Ellison and Turner'' experiments suggests that the Richardson number is

$$Ri = \frac{K_2^2}{K_1^2} \approx 0.06$$

i.e., turbulence can be maintained in a marginally stable state regulated by the mixing it produces,

References

Drazin, P.G. and L.N.Howard 1966 Hydrodynamic stability of parallel flow of inviscid fluid. Adv.Appl.Mech. 9: 1-89.

Ellison, T.H. and J.S.Turner 1955 Turbulent entrainment in stratified flows. J.Fluid Mech. 6: 423-448.

Gage, K.S. and W.H.Reid 1968 The stability of thermally stratified plane Poiseuille flow. J.Fluid Mech. 33: 21-32,

Ippen, A.T. and D.R.F.Harleman 1952 Steady-state characteristics of subsurface flow, Proc.NBS Symp.of Gravity Waves. Nat.Bur. Stand.Circ. 521: 79-93

Phillips, O.M. 1966 The Dynamics of the upper ocean. Cambridge Univ. Press.

Scotti, R.S. and G.M.Corcos 1969 Measurements on the growth of small disturbances in a stratified shear layer. Radio Science 6: 1309-1313.

Thorpe, S.A. 1971 Experiments on the instability of stratified shear flows. J.Fluid Mech., 46: 299-319.

Tritton, D.J. 1963 Transition to turbulence in the free convection boundary layers on an inclined heated plate. J.Fluid Mech. 16: 417-435.

Woods, J.D. 1968 Wave induced turbulence in the summer thermocline. J.Fluid Mech. 32: 791-800.

Notes submitted by
Friedrich A, Schott

Lecture #5. MECHANICAL MIXING ACROSS DENSITY INTERFACES

In this lecture, mechanical mixing across density interfaces will be considered, One example of this process, the mixing across the edge of a gravity current flowing down a slope, was considered in the previous lecture. In that case, the mixing was due to turbulence on one side of the interface. Lofquist (1960) did a number of experiments on this problem for the case of a nearby horizontal boundary. Other laboratory experiments will now be considered,

A convenient way to study one-dimensional mechanical mixing in a stably stratified fluid is to use a vertically oscillating grid of solid bars. Rouse and Dodu (1955) first applied this method in a two-layer experiment, and Cromwell (1960) stirred at the top of an initially stable density gradient. In the experiment of Rouse and Dodu, the interface was kept at a fixed height by adding and removing fluid from the layers, Cromwell began with the linear density gradient but too small a mesh size on his grid, resulting in strong viscous effects, which are not being considered here. In both cases however, a well-mixed layer was formed, bounded by a sharp interface which moves away from the stirrer (unless it is fixed as in the Rouse and Dodu experiment) as fluid is entrained across it from the quiescent fluid into the well-mixed layer, Thus the external stirring produces and main-

tains the well-mixed layer, and also sharpens the interfaces and causes the mixing across it. Photographs indicate that the entrainment is effected by wisps of the lower (quiescent) layer being lifted up by the upper layer eddies.

There is a question of whether stratification of the lower layer may, by carrying away energy as waves, affect the rate of entrainment. This is not the case for the latoratory experiments described above, but in the case of the oceans and the atmosphere, the question is unresolved,

There have been few detailed measurements of the interfacial structure in these experiments. The instantaneous thickness of the interface decreases as the stirring rate is increased, but the thickness depends only very weakly on the property being transferred, The mixing takes place largely through a process which looks like the intermittent breaking of steep forced internal waves, which tends to thicken the interface, followed by the sweeping away of this fluid by the stfrring in the layers, which sharpens the interface again.

Most quantitative measurements of mixing rates have been interpreted using arbitrary overall measures of length and velocity scales, derived from the geometry and stirring frequency. Thompson (1969) has shown how one can relate the entrainment rates to the properties of the turbulence. Using the same apparatus which had been used earlier (Turner 1968) to measure entrainment rates, he showed that the r.m.s. value u_1 of the horizontal component of turbulent velocity remained proportional to the stirring frequency while the turbulence decayed rapidly with increasing distance from the grid.

One can now be confident that the entrainment rates measured in Turner's experiments have been related to scales which are not arbitrary, but which are characteristic of the fluid motion near the interface. By a similar argument to that used in an earlier lecture for a turbulent gravity current, we can suppose initially that the mixing process represents a balance between buoyancy and inertia forces alone. The entrainment velocity u_e will then be a function of u_1, a measured integral

length scale l_1, and the density difference $\Delta\rho$ between the layers, which can be expressed as

$$u_e/u_1 = f(Ri_o)$$

where $Ri_o = \frac{g\Delta\rho\, l_1}{\rho u_1^2}$

The following diagram of the results of Turner (1968) and Thompson (1969) supports the choice of Ri_o as the major governing parameter. Note that the functional forms for the rates of mixing with temperature or salinity differences across the interface are different.

When both layers are stirred in similar experiments, it is found that the mixing rate in one direction through the interface is not substantially changed. This implies that turbulence is very strongly damped at an interface and the events which cause the removal of fluid are so rare that the two sides can be regarded as statistically independent. When the stirring is applied at the same rate in

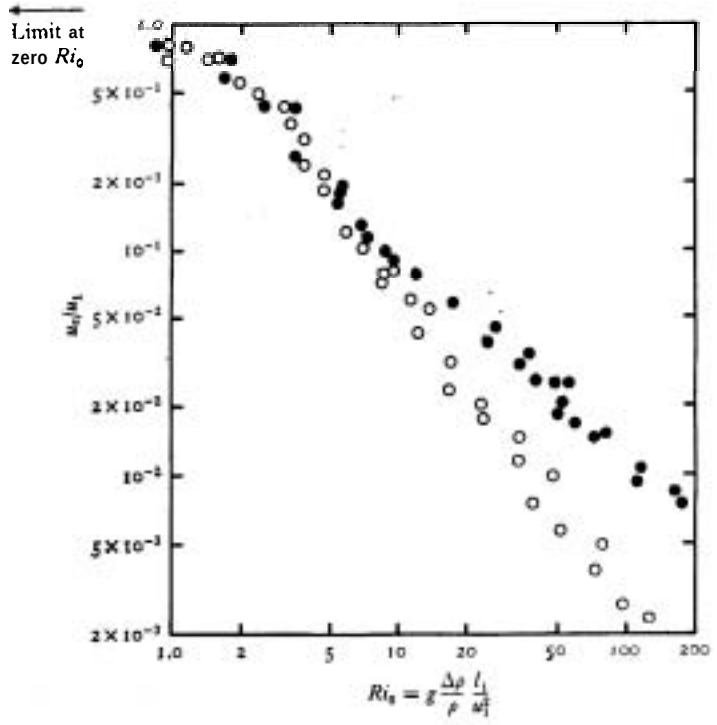

Fig.1

the two layers, the interface remains sharp and central. If the stirring is unsymmetrical, the interface moves away from the region of more vigorous stirring until the entrainment rates on the two sides balance.

The other type of mechanical mixing to be considered is mixing driven by a surface stress. Grid stirring is experimentally convenient and can be used as a model of several natural processes in which turbulent energy is put in on a scale much smaller than the layer depth, but this may not always be realistic.

Kato and Phillips (1969) used the grid stirring technique to model an ocean with density gradient, driven by a surface wind stress. To avoid end effects they used an annular tank containing salt solution with a linear density gradient, and applied a constant stress τ at the top by rotating a screen immersed just below the surface. A turbulent layer was quickly formed bounded below by a sharp interface which advanced at a decreasing rate and across which the density difference was increasing with time.

Their measurements of the Payer depth D as a function of time, together with the known initial gradient and the imposed stress are plotted in the following figure in non-dimensional form. (See Fig.2) A dimensional argument suggests that E, the ratio of the entrainment velocity to the friction velocity satisfies a relation of the form

$$E = u_e/u_* = f(Ri_*)$$

where u_* is defined by $\tau = \rho_s u_*^2$ and is used as the velocity scale and

$$Ri_* = \frac{g\Delta\rho D}{\rho_s u_*^2}$$

A particular form for f can be obtained by a dimensional argument which has an attractive physical interpretation. If $\Delta\rho$ and u_e are supposed to be separately unimportant, and to occur only as the product

$$\left(\frac{g\Delta\rho}{\rho}\right) u_e$$

(the buoyancy flux across the interface) then dimensional reasoning gives

$$g\Delta\rho u_e D \propto \rho u_*^3$$

$$E \propto Ri_*^{-1}.$$

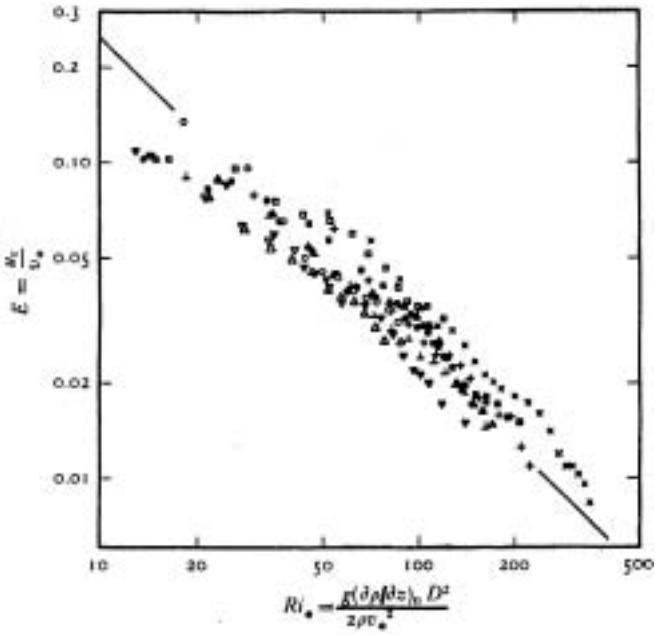

Fig. 2

The numerical constant obtained by fitting this from to Kato and Phillips (1969) experiments over the range $30 < Ri_* < 300$ implies that

$$\frac{u_e}{u_*} = 2.5\ Ri_*^{-1} = 2.5\ \frac{\rho_0 u_*^5}{g \Delta\rho D}$$

A more elaborate experiment along the same lines has been described by Moore and Long (1971). They produced a steady turbulent stratified flow in a cyclic tank by injecting and withdrawing fluid through the floor and ceiling. As is to be expected in a flow which is driven at the boundaries, two homogeneous layers formed, separated by a thin interface. Experiments with one or both layers flowing were interpreted in a similar overall way to that already described. One possible problem with this experiment is that since the flow is driven at the top and bottom by tangentially oriented jets which are turbulent, this may affect the interpretation of the mixing rates.

Thus far, the influence of molecular processes has been ignored An explicit dependence of mixing rate on Reynolds number was proposed by Rouse and Dodu (1955) on the basis of their grid stirring experi-

ments. More recent work suggests that this interpretation may be inappropriate and suggests that their results are an indication of a viscous effect occurring near the generating grid, rather than during the decay process or near the interface. Viscosity cannot explain the results of Turner (1968) and Thompson (1969) Fig.1. Since these experiments were conducted with essentially constant viscosity and the same range of density differences and stirring rates, the large differences in u_e using salt and heat can only be explained by invoking molecular diffusivity. A second dimensionless number, the Peclet number, $Pe = \frac{u_1 l_1}{K}$ enters the problem and now

$$u_e/u_1 = f(Ri_o, Pe)$$

In these experiments, u_1 and l_1 were varied little, so the major change of Pe was due to a change in K. Effectively Pe had two different constant values, one for heat and one for salt, and the experimental curves in Fig.1 are just two sections of $f(Ri_o, Pe)$. These curves tend to the same form at low Ri_o where neither buoyancy nor diffusion is important but diverge at higher Ri_o, becoming approximately $u_e/u_1 \propto Ri^{-1}$ (heat) and $u_e/u_1 \propto Ri_o^{-3/2}$ (salt).

References

Cromwell, T. 1960 Pycnoclines created by mixing in an aquarium tank. J.Mar.Res. 18: 93-82.

Kate, H. and O.M.Phillips 1969 On the penetration of a turbulent layer into a stratified fluid. J.Fluid Mech. 37: 643-655.

Lofquist, K. 1960 Flow and stress near an interface between stratified liquids. Phys.Fluids 3: 158-175.

Moore, M.J. and R.R.Long 1971 An experimental investigation of turbulent stratified shearing flow, J.Fluid Mech, 49: 635-655,

Rouse, H. and J.Dodu 1955 Turbulent diffusion across a density discontinuity. La Houille Blanche 10: 530-532.

Thompson, S.M. 1969 Turbulent interfaces generated by an oscillating grid in a stably stratified fluid. Ph.D.Thesis, University of Cambridge.

Turner, J.S. 1968 The influence of molecular diffusivity on turbulent entrainment across a density interface. J.Fluid Mech. 33: 639-656.

Turner, J.S. 1973 Buoyancy Effects in Fluids. The University Press, Cambridge.

Notes submitted by
Brian P. Hickie

Lecture #6. EXTERNAL MIXING PROCESSES IN THE OCEAN AND ATMOSPHERE

1. Mixing of a surface layer by wind stress

The mixing here at first will be considered to be entirely driven mechanically, by the wind stress at the sea surface. It is supposed that the mixing at the bottom of the surface layer is described by the proportionality between entrainment and inverse Richardson number

$$u_e / u_* = \alpha R_i^{-1}$$

(with u_* = friction velocity) which has been discussed in foregoing sections. This relation means that a fixed fraction of the energy input at the surface is used to increase the potential energy of the surface layer. Hence, for a simplified ocean with a surface layer of constant total buoyancy and depth h above a deeper layer of constant density the increase of potential energy V with the increase of the surface layer depth is given by

$$\frac{dV}{dt} = \frac{1}{2}(g h \Delta\rho)\frac{dh}{dt} = \frac{1}{2} b u_e = \text{const.}$$

i.e., the rate of deepening of the surface layer is constant and inversely proportional to the total buoyancy b.

With an arbitrary density profile $\rho(z)$ the above entrainment relation will still hold. If it is applied to a linear density gradient the depth of the interface as function of time will be given by

$$h(t) = u_* \left(\frac{15 t}{N_0^2}\right)^{1/3}$$

with N_0 the initial buoyancy frequency. This formula results with a proportionality factor α = 2.5 which was found in Kato and Phillips' (1969) experiments. There is, however, serious doubt whether such laboratory constants do hold for the ocean, for three main reasons:

(1) Surface waves may influence the energy transfer. The total work of the wind at the surface may be much larger than ρu_*^3 or τu_*

which is the underlying energy input assumption here. This means that the estimate of the factor relating surface stress energy input and potential energy change would be increased, In fact, evaluation of ocean surface layer data by Turner (1969) revealed that this factor might be almost twice as large as the one in Kato and Phillips' experiments.

(ii) For deep wind mixed layers the turbulent energy put in through wave breaking at the surface will decay with depth and contribute little to mixing at the interface.

(iii) The surface layer mixing may take place in organized motions. Cellular convection - for example in form of Langmuir cells (rolls aligned downwind) - could result in stronger mixing throughout all the surface layer.

2. Seasonal changes of a thermocline

In this case the effects of heating and cooling at the sea surface have to be taken into account in addition to the mechanical mixing. Since heating from the surface tends to make the mixed layer shallower and stirring to deepen it a balance between both effects must be possible with the thermcline remaining at a fixed depth h_1. By use of dimensional arguments Kitaigorodskii (1960) showed that then

$$h_1 = \frac{a\, v_*^3}{g'\, w'} = a\, v_*^3/B,$$

with B = buoyancy flux. This relation simply means that the kinetic input at the sea surface is used to change the density of the upper layer. If with a given constant stirring energy the heating rate is increasing the thermocline will rise and the surface layer get warmer. When the heating rate decreases the surface layer will still get warmer but deepen slowly due to the entrainment across the interface into the lower layer.

The further development when the surface is now cooled can be treated under different assumptions, limited by two extreme mixing concepts, namely no penetration at all and full penetration. In the first case the heat balance alone determines the thermocline depth, in the

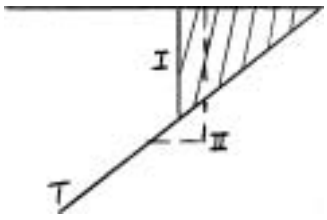

Fig,1

second case all kinetic energy produced by wind stirring and by the convection itself is used to entrain colder water upward across the thermocline. The basic difference is shown in the sketch (Fig.1); a linear temperature profile is cooled from above, In the nonpenetrative case the profile (I) results where the shaded area corresponds to the heat loss. If penetration occurs, a step is produced in the temperature profile (II).

The ideas about heating and cooling a mixed surface layer have been applied to oceanic situations with seasonally varying buoyancy flux from the surface. Kraus and Turner (1967) have treated a "saw tooth" heat flux cycle (which approximated the actual heat flux in a Pacific subarctic area reasonably well) with constant mechanical working at the surface. Their results for thermocline depth and surface temperature with different energy conservation assumptions during the cooling cycle are qualitatively shown in Fig.2.

The different curves during the cooling phase result from the assumptions of

(i) full penetration;

(ii) no penetration at all;

(iii) entrainment only due to convection, no wind stirring;

(iv) entrainment only due to wind stirring,

Measurements from an area in the Pacific where advection is small showed that two main features of the seasonal variations of the thermocline are well reproduced by the model: The maximum of heating and minimum depth occur together and the maximum surface temperature is delayed relative to the time of minimum depth,

As regards the cooling phase, Kraus and Turner applied curve (i) first, i.e., the concept of maximum entrainment due to wind and convection. Turner Later came to the conclusion that this might not be the

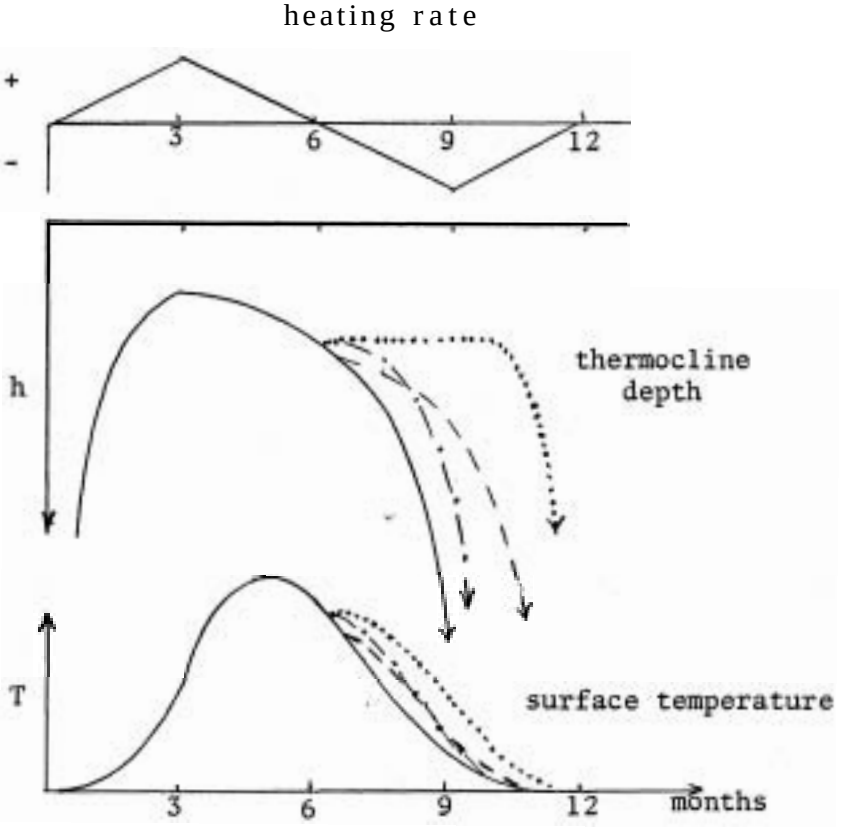

Fig. 2

appropriate case and tends more to the nonpenetrative model. Other observations in laboratory experiments, in lakes and in the ocean also suggested that the penetration effect of convection seems to be small, i.e. that in absence of wind stirring the mixed layer depth can be calculated from the heat balance alone. Recent observations have been presented from the deep convective winter mixing in the northern Mediterranean (Anati, 1971) which showed that even under presence of strong winds surface cooling and not mechanical stirring had the dominant influence on the thermocline deepening. Hence, curves (ii) or (iv) in Fig.2 should be applicable in most cases.

3. Mixing across atmospheric inversions

In an atmospheric bottom boundary layer the penetrative and the

nonpenetrative mixing process should be easily distinguishable: with penetration the temperature at a given level will first fall abruptly if the step produced by entrainment (see Fig.1) passes this level and then rise again slowly. Without penetration the temperature at a given height cannot decrease. However, observations of such a step alone is not sufficient to conclude entrainment since heat losses at the boundary top by radiation can cause the same effect.

If convection occurs in the form of thermals or plumes only a small fraction of the work done by byoyancy appears as kinetic energy, as shown by Scorer (1957). Considering that not necessarily all energy on the larger scales which is most effective for entrainment is used for this purpose, the mixing rate might be rather small. Thus, even though today's state of the art does not yet provide enough knowledge on how strong atmospheric penetration is, it can be concluded that Ball's (1960) assumption of full penetration must be wrong.

4. Other factors influencing the depth of a mixed layer

a) Rotation

In the foregoing considerations rotation was neglected, the influence of a boundary stress could practically penetrate indefinitely. However, in a rotating system this influence is confined to the Ekman layer. Noticeable deviation from the foregoing theory will have to be expected if the Monin-Obukhov length $L_B = V_*^3/B$ is not much smaller than the Ekman layer depth $L_e = V_*/f$.

b) Stable density gradient outside mixed layer

In this case energy can be lost from the layer by radiation in the form of internal gravity waves. Townsend (1968) showed this possibility for an atmospheric boundary layer. The generated waves will travel with a phase speed close to the convection velocity U of the dominant disturbances because then resonance conditions are approached. These waves will have a wavelength $\sim U/N_0$ with N_0 the buoyancy frequency in the region above the interface, The radiative energy loss may be large enough to influence the motion of the interface itself.

Necessarily, the waves can only grow large if much forcing energy falls into the frequency range $\omega < N$ with N now valid for the interface.

5. Horizontal nonuniform effects

a) Small scale

Convection in a surface mixed layer takes place in form of thermals or plumes, i.e. it is horizontally nonuniform in a small scale. This obviously implies that application of a one-dimensional eddy diffusivity concept will lead to inconsistencies. The recognition of the individual elements which carry the buoyancy flux resolves an earlier controversy about "transport against the gradient".

b) Large scale

Horizontal nonuniformal effects result from horizontal gradients of wind stress and heat flux.

c) Sloping boundaries

If a layer meets a sloping bottom and the surface is cooled (Fig.3a) the surface water in the corner gets denser because of less underlying water volume available for heat supply and a downward flow along the bottom results.

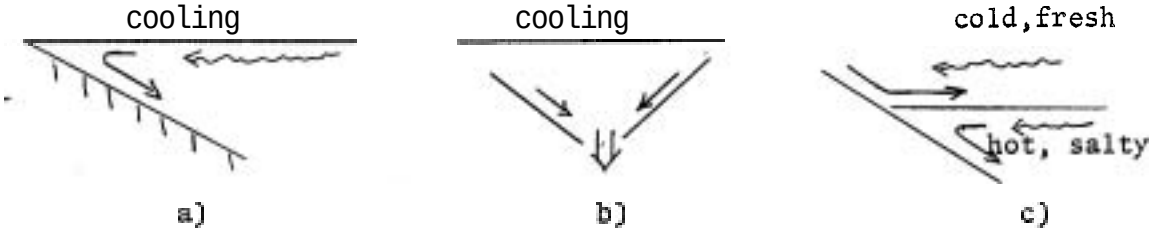

Fig.3

If sloping interfaces meet - for example in a two-layered eddy - heavier water is flowing into the intersection region and may occasionally break through the interface into the lower layer (Fig.3b), a situation which might have played a role in the development of the deep mixing observed in the northern Mediterranean during the MEDOC expedition 1969. With the double diffusive process the same effect as in Fig. 3a can happen to an interface meeting a sloping boundary, Heat

in the corner of the lower layer is diffused upward more quickly than salt with the consequence of a downflow in the lower Payer, In the upper layer downflow has to occur as well at the slope because the water in this corner warms slower than at points away from that corner. Continuity in both cases requires horizontal circulation as indicated,

References

Anati, D.A. 1971 On the mechanism of the deep mixed layer formation during MEDOC '69. Cah.Océanographiques 23: 427-443,

Ball, F.K. 1960 Control of inversion height by surface heating. Quart.J.Roy.Soc. 86: 483-494,

Kato, H. and O.M.Phillips 1969 On the penetration of a turbulent layer into a stratified fluid. J.Fluid Mech. 37: 643-655.

Kitaigorodskii, S.A. 1960 On the computation of the thickness of the wind-mixed layer in the ocean, Bull.Acad.Sci. U.S.S.R. Geophys, Ser.3: 284-287.

Kraus, E.B. and J.S.Turner 1967 A one-dimensional model of the seasonal thermocline II. The general theory and its consequencies. Tellus 19: 98-106,

Scorer, R.S. 1957 Experiments on convection of isolated masses of buoyant fluid. J.Fluid Mech. 2: 583-594,

Townsend, A.A. 1968 Excitation of internal waves in a stably stratified atmosphere with considerable wind shear. J.Fluid Mech, 32: 145-171.

Turner, J.S. 1969 A note on wind mixing at the seasonal thermocline. Deep-Sea Res. Suppl. to Vol.16: 297-300,

Notes submitted by
Friedrich A. Schott

Lecture #7. STRATIFIED TURBULENT SHEAR FLOWS

As an introduction to the study of overall very stably stratified shear flows, which are the most common in the ocean, we shall consider in turn:

1. High Reynolds number (turbulent) shear flow above a boundary, for a neutrally stratified (uniform density) fluid;

2. The effect of a buoyancy flux on such a flow, the fluid now being stratified;

3. The dependence of the flow on the degree of stratification in the convective case (unstable, with positive vertical buoyancy flux);

4. The dependence of the flow on the degree of stratification under stable conditions (with a positive vertical density flux].

1. Neutral stratification

Following Ellison (1957), we consider (Fig.1) an infinite plane z = 0 moved tangentially so as to exert a constant uniform stress τ on the fluid above, and in particular we seek the ultimate steady velocity profile, In many contexts the resulting mean velocity is the same as that generated by an externally imposed flow at a large distance above the boundary. However, in the latter case the stress may have to vanish somewhere in the profile (for example, at the centre of flow in a pipe), in which case we are only analyzing the situation fairly close to the wall,

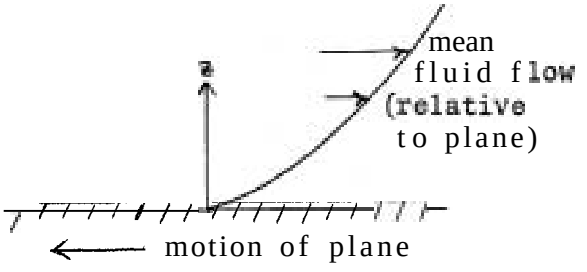

Fig. 1

Priestley (1959) considers atmospheric applications of the problem. Assuming that the flow is turbulent, corresponding to a large Reynolds number, we suppose that at a distance z above the boundary, the velocity profile is not affected by the value of the fluid viscosity. (This does exclude a thin layer close to the boundary, where viscosity is necessarily the agent of stress as the vertical velocity fluctuations w', and hence the vertical turbulent momentum transfer $\rho \overline{w'u'}$, decay to zero.) Then z and $\tau = \rho u_*^2$ (defining u_*, where is the density) are the only parameters controlling the profile. Locally, the primary profile description is $d\bar{u}/dz$. On dimensional grounds, we must have

$$d\bar{u}/dz = u_*/k z \qquad (1)$$

where k is a universal dimensionless constant (von Karman's constant), which is found by experiment to have the approximate value .41.

Integrating (1), $\bar{u} = u_*/k \left(\ln z + c\right)$ (2)

where c is another dimensionless constant. The shape of the profile (2) is universal, but the absolute magnitude of $\bar{u}$ depends on the value of c, which in turn depends on the boundary conditions.

(a) Aerodynamically smooth boundary

We suppose that the stress is ultimately transferred by a viscous sublayer, of thickness $\delta \sim \nu/u_*$, close to the boundary. Here the mean velocity is linear, but there are still velocity fluctuations with horizontal and vertical components of scale

$$(u', w') \sim u_* (z/\delta, (z/\delta)^2),$$

so that the flow is not laminar.

Writing $c = -\ln \nu/u_* + c_1$, we have from (2)

$$\bar{u} = u_*/k \left(\ln u_* z/\nu + c_1\right) \quad (3)$$

where c_1 is another universal dimensionless constant, found by experiment to be approximately 2.4. Thus the magnitude of $\bar{u}$ is determined. The profile (3) holds for z down to a few times δ.

(b) Aerodynamically rough boundary

As the boundary is approached, the momentum transfer is supposed ultimately to be directly due to roughnesses on the boundary, and their associated wakes. Clearly we suppose the roughness has a scale larger than δ. Then

$$\bar{u} = u_*/k \ln z/z_0 \quad (4)$$

where z_0 is the "roughness length", to be found by experiment in any given context. It tends to be about 1/30 the size of the objects constituting the roughness. Some estimates are

Wheat	Tall Grass	Cropped Grass	Sea in moderate wind
5 cm	3 cm	.3 cm	.1 cm

This profile gives local values for

energy production/unit mass $\varepsilon = \tau/\rho \, d\bar{u}/dz = u_*^2 \, d\bar{u}/dz = u_*^3/kz$

and "eddy viscosity" $K_m = \tau/\rho \Big/ d\bar{u}/dz = k u_* z$.

K_m increases with z as ever larger eddies (up to a scale of order z imposed by the distance to the boundary) can contribute to mixing when z increases.

The Reynolds analogy is that K_m and the thermal "eddy diffusivity" K_H (for example) are in a constant ratio throughout the flow. This is based on the idea that both momentum and heat transports occur due to the same process of turbulent mixing. The assumption is very good for neutral and weak stratification, but breaks down for a strongly stratified fluid. Success in any circumstances is perhaps somewhat surprising since momentum, unlike heat, is a vector, and may also be transferred by pressure forces.

2. Buoyancy flux

The generally accepted basis of this extension to the logarithmic profile of (1) was developed by Monin and Obukov (1954).

Figure 2 shows typical velocity profiles in different types of stratification, as observed by experiment. They agree with the idea that stability will inhibit vertical mixing and so permit greater shear.

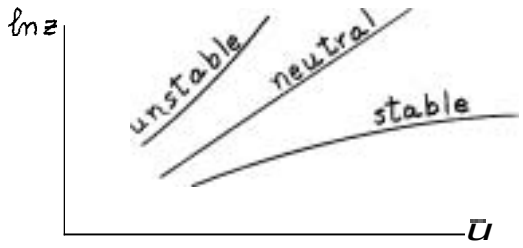

Fig.2

As in (1), we assume that u_* is uniform in height, and that z is a parameter controlling the local velocity profile. However, there is now an additional parameter, viz. the buoyancy flux

$$B = -g\overline{\rho' w'}/\bar{\rho}_0 = g/\bar{\theta}_0 \left(H/c_p \bar{\rho}_0\right)$$

where H is the heat flux, and $\bar{\rho}_0$, $\bar{\theta}_0$ reference density and potential temperature. B is assumed to be uniform with height, This is quite a severe restriction, and (for example) during morning heating of the lower atmosphere, B decreases linearly with height, so that the assumption would only hold good for a thin layer near the ground.

B and u_* combine to give a length scale (in addition to z)

$L = \bar{\rho}_0 u_*^2 / k\, g\, \overline{\rho' w'} = -u_*^3 / kB$ the Monin-Obukov length. As defined, it is positive in a stably stratified fluid, and negative for unstable stratification. It is typically some tens of metres in the lower atmosphere.

The ratio z/L measures the importance of B. Since it becomes small if either $B \to 0$ or $z \to 0$, we see that stress dominates when it is small, and buoyancy has increasing influence as it becomes larger, i.e. as the height above the bottom is increased.

Dimensional arguments now require

$$\frac{kz}{u_*} \frac{d\bar{u}}{dz} = \phi_M\left(\frac{z}{L}\right) \tag{5}$$

where the above discussion indicates $\phi_M \to 1 \ (z/L \to 0)$, ϕ_M is an increasing function of z/L. From (5) $K_M = \tau/\rho \Big/ d\bar{u}/dz = k u_* z / \phi_M$ which decreases relative to $k u_* z$ as z/L increases.

Integrating (5), $\bar{u}/u_* = 1/k \left[\ln z/z_0 + \phi(z/L)\right]$ (6)

where $\phi(z/L) = \int_{z_0}^{z} \phi_M - 1/z'\, dz' \equiv \int_0^{z/L} \phi_M(\xi) - 1/\xi\, d\xi$

Monin and Obukov plotted $\chi(4L) \equiv k/u_* \left[\bar{u}(z) - \bar{u}(4/z)\right]$ as observed experimentally against z/L, as shown in Fig.3. According to (6)

$\chi(z,L) = \ln 2z/L + \phi(z/L) - \phi(1/z) = \chi(z/L)$.

The experimental data do indeed collapse well onto the two curves of Fig.3, thus demonstrating the validity of the dimensional argument. However, no physical principle has yet been proposed which gives a satisfactory functional form for , or ϕ_M. If $\phi_M = 1 + \alpha z/L$, then

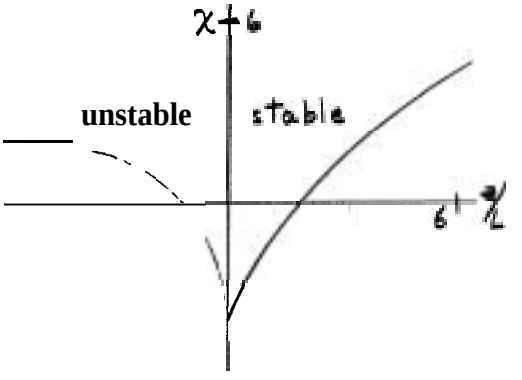

Fig.3

$$\bar{u} = u_*/k \left[\ln z/z_0 + \alpha z/L\right], \tag{7}$$

the "log-linear" profile. By experiment, $\alpha \approx 5$, but this form is only good a *priori* for small z/L, and indeed is not accurate otherwise.

Dimensional arguments also require

$$kz/T_* \, d\bar{\theta}/dz = \phi_H(z/L) \qquad (8)$$

analogous to (5), where $T_* = \overline{\theta' w'}/u_*$. The Reynolds analogy states that ϕ_M and ϕ_H are proportional.

Besides z/L, other measures of stability are

Richardson number $Ri = -g/\bar{\rho}_0 \, d\bar{\rho}/dz \Big/ \left(d\bar{u}/dz\right)^2$

and Flux Richardson number $Rf = \left(K_H/K_M\right) Ri = g\overline{\rho' w'}/\bar{\rho}_0 u_*^2 \left(d\bar{u}/dz\right) \left(= K_M/ku_*L\right)$.

$$= \frac{\text{rate of working against buoyancy}}{\text{rate of energy input by stress}} < 1.$$

In fact observations indicate that turbulence in a stratified fluid is strongly affected when the value Rf reaches about .1, so that the absolute limit 1 is not approached in practice (see section 4). As $z/L \to 0$,

$$Ri \sim Rf \sim z/L ,$$

but Ri, Rf and the value ϕ_M/ϕ_H all become different functions of z/L as this becomes larger.

3. Convection

a) Forced convection (Fig. 4) occurs when the shear-generated turbulence causes, and is unaffected by, the vertical heat transfer, In this case

$$K_H = K_M = ku_*z = k^2 z^2 \, d\bar{u}/dz$$

Then $\overline{\rho' w'} = K_H \, d\bar{\rho}/dz = k^2 z^2 \, d\bar{u}/dz \, d\bar{\rho}/dz \propto z \, d\bar{\theta}/dz$

so that $d\bar{\theta}/dz \propto z^{-1}$

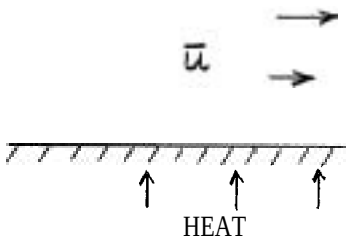

Fig. 4

b) Free convection corresponds to large negative values of z/L.

In this case, the heat flux is supposed to be driven by buoyancy effects, and not to depend on the value of the shear. Thus it is independent of u, and the derived length L. However, the turbulent energy may still have a substantial contribution from the shear flow, whose existence is indeed necessary for the dimensional argument, as it prevents a boundary layer length scale from being transferred to the heights considered by convecting elements.

Without u, and L, $g/\bar{\rho}_0 \, d\bar{\rho}/dz$ depends on z and B alone.

Hence $$B\left(g/\bar{\rho}_0 \, d\bar{\rho}/dz\right)^{-\frac{1}{2}} z^{-2} = H_* \text{ , a dimensionless constant.}$$

Thus $$-d\bar{\theta}/dz = H_*^{-2/3}\left(H/c_p\bar{\rho}_0\right)^{2/3}\left(g/\bar{\theta}_0\right)^{-1/3} z^{-4/3} \propto z^{-4/3}.$$

H_* is the non-dimensional heat flux. Whereas this is a universal constant for free convection, we have for forced convection

$$H_{*\,\text{forced}} = -g\,\overline{\rho'w'}/\bar{\rho}_0\left(g/\bar{\rho}_0 \, d\bar{\rho}/dz\right)^{-3/2} z^{-2} = -R_f u_*^2 \, d\bar{u}/dz \left(|Ri|\left(d\bar{u}/dz\right)^2\right)^{-\frac{1}{2}} z^{-2} = k^2|Ri|^{-1/2}$$
$$= k^2\left(-z/L\right)^{-1/2}$$

Forced, free and 'natural' convection, which involves molecular processes at still larger values of $-z/L$, are discussed in Townsend (1962). The results of experiment are shown in Fig.5: the transition range of z/L between forced and free convection is very short.

Ellison suggested the following interpolation formula:

$$d\bar{u}/dz = u_*/kz\left(1-\gamma R_f\right)^{-1/4} \qquad (9)$$

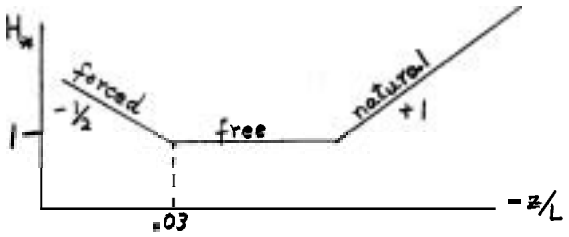

Fig. 5

(9) is correct in the limiting cases

(i) $z/L \longrightarrow 0$ (forced convection)

(ii) Large negative z/L (free convection)

(iii) Large positive z/L
(when $Rf \longrightarrow Rf_{crit} = 1/\gamma$, $K_M/ku_*z = u_*/kz \Big/ d\bar{u}/dz \longrightarrow 0$; see section 4).

Experiments indicate that γ is about 14, but the form (9) is merely a suggested interpolation; there is no theoretical reason why the single constant γ should be accurate for the three limits (i) - (iii).

(9) implies $\phi_M^4 - \gamma z/L\, \phi_M^3 = 1$

4. Stable conditions

(a) If we assume (7), viz. $\bar{u} = u_*/k \left[\ln z/z_0 + \alpha z/L\right]$,

corresponding to $d\bar{u}/dz = u_*/kz\, \phi_M$, $\phi_M = 1 + \alpha z/L$,

then $Rf = K_M/ku_*L = z/L\phi_M$, i.e., $1 = \phi_M - \alpha z/L = \phi_M(1 - \alpha Rf)$.

Thus $\phi_M = (1 - \alpha Rf)^{-1}$

Allowing z/L and Rf to increase rather beyond the range for which (7) is valid, we see that, with $\alpha = 5$, $\phi_M \longrightarrow \infty$ and $K_M \longrightarrow 0$ as $Rf \longrightarrow .2$.

Although (7) is not accurate, the suggested rapid increase of ϕ_M with Rf in the range .1 to .2 is real, and indicates that the turbulent flow will be strongly affected by buoyancy in this range. It appears that work done in raising heavier fluid against buoyancy can takk up only a small fraction of the shear energy input, most of the energy passing via the turbulence to viscous dissipation,

(b) Very stable limit

The Monin-Obukov theory includes z, u_* and B as parameters. If, however, we suppose that the stratification in a region of the fluid is sufficiently strong that no eddies extend to the boundary, it is appropriate to omit z. We are therefore no longer considering boundary turbulence. $L = -u_*^3/B$ is now the only length scale, Dimensional arguments thus imply

$$N^2 \equiv -g/\rho_0 \, d\bar{\rho}/dz = k_2^2 B^2/u_*^4 = k_2^2 u_*^2/L^2$$

$$d\bar{u}/dz = k_1(-B)/u_*^2 = k_1 u_*/L = k_1/k_2 N$$

so that both N^2 and $d\bar{u}/dz$ are uniform throughout the region. We also have

$$Rf = k_1^{-1}, \quad K_H/K_m = k_1/k_2^2, \quad Ri = k_2^2/k_1^2 = Ri_e.$$

A uniform 'equilibrium' value Ri_e for Ri is therefore implied. This, and the linear profile of $\bar{u}$, corresponds to the result for the outer edge conditions in flow down a steep slope, discussed in Lecture 4. In that context, $g\Delta\rho/\rho$ and A 4 were specified, compared with B and u_* in the present case.

References

Ellison, T.H. 1957 Turbulent transport of heat and momentum from an infinite rough plane, J.Fluid Mech. 2: 456-466.

Monin, A.S. and A.M.Obukov 1954 Basic laws of turbulent mixing in the ground layer of the atmosphere, Acad.Sci.U.S.S.R. Leningrad Geophys.Inst. 24: 163-187.

Priestley, C.H.B. 1959 Turbulent transfer in the lower atmosphere. Univ.of Chicago Press,

Townsend, A.A. 1962 Natural convection in the earth's boundary layer. Quart.J.Roy.Met.Soc. 88: 51-56.

Notes submitted by
John M. Huthnance

Lecture #8. TRANSPORTS IN VERY STABLE CONDITIONS

We should like to consider the application and significance of the uniform conditions in self-regulated very stable fluid flow (Lecture #7, section 4(b)) for large bodies of fluid.

1. Experimental evidence

(a) In the context of turbulent flow down a slope (Lecture #4 and Lecture #7, section 4(b)), it is found that the velocity profile at the interface of the two fluids is linear, This agrees with the results sf the dimensional analysis given, The equilibrium Richardson number Ri_e

which results, is found to have a value of around .1 or slightly less,

(b) Browning (1971) has made radar observations in the atmosphere, and was able to plot contours of Ri as shown in Fig.1. Minima with values between .1 and .2 were regularly obtained, indicating some balance between the tendency of turbulence to increase the Richardson number, and of large scale motions to decrease it. The larger values of Ri in these observations (compared with (a)) are probably due to the spatial averaging over distances of at least 200 m.

Fig.1

(c) Prych et *al*. (1964) carried out the experiment illustrated in Fig.2. They found that the final density profile, resulting from

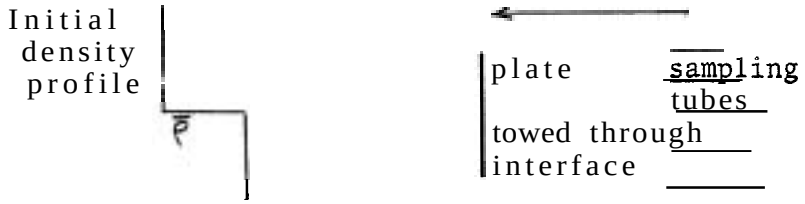

Fig. 2

towing the plate normal to itself through the interface, was linear in the region where mixing had occurred. (This agrees with the findings of Thorpe for the mixed region after Kelvin-Helmholtz instability at an interface). Before the linear profile was established after passage of the plate, however, the plate's wake successively grew, then collapsed on the large scales, and finally the small scale turbulence decayed. The large scale collapse occurred at around Ri = .1, and by the time Ri had reached .3 at any point, the turbulence had strongly decayed.

(d) Townsend (1957) set up fluid with a stable density gradient, and then introduced from the side a jet of intermediate density. He measured the density, and hence the mixing, at various points in the intruding jet, It was found that the rate of mixing began to decrease

at a value for Ri of about .05. Mixing was complete by the time Ri reached .3.

(e) Townsend, quoting Nichol (1970), also considered the experiment shown in Fig.3. It was found that, at a particular distance

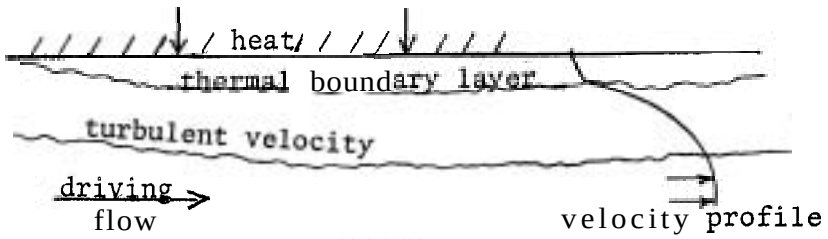

Fig.3

downstream, the turbulence in the stably stratified thermal boundary layer was dramatically reduced,

Consequently the Reynolds stress between it and the exterior flow was much less, and the thermal layer, being driven only weakly, had a much reduced velocity.

(f) Townsend (1967) interpreted the dying away of the wind at night, or during a solar eclipse, as follows: With the absence of solar heating, the ground cools by radiation and forms a thickening stable layer of air above. Eventually Ri rises to some value around .1, the driving turbulent stress is much reduced, and the wind speed in the ground layer falls correspondingly.

The evidence given so far all suggests that if the Ricahrdson number rises above about .1, strong decay of turbulence occurs, However, some observations indicate that turbulence may be present with very much larger Ri.

(g) Ellison and Turner (1960) carried out the experiment sketched in Fig.4, with the results indicated in Fig.5.

(h) Taylor (1931) made measurements in the Kattegat, where outflowing fresh water from the Baltic Sea overlies more salty water. The results are plotted in Fig.5. As for (g), Ri may increase, accompanied by a decrease of K_s/K_M so that Rf = (K_s/K_M) Ri is always less than 1.

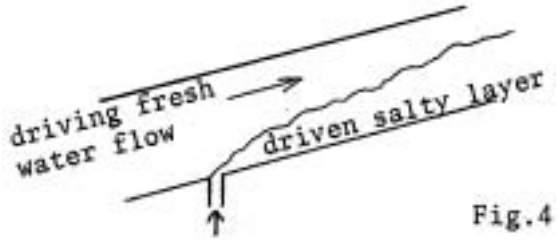

Fig.4

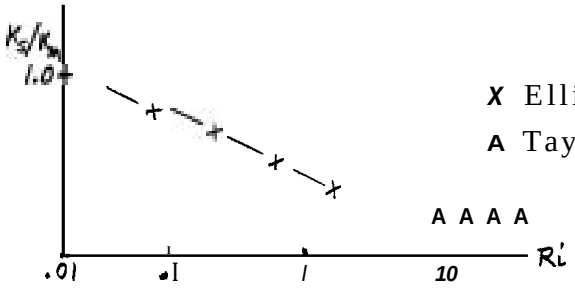

Fig. 5

2. Layering and waves

The fall of K_s/K_M as Ri rises implies that different mechanisms of salt and momentum transport are becoming important. In particular, since salinity is a passive quantity, it would appear that we require an additional means of momentum transport. Taylor, and Stewart (1969), suggested that wave motions may be important in transporting momentum.

There is also the problem of the observed existence of turbulence, even at large overall Ri. It has been proposed by Stewart that locally Ri must be very much smaller (e.g., at sharp interfaces) to support the turbulence, the large values of Ri being only space averages. We illustrate the difficulty by considering the problem in Fig.6.

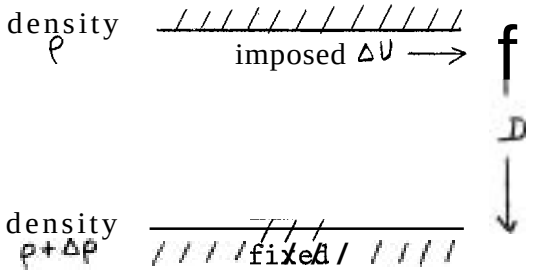

Fig.6

If, by chance, the imposed Richardson number

$$Ri_o = g\,\Delta\rho\, D/\rho(\Delta U)^2$$

should equal Ri_e (Lecture #7, section 4(b)), then the linear

gradient can be maintained by self-adjusting turbulence. If $Ri_o < Ri_e$, the shear dominates over the stratification, and the flow is externally regulated from the boundaries, as in the Monin-Obukov theory, If $Ri_o > Ri_e$ (as in the ocean), there must be internal self-regulation. However, turbulence is observed, which seems paradoxical since internally self-regulating turbulent flow implies a Richardson number Ri_e. A partial solution of this problem has been suggested by Stewart (1969). He pointed out that a small constant value (e.g. Ri_e) of Ri throughout the fluid is consistent with any overall $Ri_o > Ri_e$ provided the density and velocity profiles are sufficiently nonlinear. Essentially this is because, comparing $Ri_o = g\,\Delta\rho/\rho D\,(D/\Delta U)^2$ with $g/\rho\, d\rho/dz \,/\,(du/dz)^2$,

$g\,\Delta\rho/\rho D = g/\rho\, d\rho/dz$ whereas $(\Delta U/D)^2 \leq (dU/dz)^2$.

As an example, consider Fig.7.

Fig.7 $< \Delta\rho >$

Both the linear (solid curve) and nonlinear (broken curve) profiles have the same overall Richardson number Ri_o, which is also the local value Ri for the linear profile. However, the nonlinear profile has $Ri = Ri_e < Ri_o$ everywhere, if

$$s,t = \tfrac{1}{2}\left[2Rr + (1-R) \pm \sqrt{\left\{4Rr(1-R)(1-r) + (1-R)^2\right\}}\right]$$

where $R = Ri_e/Ri_o$, i.e. we can construct a continuous range (in r) of nonlinear profiles which have an overall value Ri_o but a local value Ri_e everywhere.

The following comments apply to Stewart's suggestion,

(a) The steady state self-regulating profile under very stable conditions was

$$d\bar{u}/dz = -k_1 B/u_*^2 \qquad (1)$$

B and u_* being supposed uniform (although the resulting Ri_e is independent of their values). Nonlinear proffles are inconsistent with this uniformity. Indeed, it appears from (1) that a region in which $d\bar{u}/dz$ is large is associated with a small value of u_*^2, i.e. small momentum transport by the turbulence. Since in regions of smaller $d\bar{u}/dz$, u_*^2 is larger, the total momentum transport there is greater. We therefore require, in regions of large $d\bar{u}/dz$, another means besides turbulence for the vertical transport of horizontal momentum. Waves provide such a means.

(b) Formation of the hypothesized layered structure from linear

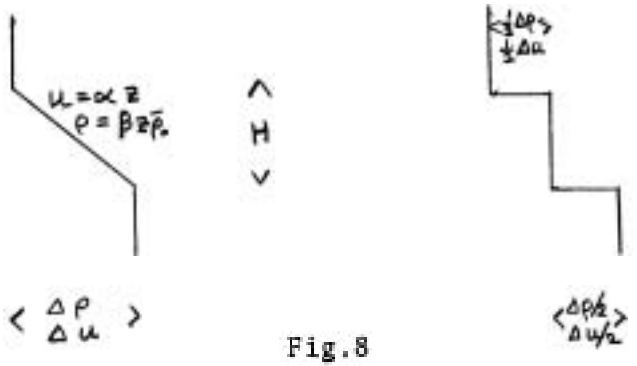

Fig.8

profiles requires energy, Consider transition from the linear to the stepped interface in Fig.8. The kinetic energy release is $\bar{\rho}_0/24\,\alpha^2 H^3$; the potential energy required is $-g\beta\,\bar{\rho}_0 H^3/12$, which is greater if $Ri_0 \left(= -g\beta/\alpha^2\right) > \frac{1}{2}$ The potential energy required to produce a profile with $Ri = Ri_e$ everywhere is greater than the kinetic energy release when $Ri_0 > \frac{1}{2}(Ri_e + 1)$. $\frac{1}{2}(Ri_e + 1)$ is always less than one, and when Ri_0 is greater than this value there is insufficient energy in the initial linear profile to form the layered structure. Again it appears that we must invoke waves, generated externally, to carry enough energy into the interior to produce the transition, A similar energy constraint limits the depth of a mixed layer resulting from Kelvin-Helmholtz instability to Ri_0 of order one at most.

(c) Consider the Reynolds number for a layered model with layers of depth h_1 and interfaces of thickness h_2. If the changes of velocity

and density across the layers and interfaces (Fig.9) are U_1 , ρ_1 , and , then Reynolds numbers might be defined by $Re_1 = h_1 U_1/\nu$ (layers.), $Re_2 = h_2 U_2/\nu$ (interfaces) whereas the overall Reynolds number for the combination is

$$Re = (h_1+h_2)(U_1+U_2)/\nu$$

For a sharp interface, $Re_2/Re \longrightarrow 0$ (as $h_2/h_1 \longrightarrow 0$).

For a broader interface, $Re_1/Re \longrightarrow 0$ (as $U_1/U_2 \longrightarrow 0$).

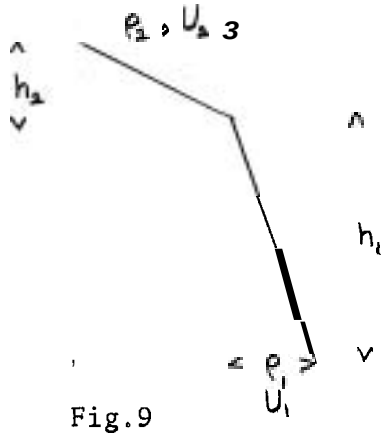

Fig.9

At some intermediate interface thickness, Re_1/Re and Re_2/Re will be equal, with value Re_c/Re (say). In general, either $Re_1 \leq Re_c$ (for a broad interface) or $Re_2 \leq Re_c$ (for a sharp interface). Now $Re_c = \frac{Ri_c}{3Ri_c + Ri_0}(Re) \ll Re$ when both layers and interfaces have . $Ri = Ri_c \ll Ri_0$, the overall Richardson number. We therefore see that strong density gradients may additionally suppress turbulence by essentially reducing the vertical length scale of the Reynolds number.

3. Processes leading to patchiness and local steps

(a) If an interface already exists, introduction of shear (for example, due to an internal wave on the interface) may induce shear instability and give a turbulent patch.

(b) Resonant interactions may occur on an interface. If a first mode wave travels on an interface of small but finite thickness, with a third mode wave of appropriate wave number in the opposite direction, a second mode wave may be generated (see Fig.10), where the dispersion curves of the three modes are shown. The possibility of a parallelogram as shown indicates

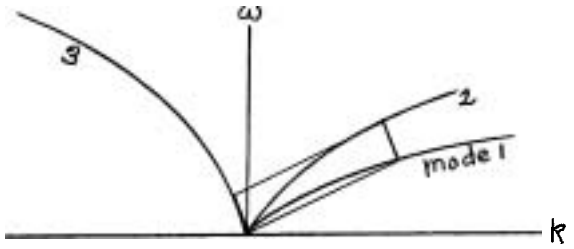

Fig.10

$\omega_2 = \omega_1 + \omega_3$, $k_2 = k_1 + k_3$ and resonant interaction). The second mode consists of alternate thickening and thinning of the interface, The shear due to the first mode causes a breakup of the bulges due to the second. The interface is most unstable where it is thickest, in son-trast to the Kelvin-Helmholtz mechanism, which is more effective the thinner the interface.

(c) In a continuously stratified fluid, internal waves commonly exist in the form of lee waves behind an obstacle (Fig.11).

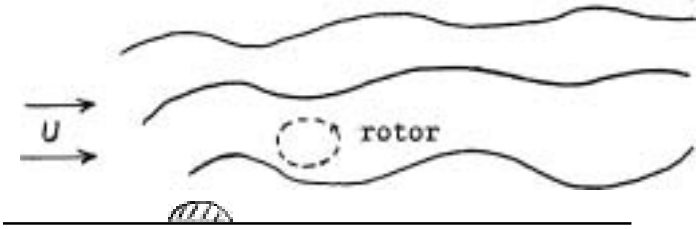

Fig.11

If the amplitude of these waves is very large, rotors, in which over-turning occurs, may form behind the obstacle. If the velocity in-ducing the lee waves vanishes at a height z_0 , additional phenomena

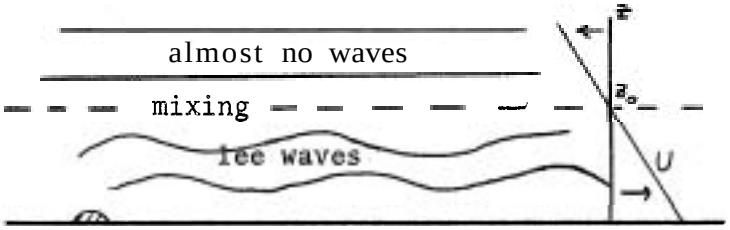

Fig,12

occur at this "critical level". Almost no waves exist above the level, where they have a sharp cut-off, so that the energy and momentum be-ing carried upward by the lee waves below must be transferred to the mean flow in this very thin layer. The result is that mixing occurs (at Least in the laboratory).

In this connection, Bretherton (1969) showed that momentum put into lee waves by drag over the Welsh hills may be absorbed far above, where association with any particular hill has been lost. In such eases, the possibility of resonant interaction prevents solution of problems by superposition, and may also lead to local breakdown of the flow in turbulent patches. (McEwan, 197'1).

In the ocean, the most vigorous events occur near the surface. However, as explained in lecture 4, strong vertical density gradients, through their correlation with strong velocity shear, tend to be less stable, and in the ocean they occur nearer the surface. Hence, as a disturbance travels downwards, the sea becomes more and more stable to it. This is reflected in the observed decrease in the proportion of turbulent patchiness downward through the ocean. (The effect should be heightened by the inability of an increasfng proportion of the disturbance to travel downward as N^2 decreases.)

Throughout these lectures we have ignored the effects of rotation. If the motions have a sufficiently small time and length scale, this should not be significant. In general, rotation may tend to extend the horizontal length scales which occur,

References

Arya, S.P.S. 1972 The critical condition for the maintenance of turbulence in stratified flows. Quart.J.Roy.Met.Soc., 98: 264-273.

Bretherton, F.P. 1969 Momentum transport by gravity waves, Quart.J. Roy.Met.Soc., 95: 213-243.

Browning, K.A. 1971 Structure of the atmosphere in the vicinity of large amplitude Kelvin-Helmholtz billows. Quart.J.Roy.Met.Soc., 97: 283-299.

Davis, R.E. and A. Acrivos 1967 The stability of oscillatory internal waves. J.Fluid Mech., 30: 723-736.

Ellison, T.H. and J.S.Turner 1960 Mixing of dense fluid in a turbulent pipe flow. J.Fluid Mech., 8: 514-544.

McEwan, A.D. 1971 Degeneration of resonantly excited standing internal gravity waves. J.Fluid Mech,, 50: 431-448.

Nichol, C.I.H. 1970 Some dynamical effects of heat on a turbulent boundary layer, J.Fluid Mech., 40: 361-384.

Prych, Harty and Kennedy 1964 M.I.T. Hydrodynamics Laboratory Report 65.

Stewart, R.W. 1969 Turbulence and waves in a stratified atmosphere. Presented at a colloquium on "Spectra of Meteorological Variables", Stocknolm. Radio Science 4: 1269-1278 (Supplement),

Taylor, G.I. 1931 Internal waves and turbulence in a fluid of variable density. Collected Works, Vol. III.

Townsend, A.A. 1957 Turbulent flow in a stably stratified atmosphere. J.Fluid Mech., 3: 361-372.

Townsend, A.A. 1967 Wind and the formation of inversions. Atmospheric Environment, 1: 173-175.

Turner, J.S. 1973 Buoyancy effects in fluids. Cambridge University Press.

Notes submitted by
John M. Huthnance

ANALYTIC CONTINUATION OF STOKES' EXPANSION FOR GRAVITY WAVES (Abstract)

Leonard W. Schwartz

The infinitesimal-wave expansion of Stokes for steady plane periodic gravity waves has been extended to very high order using the digital computer to perform the algebraic manipulations. This use of the computer to do algebra is in distinct contrast with both finite-difference and series-truncation methods in that it yields information about the analytic structure of the solution.

Each cycle of the fluid region in the physical or z-plane is mapped into a unit annulus according to

$$z = i\left[\log\zeta + a_1(\zeta - r_0^2/\zeta) + \ldots + a_n/n(\zeta^n - r_0^{2n}/\zeta^n) + \ldots\right]$$

where the inner radius r_0 may be identified with the water depth, and the transformation coefficients a^0 are to be determined by satisfying the dynamical boundary condition on the free surface. The coefficients a_n are each expanded in a power series in a global parameter ϵ. If we take $\epsilon = a_1$ we essentially reproduce the procedure of Stokes (1880), who conjectured that the convergence of the resulting series would extend to the highest wave of 120^0 crest angle, We show that this conjecture is incorrect. By examining the behavior of the ratio of power series coefficients c_n/c_{n-1} as n becomes large we demonstrate that convergence is limited by a square-root branch-point corresponding to a wave some ten percent short of the maximum. This result, that a_1 is not a monotonically increasing function of the wave height, is independent of the water depth. In computing the various power series in ϵ, typically we compute 50 to 100 terms.

By replacing Stokes' parameter a_1 with h, the dimensionless peak-to-trough wave height, we have obtained the highest wave of the proper crest angle. A power series in h is obtained whose sum is proportional to the reciprocal of the crest velocity. Since the velocity must be zero at the sharp crest, the power series should have an infinity at the corresponding value of h. We have determined that this infinity is a simple pole, Padé approximants (rational fractions) are known to represent polar singularities especially well; by recasting our series as a sequence of Padé approximants we get rapidly convergent estimates of the maximum wave height. We compute this maximum correct to 4 to 5 places for values of D/L [water depth/wave length) larger than .1. These estimates are in very close agreement with the highest-wave analyses of Michell and Havelock (extended to finite depth by Chappelear, 1959) in the region where the latter are generally considered to be valid. Moreover the present method provides accurate results for values of D/L as small as 0.01, Even this limit is dictated only by the finite word size of the digital computer used and the domain of validity in principle extends as far as the solitary wave where the mapping (1) becomes degenerate.

When D/L is less than 0.15 another square-root branch-point appears which limits convergence of the series in h to values of the Froude number less than one (based on depth), This singularity, which corresponds to imaginary values of wave height, may be mapped away with an Euler transformation. Alternately the solution may be continued past the branch-point using Padé approximants. Their domain of convergence is determined only by the presence of non-polar singularities and is not circular as is the Taylor series.

We have also determined that the maximum surface inclination increases monotonically with h, reaching the value $\pi/6$ for the peaked wave. This result is complementary to the existence proof of Kranovskii (1960).

The present work has the following features, First, virtually all free surface waves may be computed as members of a two-parameter

family of solutions. Moreover, accurate estimates of domains of convergence are provided which may suggest mathematically rigorous convergence proofs. Finally, the high accuracy of the wave profiles obtained may be useful in calibrating finite-difference methods such as the marker-and-cell technique.

AXI-SYMMETRIC RECIRCULATING FLOWS AT HIGH REYNOLDS NUMBERS (Abstract)

Jean-Yves Parlange

The laminar steady flow around an axi-symmetric object moving in a fluid is examined in the limit of a high Reynolds number. The object is assumed to be oblate rather than prolate in shape. The main feature of the flow around such an object is the existence of a recirculating wake, In most of the wake the vorticity ω is proportional to the distance r from the axis, or,

$$\omega = A r \tag{1}$$

The constant A is unknown *a priori*. In most of the region outside the wake the vorticity is zero. Along the surface of contact between the wake and the outside region there is a thin boundary layer where the vorticity varies rapidly from the value given by Eq.(1) to zero. At the bottom of the wake the boundary layer stretches along the axis and forms an additional thin wake behind the main one.

To the lowest order, i.e., in the limit of a large enough Reynolds number, the boundary layer and the thin wake can be ignored, since the energy dissipated in these thin regions is negligible compared with the energy dissipated in the wake. The energy furnished by the object moving a constant speed must be dissipated by viscosity and the rate of dissipation per unit volume is small since the Reynolds number is large. This implies that the volume of the object is small compared with the volume of the wake. The role of the object is primarily to furnish the energy necessary to maintain the steady flow. In determining the shape of the wake and the streamlines the object can then be ignored.

The problem is now reduced to finding the shape of the wake and the flow field when Eq. (1) is satisfied inside the wake and $\omega = 0$ outside the wake. Along the surface of the wake the pressure must be continuous as well as the velocity from Bernoulli's theorem. Finally the wake moves at a constant velocity in a medium at rest. The solution to this problem is remarkably simple: the wake must be a sphere, the flow inside the wake is a Hill's vortex, the flow outside the wake is the irrotational flow over a sphere.

As an example consider a bubble rising in a liquid at rest, The bubble is so large that surface tension plays no role in determining its shape. The bubble has a spherical cap shape, i.e. it has a spherical upper part and a flat lower part. The volume V of the bubble being given, the velocity U of the bubble and radius R of the wake have to be determined. From conservation of energy, viscous dissipation must equal the energy provided by buoyancy, or,

$$30\pi\nu U^2 R = gVU \qquad (2)$$

where ν is the kinematic viscosity of the liquid and g is the acceleration of gravity. In addition, a constant pressure exists within the bubble and the dynamic forces along the front surface of the bubble must be balanced by gravity, or

$$9U^2 = 4gR. \qquad (3)$$

Equations (2) and (3) complete the determination of the flow to the lowest order.

LARGE-SCALE AIR-SEA COUPLING AS CAUSE OF SHORT-PERIOD CLIMATIC FLUCTUATIONS (Abstract)

Jerome Nemias

The purpose of this talk was to acquaint oceanographers with problems posed by phenomenological studies of large-scale and long-term atmosphere-ocean coupling. The solution of these problems may go far to make feasible forecasts of abnormal oceanic and atmospheric regimes which are observed over time periods ranging from a month upward.

In the lecture, examples were shown of anomalous regimes for months, seasons, years and decades,

The space scale of sea surface temperature (SST) deviations from normal was shown to be not far different from that of surface or upper level pressure anomalies. The coupling in the two media was related to abnormal wind stress and heat exchange. However, the suggestion from the large-scale patterns in sea and air was that anomalous SST gradients may feed back into the overlying atmosphere, thereby producing zones of increased baroclinicity which boost the intensity of cyclones. The vigorous cyclones then strengthen the SST contrast. We thus are frequently confronted with positive feedback or self-amplifying systems.

The coherence of SST patterns in time was shown to be at least an order of magnitude higher than that in atmospheric pressure patterns, and it was postulated that this difference allows the sea to serve as a "memory" for the atmosphere, The "memory" is at times, particularly in summer, erased by non-representative, very shallow thermoclines. But as storminess increases in fall and winter, the anomalous water at depths of 100 to 200 m may be mixed to the surface, again to impact the atmosphere.

Synoptic examples of these air-sea interactions were shown for:

1. The 1968-69 winter when the Aleutian Low and North Pacific High were displaced far south of normal, leading to exceptionally heavy rains over central and southern California.

2. A long wave trough in the summer and fall of 1965 which slowly migrated across the central North Pacific ultimately producing November rains in Southern California. Here the movement of the trough and the thermal response of the ocean were kept "in tune".

3. The roughly decadal regimes of the winters of 1948-57 and 1958-69, -- the former characterized by warm central North Pacific water and cold U.S.Coastal water and the latter the opposite. Through complex internal dynamics it was shown that these abberations were probably responsible for the warm eastern U.S. winters of the 1950's

and the cold winters of the 1960's. An abrupt change in both North Pacific SST patterns and U.S. temperature patterns took place in the winter of 1971-72, possibly heralding a return to a U.S. temperature pattern characteristic of the 1950's.

4. Finally, some computations based on kinematics and statistics were displayed to show that at times simple advection of water around the North Pacific gyre captures the evolution of the SST anomaly patterns over a season (1971-72 winter) and that the overlying atmospheric pressure pattern might have been a response.

Perhaps a new generation of well-trained meteorological-oceanographers will develop a more quantitative deterministic model to predict long-term atmospheric and oceanic variables.

OBSERVATIONS OF RAYLEIGH-BÉNARD CONVECTION (Abstract)

John A. Whitehead

A review is given first of the experiments of Busse and Whitehead, which reported the following properties of planar cellular convection rolls:

If the Rayleigh number is above a certain critical value, to be called R_I, perfectly planar rolls of a variety of wavelengths will be stable unless a critical Rayleigh number, R_{II}, is exceeded. Above R_{II}, two sets of rolls at right angles will be stable, henceforth to be called "bimodal flow".

I have more recently conducted a study of transition to time-dependent flow. The bimodal rolls were observed to begin to oscillate above a third limiting Rayleigh number, R_{III}. By changing experimental fluids, it was found that R_{III} was proportional to the inverse of the Prandtl number, while R_{II} was independent of Prandtl number.

Scaling arguments applied to the Navier Stokes equation indicate that disturbances which go unstable independently of the Prandtl number, like the bimodal flow, receive their energy from buoyancy

forces, Likewise, if the transition is dependent upon Prandtl number, like R_{III}, the new flow bleeds kinetic energy from the original flow.

A second series of experiments was intended to explore the role of distortions to the perfect periodic convection patterns, It quickly became clear that, in the Rayleigh number range $R_I < R < R_{II}$, small "flaws" to the periodic convection lattice generated movements which would strongly decrease R_{II}, the handwidth of possible wavenumbers, so that the roll approached a relatively unique wavelength. Comparison with the theoretical computations contained in Busse (1967) has revealed that this wavelength was quite close to that which possesses maximum kinetic energy but was quite far from other maxima such as the heat transport or vorticity maximum, It has been documented that these flows travel with a velocity inversely proportional to the Prandtl number; hence it appears to be quite probable that they also acquire their energy from kinetic energy of the undisturbed flow,

At large Rayleigh number, a new flow pattern, which we call multimodal flow, develops at flaws, It seems likely that the observations by Krishnamurti of a transition to time-dependent flow at R = 50,000 in large Prandtl number fluid is connected with oscillations we have observed in these new structures,

These results suggest that an extremalizing procedure which maximizes heat flux subject to a constraint involving the $u \cdot \nabla \cdot u$ operator might have better agreement with experiment than the present upper bounding procedures,

TAYLOR COLUNNS
(Abstract)

Andrew P. Ingersoll

The interaction of horizontal flow and bottom topography in a rapidly rotating fluid may be described in terms of the Rossby number $\epsilon = V(2\Omega L)^{-1}$ the Ekman number $E = \nu(\Omega H^2)^{-1}$, the height h of the obstacle relative to the depth of the fluid, and the stratification parameter $B = N^2H^2(2\Omega L)^{-2}$. Here V is a typical horizontal velocity,

Ω is the basic rotation rate, L and H are the horizontal and vertical length scales, respectively, ν is the kinematic viscosity of the fluid, and N is the Brunt-Väisälä frequency, If the flow is incident on an isolated obstacle (e.g., a circular mountain attached to the lower boundary), the streamlines may be either open (terminating at infinity) or closed (confined to the region above the obstacle). The pattern of streamlines depends on the values of the non-dimensional parameters ϵ, E, h, and B, and on the upstream flow condition.

In the limit of rapid rotation with zero stratification ($1 \gg \epsilon \gg E$, $B = 0$), the flow is approximately 2-dimensional, with streamlines independent of the vertical coordinate. The inviscid limit is obtained by setting $E = 0$, but then the solutions are not unique in the steady state. That is, potential vorticity is conserved along streamlines, and is determined by the upstream flow condition except on closed streamlines. On closed streamlines, which occur whenever the non-dimensional height h of the obstacle exceeds $0(\epsilon)$, the potential vorticity is arbitrary as long as the fluid is inviscid ($E = 0$). This arbitrariness may be removed by re-introducing viscosity such that ($1 \gg \epsilon \gg E^{1/2}$). Then the region of closed streamlines "spins down" due to Ekman layer suction, leading to stagnation everywhere inside the critical streamline. The critical streamline is then a free surface whose location is determined by the condition that both the normal and tangential components of velocity vanish on its boundary. This is the quasi-inviscid case treated by Ingersoll.

Other interesting cases which have been studied by various people with varying degrees of success include 1) viscous flow ($1 \gg E^{1/2}$, $\epsilon = B = 0$) treated by Jacobs, 2) inviscid flow with stratification ($1 \gg \epsilon$, $E = 0$, $B \approx 1$) treated by Hide and by Hogg, 3) flow on a β-plane and flow with upstream vorticity treated by Cottrell and Ingersoll. These cases may have relevance to flow around islands in the ocean, and to flow around Jupiter's Great Red Spot.

References

Taylor, 1923 Proc.Roy.Soc. A104: 213,

Hide, 1961 Nature 190: 895.

Jacobs, 1964 J.F.M. 20: 581.

Ingersoll, 1969 J.Atm.Sci. 26: 744.

Vaziri and Boyer 1971 J.F.M. 50: 79.

Hide, 1971 J.F.M. 49: 745,.

Hogg, 1970 G.F.D. (W.H.O.I.) and preprint 1972.

Cottrell, 1971 G.F.D. (W.H.O.I.).

VORTEX RINGS, THERMALS AND TURBULENT INTERFACES
(Abstract)

Tony Maxworthy

Although we are ultimately interested in the asymptotic state of vortex rings produced at a circular orifice, a brief review of the initial stages is appropriate. Turner (private communication) has shown that for a slug of fluid of given mass, momentum, energy and circulation ejected from an orifice, one and only one resulting inviscid ring is possible. The rings have all their vorticity concentrated into a core region. Experimental work by Sullivan and Widnall at M.I.T. (private communication) tends to confirm part of this picture. Vortieity is mainly concentrated in a core but there is evidence for a weak distribution of vorticity throughout the rest of the region of moving fluid. This latter picture is therefore, not in disagreement with the results of the present author (J.F.M. 51:1 (1972)) which required that the diffusion of the distributed vorticity be the mechanism whereby outer, stationary irrotational fluid becomes rotational and is entrained into the moving sing,

All rings, except the very smallest (initial Reynold's number, based on ring diameter, below 600) then become unstable. Azimuthal waves form on the core, the wave number depending on the size of the core and the vortieity distribution. An elegant inviscid theory has been forwarded by Sullivan and Widnall which seems to account for many

of the observed features of the initial instability. The core distortions reach finite amplitude and the core becomes turbulent; it then appears to regain its laminar form with only unsteady wave motions travelling azimuthally. These wave motions in turn induce axial flows within the core. However it does not appear to go through any other instabilities even though it seems to be within the instability boundaries of the inviscid theory. The outer regions of the moving fluid appear to be turbulent,

Extension of this author's entrainment ideas to the case of a turbulent ring predicts that the ring velocity (V) should vary as $t^{-3/4}$ or X^{-3} (where t and X are elapsed time and distance from the "virtual origin" of the motion). Recent experiments suggest that this picture is close to reality for rings that have passed through the instability phase.

Further extension to the case in which buoyancy acts to increase the ring impulse gives $V \sim t^{-1/2}$ for both laminar and turbulent entrainment.

The experimental results for this case are considerably more complicated because they also depend critically on the diffusivity of the buoyancy-producing agent, If it diffuses slower than momentum (salt ring into water) then a torus of buoyant fluid is formed which stays with the ring. If buoyancy diffuses faster than momentum (a helium ring into air) then all of the buoyant fluid is left behind in a wake behind the moving ring. In the former case experiments have shown that the ring velocity decreases only very slowly over the length of the tank and the variations predicted for turbulent rings are hard to verify or deny.

Observations of the details of entrainment by turbulent interfaces show that the diffusion of vorticity into the outer irrotational fluid followed by reingestion of this vorticity and new fluid is a plausible mechanism for explaining the observations.

WATER MOVEMENT IN POROUS MEDIA: PART I
(Abstract)

Jean-Yves Parlange

Solving the diffusion equation for variable diffusivity. As an example the method is applied explicitly to the one-dimensional diffusion equation,

$$\frac{\partial \theta}{\partial t} = \frac{\partial}{\partial z}\left[D(\theta)\frac{\partial \theta}{\partial z}\right]. \tag{1}$$

The diffusivity D is a given function of the water content θ at a point z and a time t. To simplify the problem even further the following boundary conditions are taken,

$$t \leq 0;\ \theta = 0 \tag{2}$$

$$t > 0,\ z = 0;\ \theta = 1 \tag{3}$$

For these boundary conditions a similarity solution exists with a reduced variable ϕ,

$$\phi = z t^{-1/2} \tag{4}$$

Equation (1) becomes

$$-\frac{1}{2}\phi\frac{d\theta}{d\phi} = \frac{d}{d\theta}\left[D\Big/\frac{d\phi}{d\theta}\right] \tag{5}$$

Integration of this equation between $\theta = 0$ and 1 gives,

$$-\frac{1}{2}\int_0^1 \phi\, d\theta + \left[D\frac{d\theta}{d\phi}\right]_{\phi=0} = 0 \tag{6}$$

This last equation indicates that the average order of ϕ is equal to $\left[D(d\theta/d\phi)\right]_0$. The second term of Eq.(5) can be expanded and in particular yields the term $(dD/d\theta)(d\theta/d\phi)$ which is much larger than ϕ if

$$(dD/d\theta)/D >> 1 \tag{7}$$

For instance the diffusivity can be approximated in many cases by $D \approx A \exp B\theta$ with $B \sim 10$ and inequality (7) holds since $B >> 1$. Inequality (7) holds in general and to the lowest order Eq.(5) can be replace by

$$\frac{d}{d\theta}\left[D\Big/\frac{d\phi}{d\theta}\right] \simeq 0 \tag{8}$$

Then

$$\phi \simeq \lambda\int_0^\theta D(\alpha)\,d\alpha\,. \tag{9}$$

This expression can be used to estimate the first term in Eq.(5) and also to construct an approximation to that equation better than Eq.(8), or,

$$\int_{\lambda}^{1} D(\alpha)d\alpha + \frac{d}{d\theta}\left[D \Big/ \frac{d\phi}{d\theta}\right] = 0 \qquad (10)$$

This equation is easily integrated and the unknown constant λ is chosen to satisfy Eq.(6) or, altogether

$$\phi \simeq \left[2\int_0^{\theta} \theta D d\theta \Big/ \int_0^{1} \frac{\gamma D d\gamma}{\int_0^{\infty} d\beta \int_{\beta}^{1} D(\alpha)d\alpha}\right]^{1/2} \int_{\theta}^{1} \frac{D d\gamma}{\int_0^{\infty} d\beta \int_{A}^{1} D(\alpha)d\alpha} \qquad (11)$$

It is clear that an iterative scheme can be set up to yield even better approximations. In the case of D constant Eq.(11) becomes,

$$D^{-1/2}\phi \simeq [2 \ln 2]^{1/2} \ln[(2-\theta)/\theta] . \qquad (12)$$

Table 1 compares this approximation with the exact solution, which is the well-known co-error function when D is constant. The agreement is fairly good even though Eq.(11) was derived for the case of D varying rapidly rather than constant. Hence when D does vary rapidly, Eq.(11) is always an excellent approximation, e.g. within 1% of the exact solution. The method presented here can be generalized to multidimensional problems and for general boundary conditions.

θ	1	0.9	0.8	0.7	0.6	0.5	0.4	0.3	0.2	0.1	0
$D^{-1/2}\phi$ Eq.(12)	0	0.171	0.344	0.526	0.719	0.933	1.177	1.474	1.866	2.500	∞
$D^{-1/2}\phi$ exact	0	0.178	0.358	0.545	0.742	0.954	1.190	1.466	1.812	2.326	∞

Table 1. Comparison of $D^{-1/2}\phi$ as given by Eq.(12) for D constant with the exact solution.

WATER MOVEMENT IN POROUS MEDIA: PART II: GRAVITY DRIVEN INSTABILITY (Abstract)

Jean-Yves Parlange

The one-dimensional movement of water in a porous medium obeys the equation

$$\frac{\partial \theta}{\partial t} + \frac{\partial K(\theta)}{\partial z} = \frac{\partial}{\partial z}\left[D(\theta)\frac{\partial \theta}{\partial z}\right] \qquad (1)$$

This equation differs from the one considered in Part I by the addition

of the term $\partial K/\partial z$ representing the influence of gravity. The conductivity K is a given function of the water content θ (notations are as in Part I). The method developed in Part I can be applied here: A first approximation is obtained by neglecting $\partial\theta/\partial t$ in Eq. (1) yielding,

$$z = -\int_{\theta}^{1} d\alpha\, D(\alpha)/(K(\alpha)+C(t)), \tag{2}$$

with the boundary conditions

$$t<0;\ \theta=0 \tag{3}$$

$$t\geq 0,\ z=0;\ \theta=1. \tag{4}$$

The unknown function C(t) is equal to the flux of water at the surface z = 0. C(t) is chosen so that the overall conservation equation, i.e. the equation obtained by integrating $z(\theta,t)$ over the whole space, be satisfied by $z(\theta,t)$ as given by Eq. (2). It is then found that

$$t=\int_{\theta}^{1}\theta\, D K^{-2}\left[\ln(K+C)/C - K/(K+C)\right]d\theta \tag{5}$$

At any given time there exist two values of C. One, approaching zero as $t \longrightarrow \infty$, corresponds to the capillary rise of water. The other, approaching $-K_1$ as $t \longrightarrow \infty$, corresponds to the downwards infiltration of water. (K_1 is the value of the conductivity for $\theta = 1$). For this last case C(t) also satisfies, as shown by Eq. (5),

$$-C(t) \geq K_1 . \tag{6}$$

This inequality guarantees that the front remains one-dimensional, i.e. stable, as it moves downwards. Instability can occur only if the front is slowed down by some outside agent and the flux is less than K_1.

Infiltration experiments were conducted in the laboratory with a layer of fine sand covering a layer of coarse sand. For this situation the flux of water is primarily determined by the properties of the fine sand. It is possible then to impose a flux which is less than the conductivity at saturation in the coarse sand (K_1). The front moving downwards in the coarse sand should be unstable. Experimentally it is found that water moves from the fine to the coarse sand only after the layer of fine sand is saturated with water. At the interface between the

layers, fine grains of sand are packed between the large grains, forming an interface almost impervious to water movement. Only after the fine layer is saturated with water does the water have enough of a pressure head to force its way through the interface in any measurable amount. The movement in the coarse layer is one-dimensional at first but irregularities develop. Eventually "fingers" are formed which carry all the water downwards.

The fingers have a width which is determined by the properties of the coarse sand. The fingers move downwards at a speed equal to K_1. This indicates that the sand in the fingers is essentially saturated with water. It is possible to fix the position of the fingers by creating artificial imperfections at a given point of the interface. In general the water passing through the interface tends to disrupt it by creating openings at the weakest points. Eventually the water moves mostly through those openings, feeding the fingers underneath.

The situation is similar to the infiltration of water through a slab of porous material of finite thickness, Once the slab is saturated with water any additional water drips out of the slab at points where imperfections are present. When coarse sand is added underneath the slab, drops cannot form since the water is absorbed immediately by the coarse sand and as a result fingers are formed.

EXPERIMENTS ON DOUBLY DIFFUSIVE CONVECTION
(Abstract)

William R. Lindberg

Preliminary results of an experiment* in doubly diffusive convection are presented. The experiment employs a volume of water bounded by porous horizontal boundaries and insulated vertical sidewalls. The two diffusing species which contribute to the internal density gradient (one gradient is stabilizing and the other destabilizing) are maintained by diffusion across the membranes from constant

property reservoirs into the convecting system, In the present experiment, the stabilizing species (salt) has a mueh smaller molecular diffusivity than the destabilizing gradient (temperature).

"Quasi-steady state" layers (regions of large density gradients separated by regions of small density gradients) are found to exist for sufficiently high stability numbers ($\beta_c \Delta C / \beta_T \Delta T$) and thermal Rayleigh numbers ($g \alpha \Delta T L^3 / \nu K$). Experiments have been performed with the layered structure remaining essentially stationary for periods up to four weeks.

To date, thick layers have been the most carefully studied. These layers are characterized by a central non-convecting region bordered by boundary layers which are convecting into deep regions of essentially constant mean density. The layered regions exhibit tank seiche and internal wave motions along with apparent turbulent fluctuations which are intermittent in character, Transport (flux) estimates across the layered regions show general agreement with those of Turner (1965), while the fluxes in the convecting region (bounded by the conduction layers) appear to increase with thermal Rayleigh number and decrease with stability number, Insufficient measurements of transport have yet been made to compare with some theoretical arguments of Lindberg (1971) and Huppert (1972), although the not-surprfsing predicted trends are observed. Some verification of Huppert's (1971) analysis of layer stability was noted, however.

References

Huppert, H.E. 1971 On the stability of a series of double-diffusive layers. Deep-Sea Res. 18 (10): 1005-1022.

Huppert, H.E. 1972 The mean-field equations in double-diffusive eonvection, W.H.O.I.-G.F.D. Notes.

Lindberg, W.R. 1971 An upper bound on transport processes in turbulent, thermohaline convection. J.Phys.Oceanog. 1 (3): 187-195.

Turner, J.S. 1965 The coupled turbulent transport of salt and heat across a sharp density interface, Int.J.Heat Mass Transfer 8: 759-767.

*Note: These experiments are presently being conducted by Dr. R.D.Haberstrok and colleagues at Colorado State University and the material presented here constitutes part of a master's thesis by Mr. James Broughton at Colorado State University.

TRACER DISTRIBUTION IN THE ABYSS
(Abstract)

George Veronis

In an earlier paper (Kuo and Veronis, Deep-Sea Res. 1970) Stommel's abyssal circulation model was used to determine the velocity field for the abyssal World Ocean, given a uniform upwelling through a level surface at 2 km depth and equal sources in the polar regions of the North and South Atlantic. This velocity distribution was then used as a known field in the adveetive-diffusive-decay equation for oxygen and ^{14}C to determine the distribution of the tracer whose values are given in the source regions. The calculation was restricted to small values of the Peclet number beeause the numerical relaxation method broke down for larger values. A non-centered, weighted difference scheme was used to circumvent the problem of numerical instability so that results could be obtained for all realistic values of the Peclet number. The results of the calculation indicate that a best choice of parameters (i.e., that choice that gives best agreement with the observed distribution of dissolved oxygen) is:

horizontal mixing coefficient = 6×10^{7} cm^{2} sec^{-1},
vertical upwelling = 1.5×10^{-5} cm sec^{-1},
oxygen consumption = 2×10^{-3} ml l^{-1} yr^{-1},
Antarctic recirculation transport = 35×10^{7} m^{3} sec^{-1}.

CONVECTION AT THE MELTING POINT:
A THERMAL HISTORY OF THE EARTH'S CORE
(Abstract)

Willem V.R. Malkus

Higgins and Kennedy (1971) concluded that the Earth's fluid core has a stable stratification if it is at its melting point. Busse (1972) and Elsasser suggested as an alternative that a hydrostatic-isentropic distribution of particulate solid can produce neutral stability in a partially molten core. Here this suggestion is quantified and a determination is made of the efficiency of the production of fluid motion

from the heat flux. This is used to establish that macroscopic convection can exist only if the particulate solid is of sufficiently small size. A thermal history of the core compatible with upper mantle heat flux is advanced in which it is suggested that the inner core is a fairly recent feature. The implication of these results for convection-driven and precession-driven dynamos is that both can function for a small enough suspended particulate, that the convection-dynamo will fail for particles greater than one micron in diameter, and that the precession-driven dynamo probably can not survive particles greater than ten microns in diameter. Various alternatives to these conclusions are discussed. Each alternative requires that the premise of an inner-core core-fluid interface at the melting point be abandoned.

LABORATORY OBSERVATIONS OF SHEAR INSTABILITY AND TRANSITION TO TURBULENCE IN A STRATIFIED FLUID
(Abstract)

Frederick K. Browand

Certainly shearing motions are an important source of turbulence in the atmosphere and oceans. Both turbulence production and the structure of the resulting turbulence are strongly affected by the presence of stable stratification. What follows is an attempt to understand the effect of stable stratification upon the instability of a simple, unbounded shear layer. The geometry is sketched below. Two laminar, horizontal streams having different velocities and salinities are merged downstream of a splitter plate. Reynolds numbers based upon shear layer thickness, h, are 40-300. Since the diffusion rate of salt is much smaller than the rate of momentum diffusion, the ratio of thickness, h/δ is initially about 16,

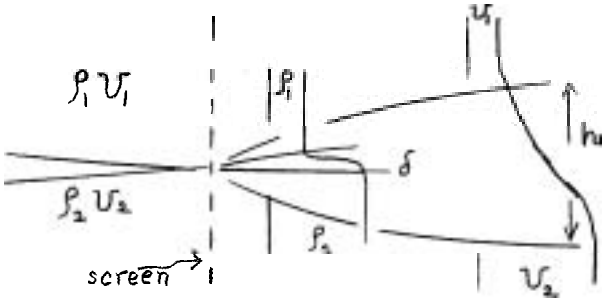

Such a flow is observed to be unstable for a wide range of Reynolds numbers and Richardson numbers ($J_0 = g\frac{\Delta\rho h}{\rho(\Delta U)^2}$). Theoretically, Holmboe (1962) considered the case $h/\delta \longrightarrow \infty$, $R_e \longrightarrow \infty$, and approximated the shear layer as a region of constant vorticity, He showed that two distinctly different modes of instability are possible. One mode is similar to the instability occurring in the absence of a density difference, and could be called the Rayleigh wave. The Rayseigh wave is less unstable when the interface is added. However, a second mode is actually destabilized by the presence of the interface, as described by Holmboe, and might be called the Holmboe wave. As a result of their different dynamical origins, the two waves break differently. Rayleigh waves break by rolling up and concentrate the shear layer vorticity into discrete lumps along the interface. Holmboe waves do not roll up but rather become sharply peaked at the crests. In breaking, fluid is torn away at the crests similar to the breaking of a surface wave in deep water. The reason for the difference can be explained by allowing the unstable wave to be the superposition of three disturbances -- two riding along the boundaries of the constant vorticity region, and one riding the interface. At sufficiently low Richardson number, the three waves can lock in phase, which allows the growing disturbance to pinch off lumps of vorticity (Rayleigh wave).

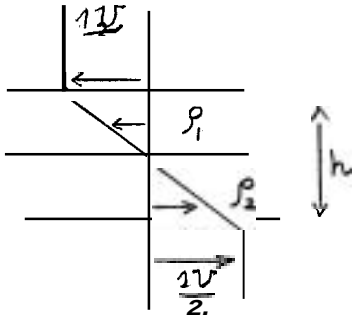

At higher Richardson numbers, the phase locking is no longer possible. The two waves at the boundaries of the shear layer now travel in oppo-

site directions and the interface performs a standing oscillation of increasing amplitude (Holmboe wave).

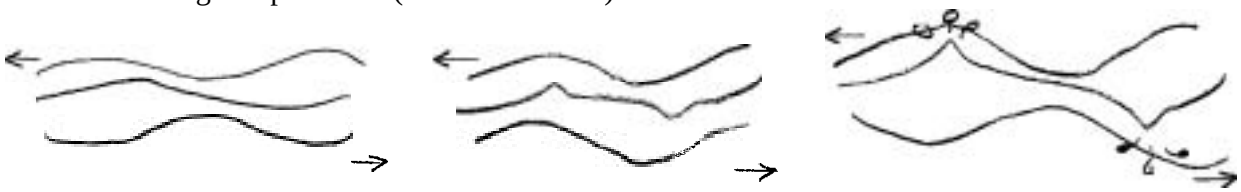

The breaking of Rayleigh or Holmboe waves produces an irregular flow with smaller scales of motion. When the initial Richardson number is low $J_0 \approx .02$ the following events are seen to occur in the developing shear layer.

1. Rayleigh waves grow and pinch off lumps of vorticity. Small scale turbulence is produced within the lumps -- probably due to overturning.
2. Adjacent vortical lumps combine to form larger vortical lumps with twice the original spacing.
3. Vortical lumps can no longer pair, and the vortfcity within the lumps is redistributed along the interface. The collapse generates Holmboe waves which grow for a time.
4. Eventually the Holmboe waves decay as does the residual small scale turbulence, and the shear layer approaches a laminar flow.

This is in marked contrast to the homogeneous case in which adjacent vortical lumps continue to pair to provide the mechanism of growth for the shear layer (C.D. Winant, Ph.D. Thesis, USC). One would conclude that any density difference, however slight, is sufficient to eventually destroy the turbulent shear flow and bring a return to the laminar state. This self-destruction might explain the strongly intermittant character of turbulence production observed in the oceans and atmosphere.

NONLINEAR INSTABILITY OF PLANE POISEUILLE FLOW
(Abstract)

Edward A. Spiegel

We expand the equations describing plane Poiseuille flow in Fourier series in the coordinates in the plane parallel to bounding walls. These results an infinite system of equations for the amplitudes which are functions of time and of the crossstream coordinate. This system is drastically truncated and the resulting set of equations are solved accurately by a finite difference method. Three truncations are considered: (I) a single mode with only dependence on the downstream coordinate and time, (II) the mode of I plus its first overtone, (III) a single three-dimensional mode. For all three cases, for a variety of initial conditions, the solutions evalue to a steady state as seen in a particular moving frame of reference. No runaways are encountered.

For Reynolds numbers below a critical value (2707 in case II) any initial disturbance to the parabolic profile dies away. For Reynolds numbers (R) and disturbance wavenumbers (α) for which linear theory predicts instability, an initial disturbance of any amplitude goes to a particular, steady, finite-amplitude solution, For R greater than the critical value mentioned above, but outside the linear instability region, "subcritical instability" occurs for wavenumbers in a given band. That is, if the initial disturbance to the parabolic profile has an energy (E) above a critfcal value, a steady finite-amplitude solution is achieved as in the unstable case. There is also a second finite-amplitude steady solution with E equal to the critical value. This is the subcritical solution discussed by several others and it is always unstable.

The location of these steady finite-amplitude solutions in R-α-E space is mapped out and their properties are outlined. The connection of these solutions to previously discussed ones is briefly indicated and the question of the relevance of them to the development of observed instabilities is broached,

THERMOCLINE MICROSTRUCTURE: FIELD MEASUREMENTS IN A FRESH WATER RESERVOIR

(Abstract)

Frederick K. Browand

Measurements of vertical thermal structure in a fresh water reservoir have been made over a one-year period. The reservoir, near Los Angeles, is approximately 1½ miles in length, 600-1000 feet in width, with water depths between 100-200 feet. The thermocline has a temperature difference of as much as 15°C during the summer months. The gross structure of the thermocline varies with the season, and four quite distinct shapes can be identified. Fall and spring thermocline shapes are similar, with a well-mixed surface layer and a

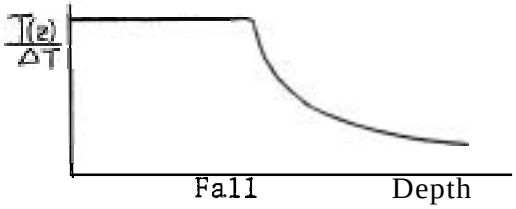

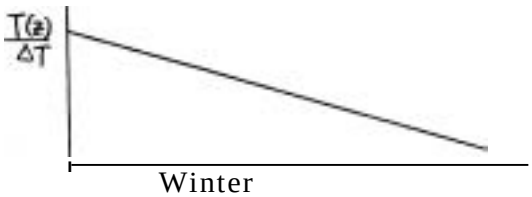

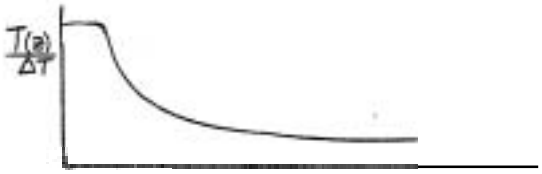

relatively sharp thermocline. The well-mixed layer is mueh deeper in the fall, however. In the summer, the sharp thermocline is replaced by a much broader region of nearly linear temperature variation. In the winter only a very small temperature difference exists ($\approx .5^{\circ}C$) and the profile is nearly linear over the entire water mass.

A rich microstructure, similar to the sheets and steps observed in the ocean, develops in the spring and remains until winter. It can be concluded that double diffusion, tidal motions, and significant surface wave activity, all absent in the reservoir, are not essential to the formation of this typical sheet and step structure. Also, the scales observed in the summer are not much different from those observed

by Woods in the Mediterranean, with sheets of order 10-20 cm and steps of order 1.0 meter predominating. There is evidence that sheet and step sizes do scale at least roughly with the thermocline thickness, whish is smaller in spring and fall. Sheets of 10-20 cm thickness are observed to have life times of at least several hours. The appearance and disappearance of sheets has been noted, but is not yet understood. Internal wave motions have been measured with peak-to-peak amplitudes of 10-20 cm in the summer and approaching one meter in the fall. The sporadic internal wave activity appears grouped into two frequency bands -- one band centered around one cycle per hour, and one with frequencies of three to six cycles per hour. These frequencies are in qualitative agreement with the lowest longitudinal and lateral interfacial sloshing modes for the reservoir.

SHEAR FLOW INDUCED BY A MOVING HEAT SOURCE: A MODEL OF VENUS' 4-DAY CIRCULATION (Abstract)

E. John Hinch

The flow induced by a periodic moving heat source is studied, with particular interest in the rectified component created by the propagating wave, This is Schubert and Whitehead's dynamical model of Venus' 4-day atmospheric circulation.

Two basic problems to be answered are the direction of the mean flow (opposite to the thermal wave for Venus) and its magnitude (30 times the wave speed for Venus), How do the vertical buoyancy forces generate horizontal momentum? How can the fluid move so much faster than its forcing?

The direction of the mean flow can be determined and understood from the linearized analyses, The key to the physics is the tilt in the convection cells, The tilt reflects the finite speed of which the information that the thermal wave is not stationary can travel away from the fixed boundaries. The details of the formation of the tilt due to thermal diffusion, vorticity diffusion and boundary layer

pumping were presented. For the Venus model with a heat flux at the upper boundary, the direction implies that the fluid motion penetrates to the bottom rigid boundary and that the thermal tilting is small,

Although the fluctuating velocities may be small compared with the wave, the mean flow can be larger. The small Reynolds stress must balance a shear stress: when the viscosity is small enough, the mean shear rate becomes compensatingly large, Because the mean flow can be large when the fluctuations are small, the nonlinear mean field equations are an appropriate asymptotic system to consider,

Finally a problem was solved with a periodic moving heat flux at an upper rigid-slippery boundary, with small viscosity and small thermal tilting, using the mean field equations. The problem could be reduced to a third order nonlinear ordinary differential equation in the mean flow with a single parameter which could be related to the external parameter group through various integrations of the mean flow itself. The asymptotic solution for strong streaming was given, The answer exhibits Malkus' doppler shift reduction.

Applying the results to Venus gives a fair prediction of the temperature fluctuations and the mean flow. The mean field linearization was not however applicable. There must also be some doubts about the neglect of stratification and the existence of a convenient rigid lower surface.

CHEMICAL OSCILLATIONS, DIFFUSION AND SPONTANEOUS PATTERN FORMATION (Abstract)

Louis N. Howard and Nancy J. Kopell

Spontaneously forming spatial patterns such as salt layers and Bénard cells are well-known phenomena of hydrodynamics, A chemical oscillator, discovered by Belousov (1), provides a simpler example in which diffusive effects combine with nonlinearities to cause the formation of regular spatial inhomogeneities, The inhomogeneities are seen as patterns of blue and purple when the appropriate indicator is added.

If a thin layer (about 2 ml) of fluid is mixed up and allowed to stand undisturbed, round target patterns of evenly-spaced blue and purple rings appear in the fluid. The rings propagate outward, The spacing and propagation speed are uniform within each pattern, but vary from pattern to pattern. At each point in the fluid there is a temporal oscillation, the frequency being uniform within each pattern, and higher than in the surrounding undifferentiated fluid. Some of these features were described by Zaiken and Zhabotinsky (2).

It is our hypothesis that the observed features of the patterns can be derived as consequences of equations describing the interaction of the chemical kinetics and diffusion. Despite detailed work by chemists (e.g. (3)), the kinetic equations of this very complicated system are not known (in enough detail to be usable]. Our method is to show that the patterns can be formed whenever the kinetic equations belong to a large class of systems having some simple mathematical properties, and to look for experimental corroboration of these properties. We also attempt to check experimentally the qualitative predictions of the overall equations of kinetics plus diffusion. For convenience, we assume that the diffusion constants are all the same; we think that the differences among diffusion rates is not an important mechanism for the phenomenon we are studying,

Very briefly, the mathematical assumptions are as follows: We study a reduced system of kinetic equations which deals only with the small number of rapidly varying concentrations and fixes the rest, possibly at non-equilibrium values. We ignore the slow drift of those values toward their stable equilibrium. We require first, that the reduced system

$$\frac{d\bar{x}}{dt} = F(\bar{x}), \quad \bar{x} = (x_1, \cdots x_n), \quad F = (f_1, \cdots f_n)$$

have an unstable equilibrium point at which the linearization has a pair of complex-conjugate eigenvalues with positive real part, It can then be shown by the Hopf bifurcation theorem, that the equations

$$\bar{x}_t = F(\bar{x}) + k\nabla^2\bar{x} \qquad (k \text{ the diffusion constant})$$

have a one-parameter family of periodic solutions of the form

$$\bar{x}(t,\bar{z}) = \bar{y}(\sigma t - \bar{\alpha}\cdot\bar{z}),$$

i.e., plane wave solutions. (Here $\bar{z}$ is the two-dimensional spatial variable.) Each of these solutions has an associated frequency σ and a wave number $\alpha = |\bar{\alpha}|$; the dispersion function relating these can be calculated by perturbation methods from the kinetic equations. The other major requirement is that this dispersion function $L(\sigma) = \alpha^2$ satisfy $L' > 0$ near the bifurcation parameter values σ_0 and α_0. This forces the kinetic equatfons to be highly nonlinear.

We have experimental evidence that there is a one-parameter family of target patterns (i.e., σ and α do not vary independently) and the dispersion relation does satisfy $L' > 0$. Excluding the very centers, these patterns appear much like plane wave solutions in their regular spacing and uniform frequency.

Using the above hypotheses, one can study solutions to the equations representing slowly varying waves, and use these to study the evolution of the patterns as well as to explain their roundness. One can also get solutions which represent the whole developed target pattern.

The full initial value problem is still not understood. A key difficulty is understanding in detail the propagation of the pattern into undifferentiated regions, which causes the overtaken portions to oscillate faster. However, some aspects of the initial value problem can be crudely understood in terms of the nonlinearities of the kinetics forced by $L' > 0$, even without diffusive interaction. In such a nonlinear system, the time necessary for one "full cycle" is not a fixed constant; rather, there is a whole range of possible "frequencies". If the initial scale of heterogeneity is large enough, the points of the fluid act, for a short time, as uncoupled oscillators having different frequencies. It can easily be shown that, under such circumstances, there is a tendency to form structures of continually decreasing size. We believe that the final size of the rings in the

Belousoz fluid is a balance between that tendency and diffusion, as it is in the plane wave solutions of our mathematical model.

References

Belousov, Sborn. 1959 referat.radiats.med. za 1958, Midgiz, Moscow,

Zaikin and Zhabotinsky, 1970 Nature, 225: 535.

Field, Koros and Noyes 1972 J.Amer.Chem.Soc. 94: 1394,

STRATIFIED EKMAN BOUNDARY LAYER MODELS - BOTTOM AND TOP (Abstract)

Rory Thompson

1. Introduction. In many geophysical fluid dynamic models, dissipation is necessary. Physically, the dissipation is controlled by small-scale turbulent processes which are not well understood. A common way to model the effect of turbulence is to assume some arbitrary "eddy viscosity", usually constant, and often chosen so as to make the final answer "look right". Here is a simple attempt to parameterize the turbulence without allowing free parameters.

In many fluid problems, there is little transfer of conserved quantities until some physical number exceeds a critical value, when turbulence will rather suddenly grow, and transfer a great deal, tending to decrease the number. This suggests a "hard limiting" approach: there will be no transfer when the number (Rayleigh, Rossby, Froude, etc.) is below critical; but there will be so much above critical that an adjustment back to critical is forced, on a time scale which is short compared to that of the large-scale physics, In many problems this approach will be simpler and less arbitrary than assuming an eddy diffusivity, and may be more physically correct as well, in that the instability is explicitly recognized,

2. Bottom layer. Think of a geostrophic flow U of a stratified fluid over a horizontal surface. The rubbing against the surface will cause turbulence which will mix the fluid near the surface, forming a layer with relatively homogeneous properties, capped by an inversion with a

strong shear. Adopt a "momentum-integral" model, as sketched in Fig.2.1:

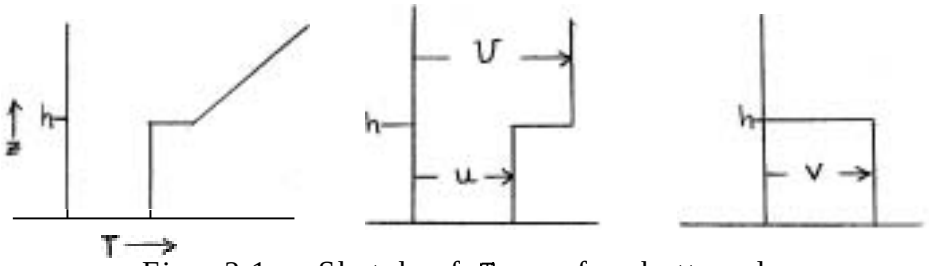

Fig. 2.1. Sketch of T,u,v for bottom layer.

so (potential) temperature is T, x-velocity is u, and y-velocity is v up to height h, at which there is a jump to the internal values. For definiteness, take the initial temperature (in Boussinesq approximation) to be Γz, and the geostrophic velocity U to be constant and in the x-direction.

Then the surface drag is $-c_D \underset{\sim}{u}|\underset{\sim}{u}|$, where the drag constant c_D is about 0.0018 (Deacon and Webb, 1962) for wind over the sea. The drag across the interface at height h is taken to be due only to entrainment, so is $(\underset{\sim}{u} - \underset{\sim}{U})\, dh/dt$. Integrating across the layer, we have the equations for conservation of momentum:

$$h \frac{du}{dt} = fhv - c_D u \sqrt{u^2 + v^2} - (u - U)\frac{dh}{dt} \qquad (2.1)$$

$$h \frac{dv}{dt} = -fhu - c_D v \sqrt{v^2 + u^2} - v \frac{dh}{dt} + fhU , \qquad (2.2)$$

where the last term in (2.2) is the pressure gradient. If there is no heating, the temperature is simply

$$T = \Gamma h/2 \qquad (2.3)$$

The system of equations will now be closed by an assumption that the layer Richardson number based on the jumps across the interface shall not be allowed to drop below 1, and while the layer is deepening, remains at critical:

$$\propto g(\Gamma h - T)h = (u - U)^2 + v^2, \qquad (2.4)$$

where $\propto$ is the expansivity and g is gravity. Richardson used essentially this criterion for maintenance of turbulence based on a Richardson number. Pollard, Rhines, and Thompson (1972) give further discussion

of a similar case.

The system ((2.1) - (2.4)) is nonlinear, but it turns out one can solve the steady problem. With $d/dt = 0$, one can eliminate the square root between (2.1) and (2.2) to get

$$u^2 + v^2 = uU.$$

This means (u,v) must fall on a circle as sketched in Fig. 2.2:

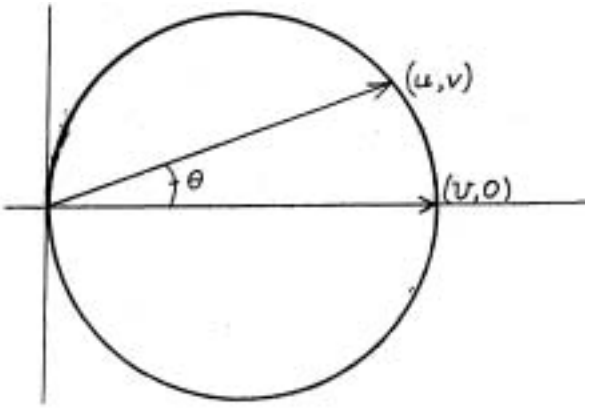

Fig. 2.2 - Relation of layer wind to geostrophic wind.

Defining

$$c = \frac{c_p}{f}\sqrt{\frac{\alpha g \Gamma}{2}} \quad , \tag{2.5}$$

one can show

$$u = \frac{U}{1+c} \tag{2.6}$$

$$v = U\frac{\sqrt{c}}{1+c} \tag{2.7}$$

$$h = U\sqrt{\frac{2}{\alpha g \Gamma}}\sqrt{\frac{c}{1+c}} \quad . \tag{2.8}$$

Thus the boundary layer flow is at an angle $\theta = \arctan\sqrt{c}$ to the geostrophic, with a component toward low pressure.

3. Typical values. Thinking of the tropical trade inversion, one might try $U \sim 15$ m/sec, $\Gamma \sim 2^{\circ}C/km$, $\alpha \sim 1/300^{\circ}C$, $f \sim 3.8*10^{-5}sec^{-1}$ (15° latitude) to get $c \sim 0.3$, $u \sim 12$m/sec, $v \sim 6$ m/sec, $\theta \sim 28^{\circ}$, $\Gamma h - T \sim 1.2^{\circ}C$, and $h \sim 1.2$ km, which is rather thick for a boundary layer, but not much thinner than the height of the trade inversion. If the latitude is reduced to 10°, the results do not change greatly

in that $u \sim 11$ m/sec, $v \sim 7$ m/sec, $\theta \sim 33^{\circ}$, and $h \sim 1.4$ km.

4. "Ekman Transport". Equations (2.7) and (2.8 imply a definite mass flux across isobars, namely

$$hv = \frac{c_D U^2}{f} (1 + c)^{-1.5} . \qquad (4.1)$$

The most important feature of (4.1) is that it is definite; in a given physical circumstance, there are no adjustable parameters. Another feature of (4.1) is that the dependence of the transport on the stratification is rather weak. Noting that typical values of c are rather small, especially for the ocean, the boundary layer transport is given in first approximation by

$$\int v \, dz = c_D U^2 / f . \qquad (4.2)$$

This simple form is independent of the stratification, despite the very existence of the layer depending on the stratification.

The transport of an Ekman layer would be $U\sqrt{\nu/2f}$, so the effective viscosity to give the transport (4.2) is

$$\nu = \frac{2\,(.0018)^2\,U^2}{f} . \qquad (4.3)$$

Typical values of U and f yield a typical value for ν of 10^5 cm^2/sec for the atmospheric bottom boundary layer, 6 cm^2/sec for the oceanic bottom boundary layer.

Assuming equilibrium and $\underset{\sim}{U} = \hat{k} \times \nabla p/(f\rho)$, the vector form of (4.2) gives the flux across isobars as

$$\underset{\sim}{F} = \frac{c_D}{f^3 \rho^2} |\nabla \rho| \nabla \rho . \qquad (4.4)$$

The easiest way to numerically calculate the divergence is probably to compute this flux, and then to take the divergence directly. This then gives an Ekman drag.

5. Time-dependence. While (2.6-8) give the steady solution to (2.1-4), it is necessary to show this steady solution is relevant. Non-dimensionalizing u and v by U, t by f^{-1}, and h by $U\sqrt{2/(\alpha g \Gamma)}$ transforms (2.1-4) into

$$h\frac{du}{dt} = hv - c\sqrt{u^2 + v^2}\,u + (1-u)\frac{dh}{dt} \qquad (5.1)$$

$$h\frac{dv}{dt} = -hu - c\sqrt{u^2 + v^2}\,v - v\frac{dh}{dt} + h \qquad (5.2)$$

$$h^2 = (1-u)^2 + v^2 \,. \qquad (5.3)$$

It is important to remember that (5.3) is actually an inequality; h is not allowed to decrease. "Unmixing" would seem to violate the second law of thermodynamics. Thus, (5.3) becomes an algorithm:

if $h < (1-u)^2 + v^2$, increase h until the equality holds; otherwise do nothing, Starting from h = u = v = 0, it is not hard to numerically solve (5.1-3) versus time. The solution for c = 0.1 is plotted in Fig. (5.1).

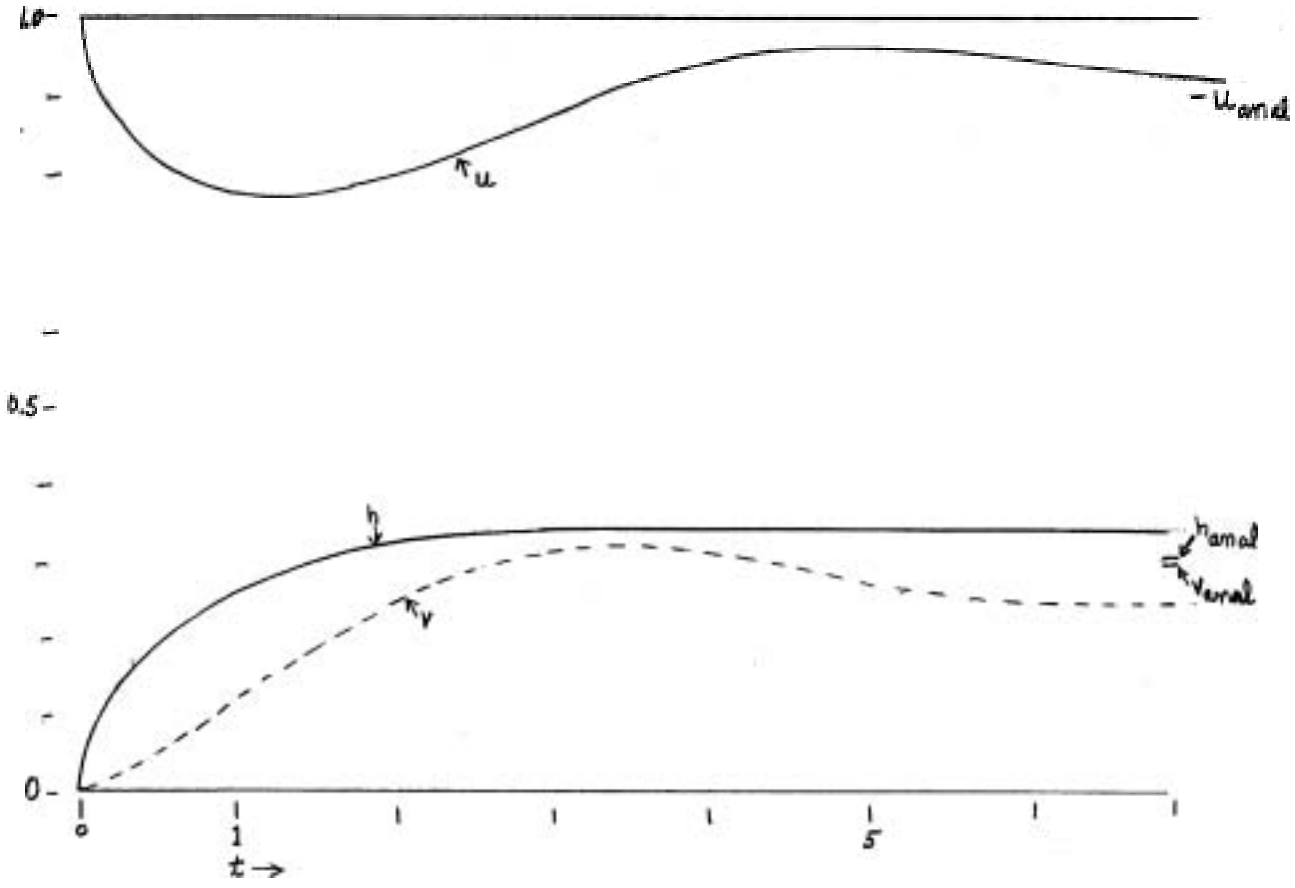

Fig. (5.1). numeric solution of (5.1-3) with c = 0.1.

The solution adjusts in an inertial period, and settles near the previously-found steady solution

$$u = 1/(1 + c), \qquad v = \sqrt{c}/(1 + c), \qquad h = \sqrt{c/(1 + c)}, \tag{5.4}$$

but not exactly at it. Apparently the solution over-shot, with the damped inertial oscillation adding to the steady shear to cause the layer to deepen. This model contains no mechanism to let h decrease again. The transport hv however remains close to that predicted by (5.4). From other trials, it appears that the analytic solution holds very well for large c (large drag) and reasonably well for small. In fact, the case presented in Fig.(5.1) for c = 0.1 is about as bad as any.

6. Surface layer. The free surface layer has already been discussed by Pollard, Rhines and Thompson (1972), but that paper omitted an analytic solution which will be presented here.

Consider a wind-stress acting on the surface of a stratified ocean. The mixing and evaporation may cause a well-mixed layer, which will be idealized as in Fig.(6.1).

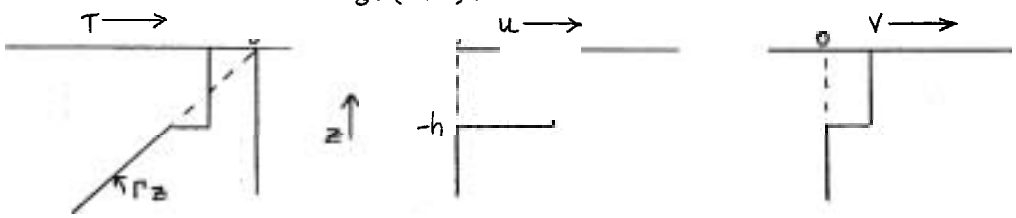

Fig.(6.1) Sketch of T,u,v for surface layer.

Behind the picture is an idea that once the initial stratification is destroyed, there is little resistance to further mixing, so u, v, and T are independent of z to a depth h, below which the initial field is undisturbed. With this layer assumption, the conservation equations are

$$\frac{d(hu)}{dt} = fhv + \frac{\tau_1}{\rho} \tag{6.1}$$

$$\frac{d(hv)}{dt} = -fhu + \frac{\tau_2}{\rho} \tag{6.2}$$

$$\frac{d(hT)}{dt} + \frac{d}{dt}(\tfrac{1}{2}\Gamma h^2) = \frac{Q}{c_v \rho} \tag{6.3}$$

where (τ_1, τ_2) is the wind stress, and Q is the net heating through the surface. Again we impose a criterion that a slab Richardson number should not become too small:

$$\frac{g\alpha(\Gamma h + T)h}{u^2 + v^2} \geq 1. \tag{6.4}$$

It may be noted that this model with heating differs from that of Pollard *et al.*, (1972) in that (6.4) is taken to hold even if Q is non-zero.

The following problem suggested by a frontal passage is easy to solve analytically: at $t = 0$, $h = u = v = 0$; for $t > 0$, $\tau_1 = \tau = $ constant, $\tau_2 = 0$, Q constant. Then

$$hu = \frac{\tau}{f\rho}\sin(ft), \qquad hv = \frac{\tau}{f\rho}(-1 + \cos(ft)),$$
$$h(T + \tfrac{1}{2}\Gamma h) = \frac{Q}{c_v\rho}t \tag{6.5}$$

with

$$u^2 + v^2 = g\alpha(T + \Gamma h)h. \tag{6.6}$$

While these are nonlinear equations, they can be solved fairly easily, since

$$h^2u^2 + h^2v^2 = \frac{2\tau^2}{f^2\rho^2}(1 - \cos(ft)) = g\alpha(\tfrac{1}{2}\Gamma h + \frac{Q}{c_v\rho h}t)\,h^3,$$

$$\text{so } h = \sqrt{\frac{-g\alpha Qt + \sqrt{g^2\alpha^2Q^2t^2 + 4t^2f^{-2}\Gamma g\alpha c_v^2(1-\cos ft)}}{\Gamma g\alpha c_v\rho}} \tag{6.7}$$

The equation (6.7) can only be expected to hold for $0 \leq t \leq \pi/f$, for after that, one expects $Ri > 1$, so the equality (6.6) will no longer hold, as discussed below. The depth h is easily measured in an experiment, so it is worth looking at special cases of (6.7).

If $t \ll f^{-1}$, then

$$h = t^{1/2}\left(\sqrt{\frac{2\tau^2}{g\alpha\Gamma\rho^2} + \left(\frac{Q}{c_v\rho\Gamma}\right)^2} - \frac{Q}{c_v\rho\Gamma}\right)^{\frac{1}{2}} \tag{6.8}$$

If the cooling is strong, or the stratification is weak (as one expects after much cooling), then the wind stress term may not

be dominant. It is easy to look at the limit $\Gamma \to 0$ in (6.9). For heating, $Q > 0$.

$$h \to t^{\frac{1}{2}} \tau \sqrt{\frac{c_v}{g\alpha\rho Q}} \,. \tag{6.10}$$

This is interesting, in that the layer thickens at a finite rate, even though there is no initial stratification. It can be compared to the case of given total buoyancy B, (no heating and $\Gamma = 0$), for which $h = \tau t/\sqrt{B}$. These cases may shed some light on the formation of layers in homogeneous water. For cooling, $Q < 0$,

$$h \to t^{\frac{1}{2}} \sqrt{\frac{2|Q|}{\Gamma c_v \rho} + \frac{\tau^2 c_v}{g\alpha\rho|Q|}} \,, \tag{6.11}$$

so strong cooling can make the layer thicken rapidly. Note that (6.11) holds even in the limit $\tau = 0$.

The case of no velocity shear can also be treated. Then not allowing the Richardson number (with zero denominator) to drop below 1 reduces to not allowing T to drop below $-\Gamma h$. For $Q < 0$, Eqs. (6.3) and (6.4) reduce to saying the heat loss from the deepening layer is the total flux across the surface,

$$h\left(-\tfrac{1}{2}\Gamma h\right) = Qt/\rho c_v$$

or

$$h = t^{\frac{1}{2}} \sqrt{\frac{-2Q}{c_v \rho \Gamma}} \tag{6.12}$$

This answer is independent of rotation.

7. Comparison with observations, Stommel, Saunders, Simmons and Cooper (1969) took closely-spaced SID casts through the surface layer from a drifting ship. They saw a number of interesting and suggestive phenomena. For instance, in their observations on 14 March, shortly after a sudden increase in the wind, the mixed layer thickened very suggestively. However, Stommel *et al.* point out that temperature of the surface layer did not drop, as it should have if the thickening was due to mixing. They suggest advection must have been important in this case. Unfortunately, through virtually all of their observations

advection appears to have been important, For instance, on 12 March, there appears to have been a classic cooling from the surface, with isotherms becoming vertical and vanishing through the surface. However between their soundings 109 and 123, in about two hours the temperature dropped 0.5°C over a depth of at least 4 m, implying a heat loss an order of magnitude larger than the 0.2 langley/min flux estimated across the surface.

While the motion of the ship through the water, and perhaps vertical advection, renders the data very hard to use, their temperature and salinity soundings during and after a rainstorm on 19 March are rather suggestive. The fresh water is readily discernible as a well-mixed layer deepening to about 10 m. Shortly after, the sun came out and a 10 m deep step formed in the temperature which had formerly been well-mixed to at least 30 m. The net solar flux in the time the step formed was comparable with the heat stored in the step. This suggests that the buoyancy of the fresh surface layer did indeed cut off the deep mixing that had occurred earlier in the day, and allowed the solar heat to accumulate, strengthening the layer.

8. Discussion. The slab models presented here for top and bottom boundary layers in a rotating, stratified fluid may be more realistic than the usual picture of Ekman eddy coefficients, in that Ekman spirals are very rarely seen in nature, but well-mixed layers often are, The present approach, based on a slab Richardson or Froude number, gives Ekman transports, and consequent vertical velocities, which are quite definite, and involve no arbitrary eddy coefficients,

It is desirable that someone experimentally check these predicted well-mixed depths and Ekman transports. In doing so, the experimentalist should realize that behind this model is an idea of turbulence that depends on a large Reynolds number. Thus, with ν the kinematic viscosity, it is necessary to ensure that

$$\frac{Uh}{\nu} >> 100 \qquad (8.1)$$

If one thinks of spinning-up a stratified fluid, so $u \sim L\Delta\Omega$ with L a radius and Δ a fractional change of rotation rate Ω, and uses (2.8), then one requires

$$(L\Delta\Omega)^2 \sqrt{\frac{c_p}{2\Omega}} \left(\frac{2}{\alpha\Gamma g}\right)^{\frac{1}{4}} >> 100\nu.$$

with $\nu = .01$ cm^2/sec, $L \sim 10$ cm, $\Omega \sim 10$ sec^{-1}, and $\alpha\Gamma \sim .02/10$ cm, $c \sim 10^{-3}$ and $h \sim 0.3\,A$ cm, $u \sim 10\,\Delta$ cm/sec so $Uh/\nu \sim 3000$ for $\Delta = 0.1$ which ought to be enough. Thus, the conditions for the layer proposed whould not be difficult to achieve. Thus, the model discussed here suggests that many experimental trials of stratified spin-up whould form layers of the sort discussed here, rather than laminar Ekman layers.

References

Deacon, E.L. and E.K. Webb 1962 Interchange of properties between sea and air - small-scale interactions. The Sea, p.57. Interscience, N.Y.

Pollard, R.T., Peter B. Rhines, and Rory O.R.Y. Thompson 1972 The deepening of the wind-mixed layer. Geophysical Fluid Dynamics. (In press).

Stommel, Henry, Kim Saunders, William Simmons, and John Cooper 1969 Observations of the diurnal thermocline. Deep-Sea Res., supplem. to vol. 16: 269-284.